Synthesis of nitrogen-doped carbon dots/polymer composites for their application in organic-based solar cells

A dissertation submitted to the Faculty of Science, University of the Witwatersrand, in fulfilment of Master of Science degree in chemistry

by

Ms Puledi Mphago (BSc Hons)

Student Number: 548261

Supervisor: Dr Manoko S. Maubane

Co-supervisors: Prof Daniel Wamwangi and Prof Neil J. Coville

Molecular Sciences Institute, School of Chemistry

University of the Witwatersrand, Johannesburg, South Africa, May 2019

DECLARATION

I declare that this dissertation is my own, unaided work. It is being submitted for the Degree of Master of Science at the University of the Witwatersrand, Johannesburg. It has not been submitted before for any degree or examination at any other University.

.....

Puledi Mphago

On this 17th day of May 2019 in Johannesburg.

ABSTRACT

This study reports the synthesis, application and investigation of fluorescence properties of nitrogen-doped carbon dots (NCdots). The NCdots were synthesised using different precursors such as: citric acid (CA) with ethylenediamine (EDA), and fumaronitrile (FN) via microwave-irradiation method. The as-synthesized NCdots from CA with EDA (NCdots-CAEDA) and FN (NCdots-FN) were both spherical in shape and the average sizes were around 3-5 nm. Both types of NCdots demonstrated excellent fluorescence properties with excitation-dependent fluorescence behaviours. The composition of the as-synthesized NCdots was explored by X-ray photoelectron spectroscopy (XPS), showing different amount of carbon, hydrogen, nitrogen and oxygen contents. The most dominant nitrogen configuration in NCdots-CAEDA was pyridinic and in NCdots-FN was pyrrolic nitrogen. The surface functional groups of both types of NCdots were confirmed by fourier transformation infrared microscopy (FTIR). Both types of NCdots were applied in organic solar cells, modifying the active layer. The results demonstrated that the device modified with NCdots-FN outperformed the device modified with NCdots-CAEDA. In order to investigate the fluorescence properties of NCdots, various reaction conditions such as: the amount of EDA, solvent, reaction time and microwave power were varied. The results showed that 1.0 ml EDA, water, 10 min and 500 W were the optimal synthesis conditions for the preparation of the NCdots-CAEDA with good fluorescence properties. The fluorescence properties of NCdots play a crucial role in organic photovoltaics (OPVs). The functional groups on the surface of the NCdots-CAEDA were also removed by annealing the sample at 500 ℃ for 2 h at a heating rate of 10 ℃/min to further investigate the fluorescence properties of NCdots. The fluorescence properties of the NCdots-CAEDA were destroyed after annealing the sample.

DEDICATION

This dissertation is dedicated to my:

Mom: Tinny Mphago

Sister: Sandra Mphago

Granny: Francinah Monama

Uncles: Frans and Casberth Mphago

"Let the wise listen and add to their learning, and let the discerning get guidance" Proverbs 1:5

ACKNOWLEDGEMENTS

- I would like to give my appreciation to my supervisors: Dr Manoko Maubane, Prof Neil Coville and Prof Daniel Wamwangi for their constant support, advice, encouragement and guidance during this research project. It has been a wonderful experience to work with people like you and I am very grateful. May God bless!
- I would also like to extend my gratitude to the following people for helping me with different characterization techniques: Dr Werner Jordaan for XPS analysis, Ms Rhandzu Rikhotso for HRTEM and Adam Shnier for IV-Characterizations. Without your help, it would be impossible for me to complete this master's degree.
- To Prof Alexander Ziegler, thank you for allowing me to use the characterization techniques such as: TEM, SEM and PXRD to analyse my samples.
- I would like to show my sincere gratitude to Dr Bridget Mutuma. Thank you so much doc, you have been a great help!
- I would also like to thank the CATMAT research group especially the following people: Lerato Mphahlele, Tshwarela Kolokoto, Thulisile Buthelezi, Alice Magubane, Thomas Mongwe, Themba Ntuli, Lerato Mokoloko, Xiluba Mathebula, Hajeccarim Baloyi and the others for their valuable support.
- To school of physics and chemistry, Thanks for providing me with the high quality laboratories environment to perform my experiments.
- I would also like to thank my dearest mom, Tinny Mphago, for the love, support and prayers. I don't know where I would be if it was not your prayers. May the God of Mount Zion protect you!
- To my friends and family, especially, Sandra Mphago, Collen Mabafule and Dineo Raselabi. Thank you so much for your love, support and encouragement.
- I would also like to thank DRF/NRF-Centre of Excellence in Strong Materials for funding. This research project could not be possible without this funding.
- Finally, I would like to thank the God of Mount Zion for guidance, protection and mercy. Kgomo keya leboga!

"Let the wise listen and add to their learning, and let the discerning get guidance" Proverbs 1:5

PRESENTATIONS

- Frontiers of electron microscopy in materials science (FEMMS) conference, "Synthesis of nitrogen-doped carbon dots/polymer composites for applications in organic solar cell" **(Poster presentation)**, September 2017, Fourways-Indaba hotel, Gauteng.
- Catalysis and Materials (CATMAT) school of chemistry seminar, "Synthesis of nitrogen-doped carbon dots/polymer composites for applications in organic solar cell" **(Oral presentation)**, October 2017, Johannesburg-Wits University, Gauteng.
- Catalysis society of South Africa (CATSA) conference, "Synthesis of nitrogen-doped carbon dots/polymer composites for applications in organic solar cell" **(Poster presentation)**, November 2017, Pilanesberg-Bakubung Bush lodge, Northwest.
- Microscopy society of South Africa (MMSA) conference, "Microwave synthesis of fluorescent nitrogen-doped carbon dots for applications in organic solar cells" **(Poster presentation),** December 2017, Warmbaths in Belabela-Forever Resorts, Limpopo.
- Catalysis and Materials (CATMAT) school of chemistry seminar, "Synthesis of nitrogen-doped carbon dots/polymer composites for applications in organic solar cell" **(Oral presentation)**, March 2018, Johannesburg-Wits University, Gauteng.
- Centre of excellence students' presentations (CoE/AMSA) workshop, "Microwave synthesis of fluorescent nitrogen-doped carbon dots for applications in organic solar cells" **(Poster presentation),** April 2018, Johannesburg-Wits university, Gauteng
- Nanostructured materials (NanoSmat) conference, "Facile synthesis of nitrogen-doped carbon dots for applications in organic solar cell" **(Poster presentation)**, November 2018, Cape Town-The lord Charles hotel, Western Cape.

TABLE OF CONTENTS

LIST OF ABBREVIATIONS

AFM:	Atomic force microscopy
AM:	Air mass
BHJ:	Bulk heterojunction
BDA:	Butanediamine
CA:	Citric acid
Cdots:	Carbon dots
Cdots-CA+EDA:	Caborn dots from citric acid and ethylenediamine
Cdots-FN:	Carbon dots from fumaronitrile
N,SCdots:	Nitrogen, sulphur co-doped carbon dots
CVD:	Chemical vapor deposition
Da:	Daltons
DEA:	Diethylamine
DMF:	Dimethylformamide
DMSO:	Dimethyl Sulfoxide
EDA:	Ethylenediamine
EtOH:	Ethanol
ETL:	Electron transport layer
FTIR:	Fourier transform infrared spectroscopy
HOMO:	Highest occupied molecular orbital
HRTEM:	High resolution transmission electron microscopy
HTL:	Hole transport layer
ISCs:	Inorganic solar cells
ITO:	Indium tin oxide
J-V:	Current density-voltage
J_{max}:	Current density at maximum power
J_{sc}:	Current density
LiF:	Lithium fluoride
LUMO:	Lowest unoccupied molecular orbital
MWCO:	Molecular weight cut-off
MWCNT:	Multi-walled carbon nanotubes
NCdots:	Nitrogen-doped carbon dots
OSCs:	Organic solar cells

OPVs:	Organic Photovoltaics
P3HT:	Poly (3-hexylthiophene)
PAGE:	Polyacrylamide gel electrophoresis
PCE:	Power conversion efficiency
PEG:	Poly-ethylene glycol
PL:	Photoluminescence spectroscopy
PXRD:	Powder X-ray diffraction
QDs:	Quantum dots
QY:	Quantum Yield
TEM:	Transmission electron microscopy
TGA:	Thermal gravimetric analysis
TCO:	Transparent conductive oxide
Uv-vis:	Ultraviolet-visible spectroscopy
V_{max}:	Voltage at maximum power
V_{oc}:	Open circuit voltage
XPS:	X-ray photoelectron spectroscopy

LIST OF FIGURES

Chapter 1

Chapter 2

Chapter 3

Chapter 4

Chapter 5

Chapter 6

LIST OF TABLES

Chapter 2

Chapter 4

Chapter 5

Chapter 6

LIST OF SCHEMES

Chapter 4

CHAPTER 1: MOTIVATION OF THE STUDY

1.1 Solar energy

The earth receives over 86 000 TW energy from the sun, but converting it efficiently into electricity remains one of the biggest challenges faced by researchers around the world[1-4]. South Africa (SA) has been identified as one of the countries that receive the highest amount of solar irradiation. It has been reported that SA receives solar irradiation of about 2000-3000 KW/m^2/year, with the Northern Cape area receiving the highest as compared to other provinces[5]. With an increase in demand to produce green sources of energy, there has been keen interest in finding solutions to improve efficiencies in solar cells. This increase in energy demand can be due to a rapid human population growth, as well as industrialization and urbanization by mankind. Therefore, in order to ameliorate the energy crisis that the country is facing, intensive research programmes on renewable energy technologies have been developed. Solar energy is one of the renewable, abundant and inexhaustible energies that can produce clean energy without heavy machinery and noise as compared to other energy sources[2,3].

1.2 Photovoltaic solar cells

The photovoltaic industry plays an important role worldwide because it uses energy from the sun, which is abundant. Solar energy conversion is one of the few technologies that is environmentally friendly, with zero CO_2 emission and with no noise during the process as compared to other technologies[2,6,]. In photovoltaic (PV), solar cells generate electricity as a result of the photovoltaic effect. This was first discovered by Alexandre-Edmund Becquerel in 1939 when he was studying the effect of light on an electrolytic cell[7]. The PV effect occurs when a potential difference at the junction of two different materials is generated in response to visible or other radiation or it can simply be defined as the conversion of light directly to electricity[8]. For a cell to operate, a material that can absorb light to generate free electrons via this photovoltaic effect is required. There are also important factors that need to be taken into considerations for development of an ideal solar cell material. These factors include:

- a small band gap (between 1.1 and 1.7 eV),
- a direct band gap,
- an easy production method suitable for mass production,
- long term stability of the solar cell material,

- availability of the material,
- non-toxicity of the material,
- high conversion efficiency[9,10].

The most widely used PV materials are mainly semiconductors such as: silicon, cadmium telluride (CdTe), gallium arsenide (GaAs), indium phosphide (InP), copper indium diselenide ($CuInSe_2$). This category of PV cells made from the above materials is classified as first and second generation PV based materials. More recently exotic thin film PV devices have been fabricated using liquid electrolyte, organic polymers and a hybrid thereof amongst other suite of materials[10]. This is the class of the third and fourth generation PV technology. **Figure 1.1** illustrates the specific materials categorized into the four developmental generations[2].

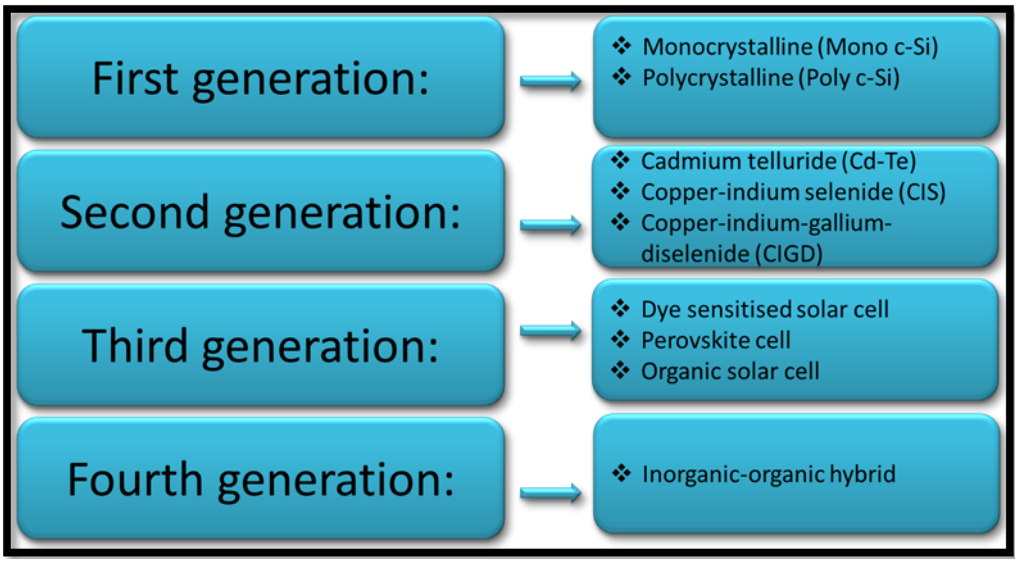

Figure 1.1: Generations of photovoltaic cell (modified from ref.2).

1.2.1 Silicon solar cells

Silicon-based solar cells are still dominantly used in the solar cell industry due to their high conversion efficiency, excellent charge transport properties or high electron mobilities[2,6,9,11,]. Silicon-based solar cells have been dominant for more than 30 years[2,9]. The conversion efficiency of PV solar cells based on silicon was reported to be around 15-20 %, particularly when used in its crystalline form[9]. Even though silicon based solar cells have a high energy conversion efficiency, their cost remains the largest barrier for wide spread sustainable commercialization as a renewable source of energy[11,12]. Other drawbacks of silicon-based solar cells include their limited lifetime and stability due to degradation when under illumination[12]. In addition to limitations of silicon-based solar cell, silicon is an indirect band gap

semiconductor, and a material with a direct band gap is required because the probability of light being absorbed in a direct band gap material is much higher than in an indirect band gap material[9,11]. Some of these problems were solved by use of thin film solar cells that used semiconductor materials such as CdTe and Cu_2ZnSnS_4. They are direct band gap semiconductors and possess unique electronic and luminescent properties requisite for photovoltaic applications[9,10]. However, these materials are toxic and the metal is expensive, thus limiting their development[13]. Therefore, in the future, society will need materials with a low production cost that are abundantly available, show long-term stability and are environmentally friendly. This is thus the driving force for the search for novel materials for PV applications to replace the energy intensive Si-based PV devices. To this end, Organic solar cells have been seen as potential candidates for low cost PV applications.

1.2.2 Organic solar cell

Organic-based solar cells can be used as alternatives to silicon-based solar cells since they are cost-effective[12,14]. They have attracted a great deal of attention due to their unique and favourable advantages including:

- mechanical flexibility,
- ease of device fabrication,
- light-weight,
- solution processability and
- low cost[14-16].

The cost trade-offs are attributed to the solution processing fabrication techniques which are not only cheap but also scalable to large area devices[14-16]. In an organic solar cell, a light absorbing material is required to absorb photons and generate charge carriers[3]. The bulk-heterojunction (BHJ) layer is made of two materials: a donor and an acceptor as shown in **Figure 1.2**. The donor in the active BHJ layer is responsible for light absorption, exciton generation, diffusion, and dissociation at the interface. It is crucial to understand the operation of a PV cell and this will be discussed in detail in **Chapter 2**.

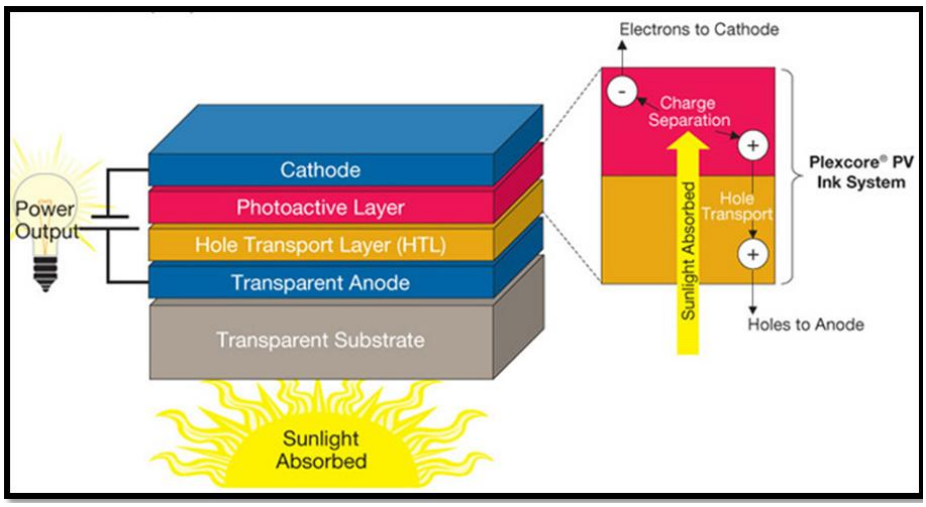

Figure 1.2: Generalised structure of an organic photovoltaic solar cell[17].

This study reports the use of nitrogen-doped carbon dots (NCdots) in an organic solar cell to improve the light absorption and charge transport in the active layer. Carbon dots (Cdots) are quasi-spherical carbon nanoparticles with diameters less than 10 nm. They exhibit excellent optical properties such as tuneable fluorescence. These excellent optical properties have been exploited for a wide range of applications[1,15]. To the best of our knowledge, the study of NCdots/polymer composites in organic solar cells as the active layer has not been reported in the literature.

1.3 Aims and objectives

The main aim of this research project is the synthesis of NCdots for applications in organic photovoltaic devices as the active layer.

Objectives:

- To synthesise NCdots using different precursors such as: citric acid (CA) with ethylenediamine (EDA), and fumaronitrile (FN) via a microwave-irradiation method.
- To investigate the optical properties of the NCdots prepared from CA with EDA, and FN using photoluminescence (PL) and Ultraviolet-visible (Uv-vis) spectroscopy.
- To study the effect of the annealing processes on the fluorescent properties of the as-prepared NCdots.

- To characterise the as-prepared NCdots using other techniques such as: transmission electron microscopy (TEM), thermal gravimetric analysis (TGA), Fourier transform infrared spectroscopy (FTIR), Laser Raman spectroscopy, X-ray photoelectron spectroscopy (XPS) and Powder X-ray diffraction (PXRD).
- To synthesise NCdots/polymer composites using the as-synthesised NCdots and the semi-conducting polymer [6,6]-phenyl-C61-butyric acid methyl ester (PCBM)
- To incorporate NCdots/PCBM composites as an electron acceptor in the organic photovoltaic device: P3HT: PCBM-NCdots
- To test the photovoltaic device using the current density-voltage (J-V) measurements.

1.4 Hypotheses and questions

Questions:

- ❖ Can NCdots/polymer composites be used in organic photovoltaic solar cells to harvest the energy from the sun to generate clean and abundant electricity?
- ❖ Are the NCdots, blended with conducting polymer, an ideal material to be used as an active layer in organic photovoltaic solar cells?
- ❖ Does the incorporation of the NCdots in P3HT:PCBM improve the performance of the cell?
- ❖ Does annealing of the NCdots have an impact on their fluorescent properties?
- ❖ Does the variability of reaction conditions have any effect on the fluorescence properties of NCdots?

Hypothesis:

- This research project suggests that by the use of nitrogen doped Cdots blended with conducting polymers, as active layer in organic photovoltaic solar cell, a clean and abundant energy can be generated with improved efficiency.
- We hypothesize that the fluorescence properties of NCdots are due to the functional groups on their surfaces. The fluorescence properties are expected to be destroyed upon annealing as the functional groups are removed.

1.5 Organisation of dissertation

Chapter 1 presents general introduction and motivation of the study. It also gives the aims and research questions on how strong material composites can be used in organic-based solar cells to enhance the efficiency.

Chapter 2 focuses on the literature review on carbon dots, how they were discovered, their advantages over non-carbon nanomaterials, and their synthesis and applications. It also provides a background on the architectures of organic solar cells and the working principle.

Chapter 3 introduces the different characterization techniques used to analyze the as-prepared NCdots. This chapter also explains how some of the sample preparations were done.

Chapter 4 focuses on the synthesis and characterization of carbon dots prepared from different precursors (CA with EDA, and FN) via a microwave-irradiation method. The properties of the as-prepared NCdots from different precursors are being compared in this chapter.

Chapter 5 presents the fabrication and characterization of the organic solar devices modified with two types of NCdots. It presents how incorporation of NCdots in the active layer can affect the performance of the devices.

Chapter 6 presents the effect of reaction conditions on the fluorescence properties of the NCdots prepared from CA and EDA as carbon and nitrogen precursor, respectively, via a microwave-irradiation method.

Chapter 7 offers general conclusions and recommendations of the overall dissertation.

References

1) Essner, J. B.; Baker, G. A. The Emerging Roles of Carbon Dots in Solar Photovoltaics: A Critical Review. *Environ. Sci. Nano* **2017**, *4*, 1216–1263.
2) Ranabhat, K.; Patrikeev, L.; Revina, A. A.; Andrianov, K.; Sofronova, E.; Lapshinsky, V. AN INTRODUCTION TO SOLAR CELL. *J. Appl. Eng. Sci.* **2016**, *14*, 481–491.
3) Dieter, W.; Dieter, M. Organic Solar Cells. *Adv. Mater.* **1991**, *3*, 129–138.
4) Bagher, A. M. Introduction to Organic Solar Cells. *Sustain. energy* **2014**, *2*, 85–90.
5) Gauché, P.; Backström, T. W. Von; Brent, A. C. A Concentrating Solar Power Value Proposition for South Africa. *J. energy South. africa* **2013**, *24*, 67–76.
6) Razykov, T. M.; Ferekides, C. S.; Morel, D.; Stefanakos, E.; Ullal, H. S.; Upadhyaya, H. M. Solar Photovoltaic Electricity: Current Status and Future Prospects. Sol. Energy **2011**, 85, 1580–1608.
7) Becquerel, A.E. Memoire sur les Effects d'Electriques Produits Sous l'Influence des Rayons Solaires. *Comptes Rendus de l'Academie des Sciences* **1839**, 9, 561-567.
8) Parida, B.; Iniyan, S.; Goic, R. A Review of Solar Photovoltaic Technologies. Renew. Sustain. Energy Rev. **2011**, 15, 1625–1636.
9) Xakalashe, B. S.; Tangstad, M. Silicon Processing : From Quartz to Crystalline Silicon Solar Cells. South. African pyrometallurgy. **2011**, 1, 83–100.
10) Goetzberger, A.; Hebling, C.; Schock, H.-W. Photovoltaic Materials, History, Status and Outlook. Mater. Sci. Eng. **2015**, 40, 1–46.
11) Lussem, B.; Riede, M.; Leo, K. Doping of Organic Semiconductors. Phys. status solidi A. **2013**, 210, 9–43.
12) Zhu, H.; Wei, J.; Wang, K.; Wu, D. Applications of Carbon Materials in Photovoltaic Solar Cells. Sol. Energy Mater. Sol. Cells. **2009**, 93, 1461–1470.
13) Yue, Z.; Lisdat, F.; Parak, W. J.; Hickey, S. G.; Tu, L.; Sabir, N.; Dorfs, D.; Bigall, N. C. Quantum-Dot-Based Photoelectrochemical Sensors for Chemical and Biological Detection. ACS Appl. Mater. Interfaces. **2013**, 5, 2800–2814.
14) Mazzio, K. A.; Luscombe, C. K. The Future of Organic Photovoltaics. R. Soc. Chem. **2014**, 2012, 1–13.
15) Zhang, H.; Zhang, Q.; Li, M.; Kan, B.; Ni, W.; Wang, Y.; Yang, X.; Du, C.; Wan, X.; Chen, Y. Investigation of the Enhanced Performance and Lifetime of Organic Solar Cells Using Solution-Processed Carbon Dots as the Electron Transport Layers. J. Mater. Chem. C **2015**, 3, 12403–12409.

16) Gunes, S.; Neugebauer, H.; Sariciftci, N. S. Conjugated Polymer-Based Organic Solar Cells. Am. Chem. Soc. **2007**, 107, 1324–1338.
17) http://www.sigmaaldrich.com/technical-documents/articles/technology-spotlights/plexcore-pv-ink-system.html accessed on **08 March 2017**

CHAPTER 2: LITERATURE REVIEW

2.1 Carbon-based materials

Carbon-based nanomaterials have received considerable attention due to their unique size dependent combination of chemical and physical properties such as: high electron density, high surface area, high structural stability and chemical inertness[1-3]. Carbon is a well-known, and an extraordinary element, which is nontoxic, relatively cheap and abundant in the earth's crust[4,5]. Carbon can be found in different allotropes such as nano-diamond, nano-horns, carbon onions, graphite, graphene, carbon nanotubes (CNTs), and fullerenes[1,6] as shown in **Figure 2.1**. Recent studies have shown that carbon nanomaterials remain promising candidates for a multiplicity of applications such as: photovoltaics, photocatalysis and biological applications etc. Their utility is driven primarily by their excellent optoelectronic, high optical-absorption within the visible spectrum, high photostability and low toxicity, respectively[6-9].

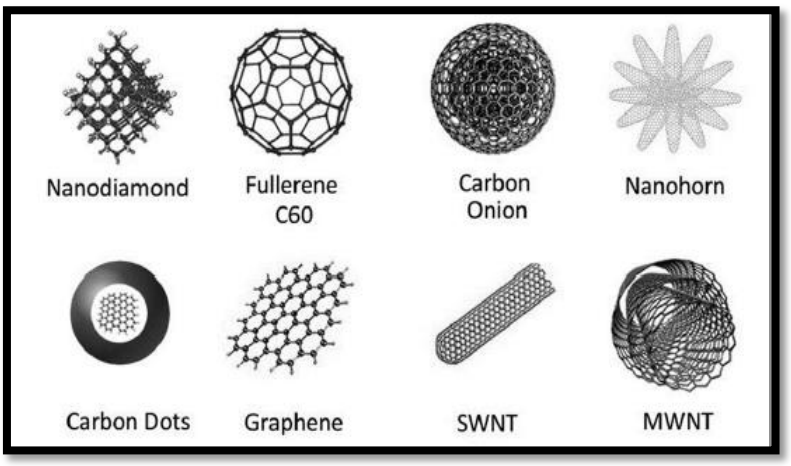

Figure 2.1: Members of the carbon materials with different shapes[1].

2.1.1 Carbon dots

Amongst the family of structured carbon nanomaterials, carbon dots (Cdots) have recently attracted a great deal of interest due to their excellent quantum confined optical properties that enables them to be used not only as light conversion materials, but also as active charge transport layers. Additionally, they offer high photostability similar to conventional semiconductor quantum dots (QDs). Cdots are also known as carbon nanodots, carbon quantum dots or carbogenic dots and are defined as quasi-spherical small carbon nanoparticles with diameters less than 10 nm showing the character of crystalline graphite[7-14]. These materials

were first discovered serendipitously in 2004 by Xu and co-workers during purification of single-walled carbon nanotubes (SWCNTs) by a preparative electrophoresis method[15]. Cdots possess many advantages compared to the non-carbon dots due to their robust chemical inertness, low cost, low cytotoxicity, high aqueous solubility, high photostability, resistance to photobleaching and good biocompatibility[8,14,16-20]. The unique properties of Cdots make them suitable for bioimaging, biosensing, solar technologies, light emitting diodes and drug delivery applications[19-25]. Therefore, Cdots can be considered as substitutes for non-carbon dots such as semiconductor QDs which consists of heavy metals which are essential elements for their high performance in certain applications. In addition, unlike semiconductor QDs, Cdots have a tuneable band gap and allow efficient charge injection.

In the past years, semiconductor QDs, particularly those that consist of cadmium or lead derivatives, have been used in applications such as solar cell devices, bioimaging, light emitting diodes and optical sensors[26-29]. This is due to the fact that these materials also possess excellent optical properties. However, they contain heavy metals that are toxic and hazardous to both humans and the environment[5,23,26,30]. In addition, these materials are expensive, and their synthesis requires expensive precursors while Cdots can be produced from an unlimited number of carbon precursors ranging from small molecules to polymers. Previous studies also showed that Cdots can be prepared from cheap, abundant raw materials/biomass as the precursors[31]. These materials include: watermelon peel[32], orange juice[33], mango peels[34], orange peels[35], starch from potatoes[36], onion waste[37], eggshell membrane[38], unripe peach[39], sweet potato[40] and banana juice[41]. Carbon is present in almost all organic materials, hence Cdots starting materials are cheap and abundant.

2.1.2 Structure of carbon dots

Cdots consists of a core-shell structure with sp^2/sp^3 carbon cores and different functional groups such as carboxylic acid, hydroxyl, amine, ether, carboxyl, epoxy and carbonyl on their surface[16,18]. The structure of Cdots is depicted on **Figure 2.2**. Different functional groups on the surface of Cdots depend on the type of precursor used in the synthesis of these materials. The functional groups on the surface of Cdots imparts them with good solubility and ease of further surface functionalization with various organic and inorganic molecules. In addition, the composition, size and optical properties of Cdots also depend on the precursors and synthesis methods used. Cdots generally fall under a class of zero-dimensional (0-D) carbon nanoparticles with a crystal lattice parameter of approximately 0.34 nm which corresponds to the (002) interlayer spacing of graphite[1,16].

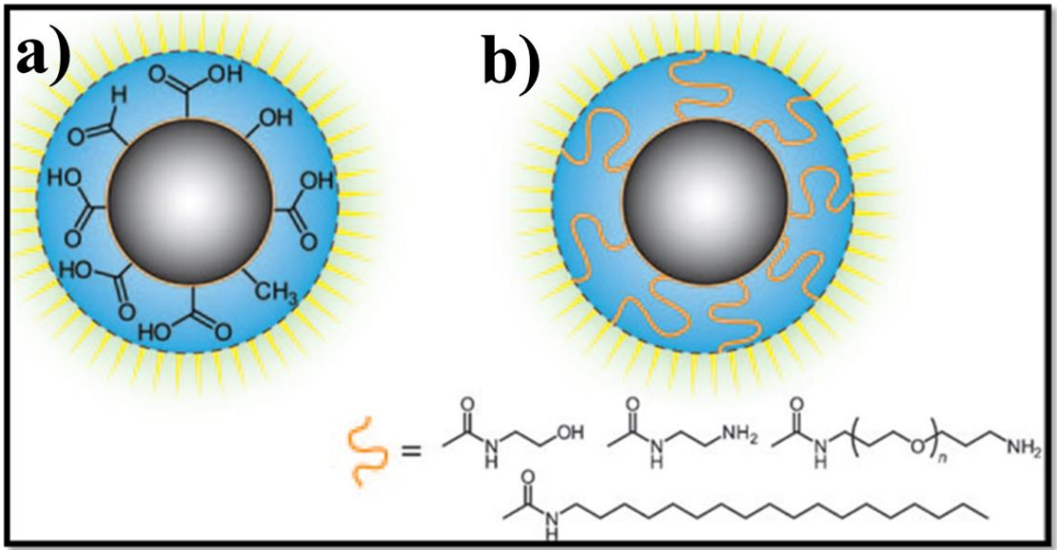

Figure 2.2: Structure of Cdots after a) surface passivation and b) functionalization[16].

2.2. Synthesis of carbon dots

In recent years, various methods have been used in the synthesis of Cdots. These methods can be categorised into two general approaches, namely: the bottom-up and the top-down approaches[5,12,13,16,25]. The physical, chemical and optical properties such as the size, crystallinity and fluorescence characteristics such as the quantum yield, are often determined by the precursors and the synthesis methods of Cdots. Therefore, the properties of these materials can be easily tuned with careful choice of the synthesis methods and the precursors. The schematic representation of the two approaches are shown in **Figure 2.3**. This section presents various preparation methods for Cdots in detail with their attributed advantages and disadvantages summarised in **Table 2.1**.

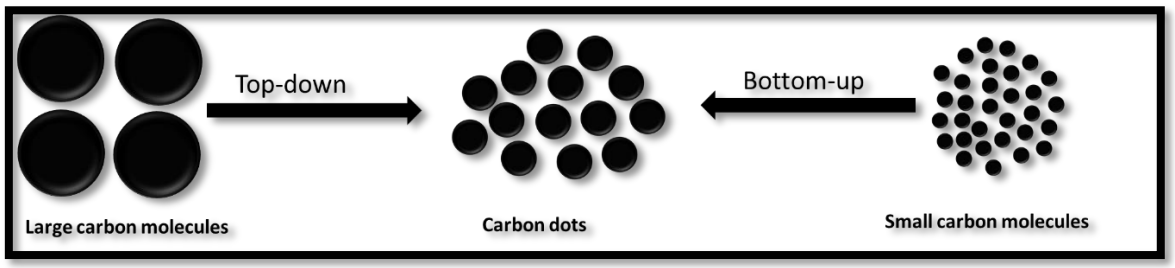

Figure 2.3: Schematic illustration of the top-down and bottom-up approaches.

Table 2.1: Comparison of the top-down and bottom-up approaches for preparation of Cdots.

Approaches	*Methods*	*Advantages*	*Disadvantages*	*References*
Top-down	Arc-discharge	-	High impurities, complicated operations, low yield	15
	Laser ablation	Controllable size, effective	Complicated operations, time-consuming, high cost, non-uniform size distribution	10,42
	Electrochemical oxidation	High purity, high yield	Low quantum yield	43,44
Bottom-up	Hydrothermal treatment	Easy operation, high quantum yield	Low yield, long reaction times	21,33
	Microwave-irradiation	Short reaction time, easy operation	Can use higher energy	11,38,45

2.2.1 Top-down approach

The top-down approach is considered the earliest approach for the preparation of Cdots. It involves cutting a large carbon structure into small carbon nanoparticles, physically, chemically or electrochemically until the required particle size is reached[10,42]. Large carbon precursors such as graphite, candle soot and multi-walled carbon nanotubes (MWCNTs) are normally used in the top-down approach. The top-down approach typically involves complicated reactions which require special equipment and purification methods that are time-consuming[10]. The preparation methods such as: arc-discharge method, laser ablation, and electrochemical oxidation fall under this approach and are discussed below.

2.2.1.1 Arc-discharge method

The Arc-discharge method can be considered the original method for preparing Cdots following their discovery by Xu *et al*[15]. In a standard procedure, 2 g crude arc was boiled with 3.3 N HNO_3 for 48 h in order to remove amorphous carbon. The sediment was washed with acidic water and then centrifuged to remove large particles. The resultant sediment was then extracted with NaOH solution to collect SWCNTs. In this method, the Cdots were obtained as

the by-products of the purification of SWCNTs derived from arc-discharge soot[15]. After purification, it was discovered that the suspension contained different classes of carbon materials, including purified SWCNTs, tubular carbon and highly fluorescent carbon materials as shown in **Figure 2.4**. The particle sizes of the fluorescent materials ranged from 3 to 6 nm. The drawback of this method is the large amounts of impurities that are produced with the Cdots and this makes the separation process to be an enormous challenge. One method that has gained attraction in the separation of Cdots from impurities is the polyacrylamide gel electrophoresis (PAGE). However, this additional step of separation process makes the Arc-discharge method to be time-consuming. In addition, the experimental apparatus used in the arc-discharge method is not readily available for many researchers.

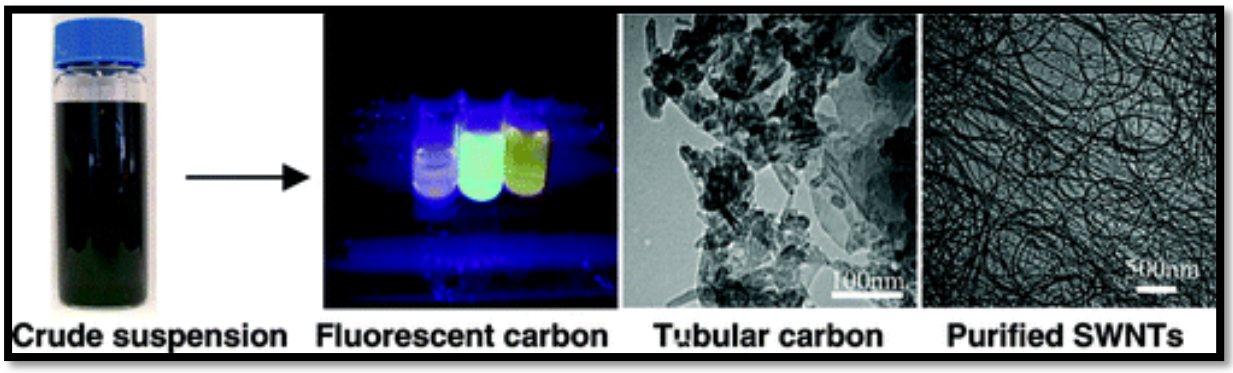

Figure 2.4: Cdots preparation via an Arc-discharge method showing different classes of carbon materials[15].

2.2.1.2 Laser ablation method

Sun *et al.* synthesised Cdots via a laser ablation method from a mixture of graphite powder and cement under argon as a carrier gas in the presence of water vapor[10]. In a typical procedure, carbon materials were prepared by hot-pressing a mixture of graphite powder and cement. This was followed by baking, curing and annealing sequentially in argon flow[10]. The obtained products showed no photoluminescence until the passivation agent poly-ethylene glycol (PEG_{1500}), an organic molecule, was added to the sample. The bright luminescence emissions were observed as shown in **Figure 2.5**. Transmission electron microscopy (TEM) demonstrated that the average particle size was 5 nm in diameter. The most fascinating feature of this method is that the particle sizes are controllable.

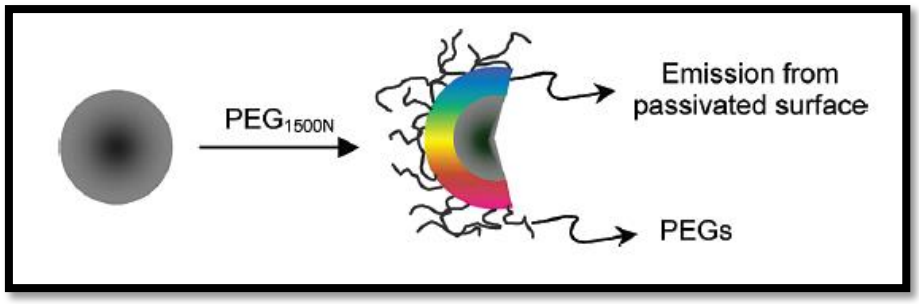

Figure 2.5: Cdots preparation via a laser ablation method showing fluorescence emission of the carbon after surface passivation[10].

2.2.1.3 Electrochemical oxidation method

The electrochemical oxidation method produces Cdots with high reproducibility, good yield and with high purity and crystallinity. Liu *et al*. produced Cdots via an electrochemical oxidation method using a three-electrode system[44]. The three-electrode system used consists of Ag\Agcl as the reference electrode, graphite as the working electrode and a platinum foil as the counter electrode. The electrolyte was made by mixing water, ethanol and NaOH. The voltage was then applied to the working electrode for 3 hours under nitrogen conditions. The resultant product was colourless and tended to be bright yellow when exposed to air at room temperature (**Figure 2.6**). It was concluded that the colour change was due to the oxidation processes taking place. The average diameter of the obtained Cdots was 4.0 nm with high crystallinity and a lattice spacing of 0.31 nm.

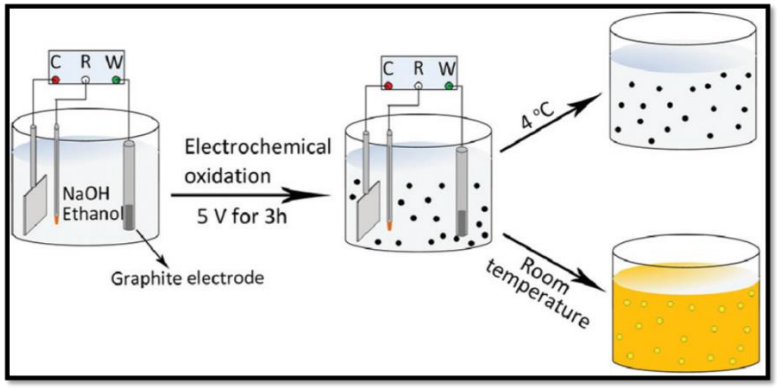

Figure 2.6: Schematic representation of Cdots preparation via an electrochemical oxidation method using a graphite electrode[44].

2.2.2 Bottom-up approach

The bottom-up approach is one of the procedures used that has received considerable attention due to its easy operation as compared to its counterpart the top-down approach. The bottom-up approach involves building Cdots from small organic molecular precursors by various method: hydrothermal method, pyrolysis method, microwave-irradiation method, acid dehydration method, ultrasonic method or combustion methods[12,13,16]. Unlike the top-down approach, the bottom-up approach involves the use of abundant and cost-effective starting materials. The bottom-up method is preferred over the top-down method because it tends to avoid many problems such as carbonaceous aggregation, poor size control, uniformity and unwanted surface properties which are faced by the majority of the methods using the top-down approach[10,23]. Among the methods using bottom-up approach, the hydrothermal treatment and microwave-irradiation methods are the most commonly used and are discussed in more detail below:

2.2.2.1 Hydrothermal treatment method

The hydrothermal treatment is a method that has been used for the preparation of Cdots for a very long time. It produces Cdots with high quality, high yield and tunable morphology. The disadvantage of this method is its long reaction times and the high energy requirement as compared to the microwave-irradiation method. Sahu *et al*. produced highly green-fluorescent Cdots from orange juice via a hydrothermal treatment method as shown in **Figure 2.7**[33]. In a typical procedure, 40 ml orange juice and 30 ml ethanol were mixed and the transferred into a Teflon-lined stainless-steel autoclave. The mixture was then heated at 120 ˚C for 150 min. The resultant dark brown solution was centrifuged to remove large particles[33]. In addition, centrifugation speed was optimized in order to separate highly fluorescent Cdots from less fluorescent materials. TEM images revealed an average Cdots particle size of 2.5 nm in diameter.

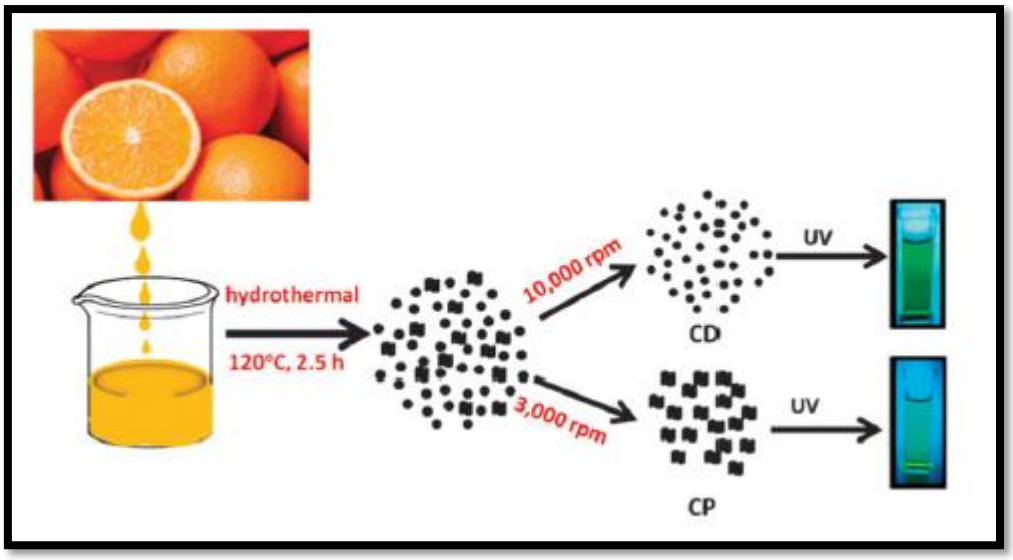

Figure 2.7: Schematic illustration of Cdots preparation via the hydrothermal treatment of orange juice[33].

2.2.2.2 Microwave-irradiation method

The microwave-irradiation method is a simple, flexible, clean and efficient method used for the production of Cdots as compared to other methods. The most fascinating feature about the microwave-irradiation method is the use of short reaction times and homogeneous heating which results in Cdots being produced on a large scale[11,45]. During a microwave-irradiation synthesis, the precursors are mixed with solvents and then heated at a certain microwave power or temperature to break the chemical bonds of the starting materials. The precursors then become carbonized. After carbonization, the graphitic or amorphous cores are formed and the functional groups remain on the surface of the Cdots. Yang *et al*. produced nitrogen, sulphur co-doped Cdots (N,SCdots) from a mixture of ammonium citrate and cysteamine hydrochloride via a microwave-irradiation method. These materials were used for chromium (VI) and ascorbic acid sensing as shown in **Figure 2.8**[45]. In a standard procedure, 0.2 g cysteamine hydrochloride and ammonium citrate were dissolved in 30 ml ultrapure water. The mixture was then heated in a microwave oven at high power mode for 4 min. The obtained N,SCdots after purification showed excitation-independent emission behaviour with a QY of 54.8%. The average size of the Cdots was determined to be 3.6 nm as shown in **Figure 2.9**. This method is efficient as the product was obtained in 4 min.

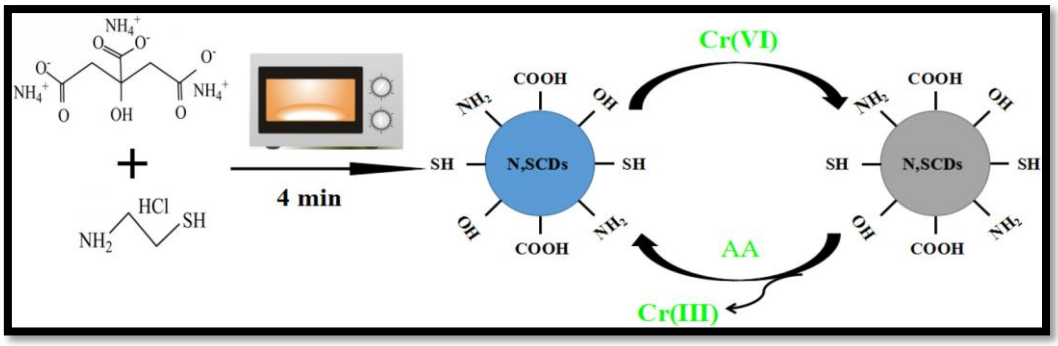

Figure 2.8: Schematic illustration of Cdots preparation via a microwave-irradiation method[45].

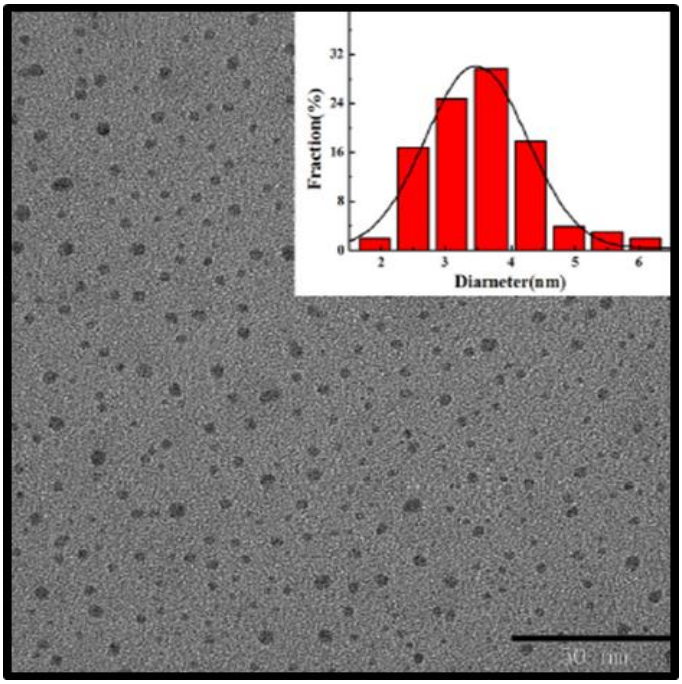

Figure 2.9: TEM image of the N,SCdots (inset: Its corresponding size distribution histogram)[45].

2.3. Optical properties of carbon dots

Carbon dots generally demonstrate unique optical properties irrespective of the different precursors used for their synthesis. They possess excellent optical properties such as tunable excitation and emission wavelengths, high fluorescence stability, nonblinking, etc. This section presents and discusses the common optical properties of Cdots.

2.3.1 Ultraviolet-visible (uv-vis) absorption properties

Cdots typically show two uv-vis absorption peaks at 240-320 nm and 340-550 nm, corresponding to a $\pi \rightarrow \pi^*$ transition of the aromatic sp^2 domains and a $\pi \rightarrow n$ transition of functional groups or surface defects in which the excited state energy is trapped and a strong emission is observed[19,46]. However, it has been reported that the optical absorption characteristics of Cdots appear to be restricted within the UV region[47,48]. This limits their applications in solar cells which requires the utilization of materials that absorb in the visible region to harvest more solar energy. However, energy exchange or down conversion processes can be used to quantum cut the light emitted by Cdots to the visible range.

2.3.2 Photoluminescence (PL) properties

The most fascinating property of Cdots is their photoluminescence and it can play a significant role in numerous applications. The photoluminescence mechanism of Cdots is not yet understood in detail. However, several studies reported that the photoluminescence emissions of Cdots can be due to various factors including; the excitation wavelength, a quantum confinement effect and doping with heteroatoms[14,19]. These factors are discussed below:

2.3.2.1 The excitation wavelength

PL emissions of Cdots can be λ_{ex}-dependent or λ_{ex}-independent depending on the precursors or/and methods used in their synthesis. Different carbon sources and different methods produce Cdots with different optical properties. Bhunia *et al*. produced Cdot/polymer films with different luminescence colors using different carbon precursors (glucose, ascorbic acid and vitamin B_1 plus oleic acid). The Cdots had different fluorescence emissions as shown in **Figure 2.10**[22]. These Cdots demonstrated λ_{ex}-dependent fluorescence behaviors. There was a red-shift of the emission wavelengths (from UV to the near-infrared region) upon increasing the λ_{ex} from UV to the visible light. Other studies reported similar results[19,21].

Zhao *et al*. produced different Cdots with λ_{ex}-dependent and λ_{ex}-independent PL behaviors from citric acid (CA) and ethylenediamine (EDA) as carbon and nitrogen precursors,

respectively, via a hydrothermal treatment method[49]. Dong *et al.* also produced nitrogen and sulfur co-doped Cdots that showed λ_{ex}-independent PL from CA monohydrate and glycine precursors using a hydrothermal treatment method[46]. He observed an unchanging emission peak upon increasing the λ_{ex}. It has been reported that the λ_{ex}-dependent fluorescence behaviors of Cdots is related to their size distribution or heterogeneity while λ_{ex}-independent fluorescence behaviors are due to homogeneity of Cdots[50-52].

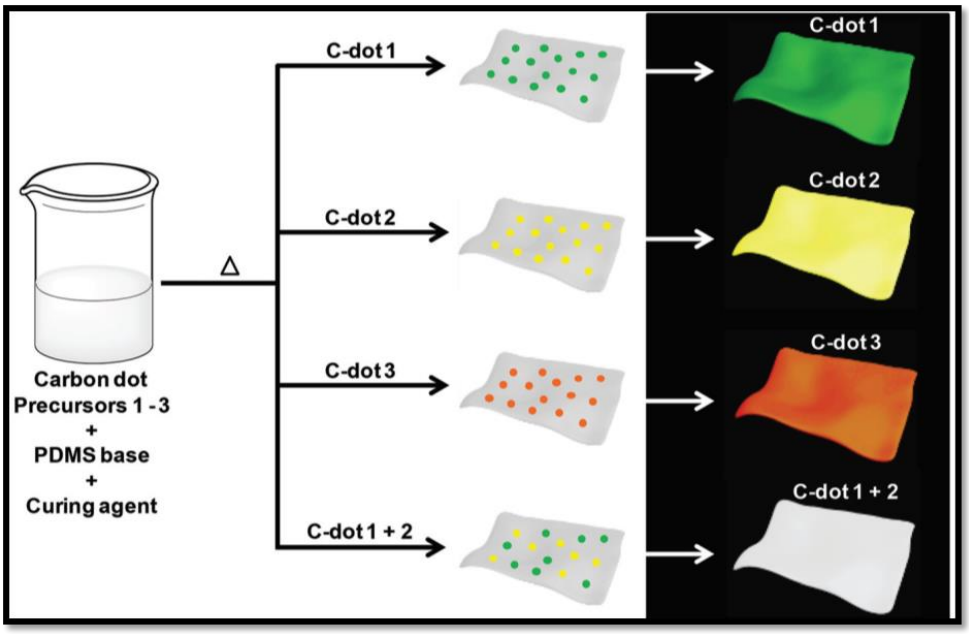

Figure 2.10: Cdot/polymer films with different luminescence colours from different precursors[22].

2.3.2.2 Doping with heteroatoms

Doping with heteroatom is an attractive process that allows the intrinsic properties of Cdots to be tunable and exploited for their desired potential applications. Previous studies have shown that doping Cdots with heteroatoms enhances the optical properties and increases the quantum yield (16% to 83%)[11,20,53,54]. Zhao *et al.* produced nitrogen-doped Cdots with excellent photoluminescence properties from citric acid and ethylenediamine as carbon and nitrogen precursors, respectively[49]. Other elements that were previously used to dope Cdots are phosphorus and boron[55-58]. In addition, nitrogen doping of Cdots introduces an extra electron, thus increasing the electron transfer process and reducing the chance of recombination. The generation of the extra electron enables Cdots to be used as acceptors or charge injection layers and thus makes doped Cdots beneficial to potential applications such as solar cells, photocatalysis and other applications.

2.3.2.3 Quantum confinement effect (QCE)

Quantum confinement is considered one of the factors affecting the PL properties of Cdots[51]. It occurs when the PL properties of Cdots are largely dependent on their particle sizes. In fact, quantum confinement effects occur when the nanoparticle sizes fall in the quantum-confined regime (smaller than the Bohr radius of its constituent compound), which is in between the highest occupied molecular orbital (HOMO) and the lowest unoccupied molecular orbital (LUMO)[59,60]. This effect results in the restriction of energies at which the electrons and holes can exist in the particles. The PL spectrum of different-sized Cdots typically vary in breadth with discrete energy levels and different optical and electronic properties[59,60]. Therefore, QCE determines the PL properties as the absorption energy and the emission wavelengths of the resulting photons are related to each other. In addition, the PL properties of Cdots can be tuned, depending on their particle sizes[60]. The smaller the nanoparticles, the larger the energy band gap, resulting in a greater energy for the optical emission[51,61]. This can also be due to the fact that the surface-to-volume-ratio of nanoparticles is very high or due to the repulsion of the electronic wave function due to the size/interatomic spacing reduction. **Figure 2.11** depicts a diagram of nanoparticles having a higher energy band gap than the bulk materials.

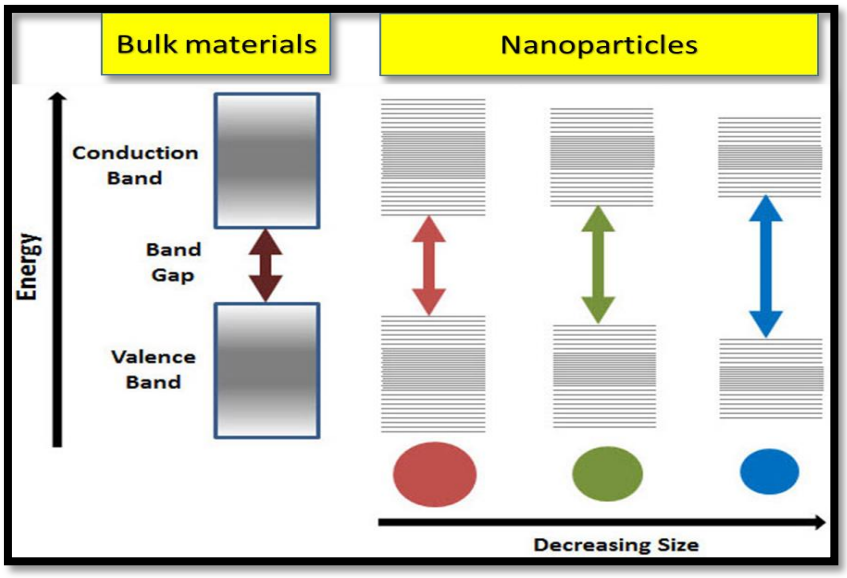

Figure 2.11: Energy band gap of nanoparticle increases with decreasing nanoparticle sizes[61].

2.4 Applications of carbon dots

Cdots have been used in a wide variety of applications such as: bioimaging, biosensing, fuel cells, supercapacitors, catalysis, solar cells, lithium ion batteries, drug delivery and light emitting diodes, owing to their outstanding chemical, physical and optical properties[5,8,16,17]. Their properties such as low toxicity, good aqueous solubility and small size make them good candidates for biological applications[16]. In addition, their good biocompatibility property is due to their smaller particle size (less than 10 nm) and it is easier for them to enter a cell in vivo, which makes them good candidates in biological applications. These properties also make them strong competitors to semiconductor quantum dots which consist of toxic and expensive metals. The following section provide the theoretical background on the operation of the organic solar cells. This includes the mechanisms of photoabsorption, excitation generation, the diffusion of the quasi particle to the donor-acceptor interface, the dissociation of the exciton and subsequent charge transport or collection at the electrodes.

2.4.1 Working principle of organic solar cells

It is crucial to understand how organic solar cells work in order to develop the most efficient device. There are four fundamental steps that are involved in the mechanism of an organic solar cell (**Figure 2.12**)[62]. The first step is the absorption of incident light which is followed by the generation of the bound electron-hole pair (exciton), held together by coulombic attraction. In order for a photon to be absorbed by the active layer, its energy should be equal or greater than the energy band gap of the donor materials which is usually a small molecule or polymer for the case of organic solar cells[62,63]. The second step is the diffusion of the exciton to the donor-acceptor interface. For successful exciton diffusion, the exciton diffusion length must be within the range of the donor-acceptor interface separation length. This forms the basis of the BHJ or the interconnected network. The third step is the dissociation of the exciton whereby the electron-hole pair splits into free charges. This is very important because the electric current generated by the photovoltaic solar cell corresponds to the number of charges collected at the electrodes[64,65]. The fourth step is the charge collection by the transparent conductive oxide (TCO), with a relatively high work function, and a metal with a relatively low work function as the electrodes[63]. The electrons are collected by the cathode and the holes by the anode.

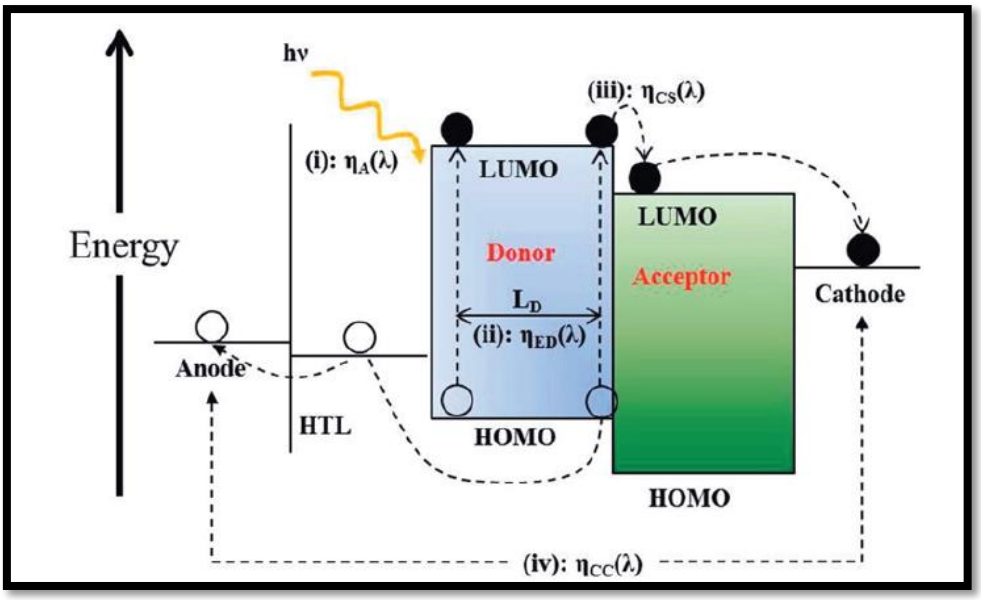

Figure 2.12: Mechanism of operation of an organic solar cell[62].

2.4.2 Organic solar cell architectures

Organic solar cells are devices that utilize semiconducting polymers to convert solar energy into electrical energy via the photovoltaic effect[66]. They normally use a conjugated polymer and a fullerene derivative as the active layer[64,66]. The conjugated polymer acts as the electron donating material while the fullerene derivative acts as the electron accepting material. Organic solar cells consist of different distinct layers depending on the type of the device architecture. There are different types of organic solar cell architectures; the single layer, bilayer and bulk heterojunction (BHJ) (**Figure 2.13**)[63,64,67,68]. These architectures vary in their active layer that is responsible for the absorption of light. The single layered architecture comprises of one active material and both the bilayer and BHJ architectures comprise of two active materials (electron donor and acceptor materials).

The first organic solar cell was based on a single organic layer sandwiched between two metal electrodes[64]. Compared to the bilayer and BHJ architectures, single layered organic solar cells possess a lower efficiency due to a high series resistance that leads to a low FF[64]. In addition, its photoactive layer is not thick enough to absorb the majority of the incident light. The photoactive layer must be at least 100 nm thick for it to absorb most of the incident light[69].

In a bilayer architectured organic solar cell, the electron donating and accepting materials are sequentially stacked on top of each other[63,64,66]. In an organic solar cell, charge separation is only efficient at the donor-acceptor interface. Therefore, a photoexcitation process that takes

place anywhere far from the donor-acceptor interface results in recombination of charge carriers before diffusing to the junctions[70]. The excitons that are generated near the donor-acceptor interface tend to live long enough to dissociate into free charges (electrons and holes) and are transported to their respective electrodes[70]. This limitation in a bilayer architecture brought forward the introduction of the BHJ architecture.

In a BHJ device, the donor and acceptor materials are nanoscopically mixed together. The donor-acceptor interface is randomly distributed throughout the active layer as compared to the bilayer architecture. What makes the bulk heterojunction architecture special is that, the generated electron-hole pair can be dissociated anywhere in the active layer since the donor-acceptor interface is all over the bulk[71]. Therefore, the BHJ is reported to be the most efficient device architecture for use in organic solar cells[71,72].

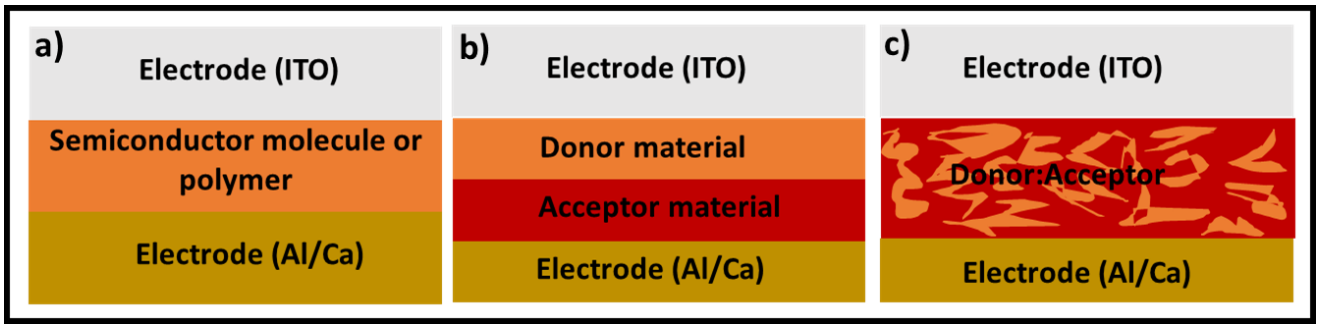

Figure 2.13: Device architectures of Organic solar cell. a) Single layer, b) bilayer and c) bulk-heterojunction (Modified from ref.66).

2.4.3 Cdots in organic solar cell applications

The excellent optical and electronic properties of Cdots make them good candidates for organic solar cell applications. Zhang *et al.* reported the use of Cdots as an electron transport layer (ETL) in an organic solar cell[73]. It was discovered that the devices with Cdots as the ETLs had a higher charge transport and collection efficiency[73]. In addition, lifetimes of the devices with Cdots as the electron transport layers were found to be improved significantly due to the better air-stability of Cdots materials compared to other materials used in ETLs[73]. Cdots as the ETLs have advantages over other materials used in ETLs, such as LiF and Ga, because it can efficiently prevent the formation of an unstable cathode contact for the diffusion of Al ions at the interface. LiF and Ga have been used also in organic photovoltaic solar cells, but their thickness and evaporation rate were difficult to control, and this resulted in high cost in the

fabrication of large area devices. These materials were also found to be very sensitive to moisture and oxygen, resulting in poor performing devices[73].

2.5 Conclusions

In conclusion, Cdots can be synthesised using different methods from different precursors. Their PL properties play a significant role in solar cells applications. Cdots possess excellent optical properties which make them potential candidates in organic solar cells. Besides their excellent optical properties, they were found to be strong competitors to semiconductor QDs which consist of toxic and expensive metals. Therefore, Cdots blended with conducting polymers in organic solar cell can be a solution of energy crisis in the world since they are economically viable and have the ability to absorb light.

References

1) Baptista, F. R.; Belhout, S. A.; Giordani, S.; Quinn, S. J. Recent Developments in Carbon Nanomaterial Sensors. *Chem. Soc. Rev.* **2015**, *44* (13), 4433–4453.
2) Plaksin, G. V.; Baklanova, O. N.; Lavrenov, A. V.; Likholobov, V. A. Carbon Materials from the Sibunit Family and Methods for Controlling Their Properties. *Solid Fuel Chem.* **2014**, *48* (6), 349–355.
3) Wen, J.; Xu, Y.; Li, H.; Lu, A.; Sun, S. Recent Applications of Carbon Nanomaterials in Fluorescence Biosensing and Bioimaging. *Chem. Commun.* **2015**, *51* (57), 11346–11358.
4) Zhang, Y.; Yin, Q.-Z. Carbon and Other Light Element Contents in the Earth's Core Based on First-Principles Molecular Dynamics. *Proc. Natl. Acad. Sci.* **2012**, *109* (48), 19579–19583.
5) Zuo, P.; Lu, X.; Sun, Z.; Guo, Y.; He, H. A Review on Syntheses, Properties, Characterization and Bioanalytical Applications of Fluorescent Carbon Dots. *Microchim. Acta* **2016**, *183* (2), 519–542.
6) Nasir, S.; Hussein, M. Z.; Zainal, Z.; Yusof, N. A. Carbon-Based Nanomaterials/Allotropes: A Glimpse of Their Synthesis, Properties and Some Applications. *Materials (Basel).* **2018**, *11* (2), 1–24.
7) Bernardi, M.; Lohrman, J.; Kumar, P. V; Ferralis, N.; Grossman, J. C. Nanocarbon – Based Photovoltaics. *ACS Nano* **2012**, *6* (10), 8896–8903.
8) Namdari, P.; Negahdari, B.; Eatemadi, A. Synthesis, Properties and Biomedical Applications of Carbon-Based Quantum Dots: An Updated Review. *Biomed. Pharmacother.* **2017**, *87* (88), 209–222.
9) Zhu, H.; Wei, J.; Wang, K.; Wu, D. Applications of Carbon Materials in Photovoltaic Solar Cells. *Sol. Energy Mater. Sol. Cells* **2009**, *93* (9), 1461–1470.
10) Sun, Y. P.; Zhou, B.; Lin, Y.; Wang, W.; Fernando, K. A. S.; Pathak, P.; Meziani, M. J.; Harruff, B. A.; Wang, X.; Wang, H.; et al. Quantum-Sized Carbon Dots for Bright and Colorful Photoluminescence. *J. Am. Chem. Soc.* **2006**, *128* (24), 7756–7757.
11) Gong, X.; Lu, W.; Paau, M. C.; Hu, Q.; Wu, X.; Shuang, S.; Dong, C.; Choi, M. M. F. Facile Synthesis of Nitrogen-Doped Carbon Dots for Fe3+sensing and Cellular Imaging. *Anal. Chim. Acta* **2015**, *861*, 74–84.

12) Zhu, S.; Song, Y.; Zhao, X.; Shao, J.; Zhang, J.; Yang, B. The Photoluminescence Mechanism in Carbon Dots (Graphene Quantum Dots , Carbon Nanodots , and Polymer Dots): Current State and Future Perspective. **2015**, *8* (2), 355–381.
13) Lim, S. Y.; Shen, W.; Gao, Z. Carbon Quantum Dots and Their Applications. *Chem. Soc. Rev.* **2015**, *44* (1), 362–381.
14) Paulo, S.; Palomares, E.; Martinez-ferrero, E. Graphene and Carbon Quantum Dot-Based Materials in Photovoltaic Devices : From Synthesis to Applications. *Nanomaterials* **2016**, *6* (Figure 1157), 1–20.
15) Xu, X.; Ray, R.; Gu, Y.; Ploehn, H. J.; Gearheart, L.; Raker, K.; Scrivens, W. A. Electrophoretic Analysis and Purification of Fluorescent Single-Walled Carbon Nanotube Fragments. *J. Am. Chem. Soc.* **2004**, *126* (40), 12736–12737.
16) Baker, S. N.; Baker, G. A. Luminescent Carbon Nanodots: Emergent Nanolights. *Angew. Chemie - Int. Ed.* **2010**, *49* (38), 6726–6744.
17) Zhang, J.; Yu, S. H. Carbon Dots: Large-Scale Synthesis, Sensing and Bioimaging. *Mater. Today* **2016**, *19* (7), 382–393.
18) Himaja, A. L.; Karthik, P. S.; Singh, S. P. Carbon Dots: The Newest Member of the Carbon Nanomaterials Family. *Chem. Rec.* **2015**, *15* (3), 595–615.
19) Roy, P.; Chen, P. C.; Periasamy, A. P.; Chen, Y. N.; Chang, H. T. Photoluminescent Carbon Nanodots: Synthesis, Physicochemical Properties and Analytical Applications. *Mater. Today* **2015**, *18* (8), 447–458.
20) Wang, Y.; Hu, A. Carbon Quantum Dots : Synthesis , Properties and Applications. *J. Mater. Chem. C Mater. Opt. Electron. devices* **2014**, *2*, 6921–6939.
21) Zhu, S.; Meng, Q.; Wang, L.; Zhang, J.; Song, Y.; Jin, H.; Zhang, K.; Sun, H.; Wang, H.; Yang, B. Highly Photoluminescent Carbon Dots for Multicolor Patterning, Sensors, and Bioimaging. *Angew. Chemie - Int. Ed.* **2013**, *52* (14), 3953–3957.
22) Bhunia, S. K.; Nandi, S.; Shikler, R.; Jelinek, R. Tuneable Light-Emitting Carbon-Dot/Polymer Flexible Films Prepared through One-Pot Synthesis. *Nanoscale* **2016**, *8* (6), 3400–3406.
23) Moon, B. J.; Oh, Y.; Shin, D. H.; Kim, S. J.; Lee, S. H.; Kim, T. W.; Park, M.; Bae, S. Facile and Purification-Free Synthesis of Nitrogenated Amphiphilic Graphitic Carbon Dots. *Chem. Mater.* **2016**, *28* (5), 1481–1488.
24) Tuerhong, M.; XU, Y.; YIN, X. B. Review on Carbon Dots and Their Applications. *Chinese J. Anal. Chem.* **2017**, *45* (1), 139–150.
25) Goryacheva, I. Y.; Sapelkin, A. V.; Sukhorukov, G. B. Carbon Nanodots: Mechanisms

of Photoluminescence and Principles of Application. *TrAC - Trends Anal. Chem.* **2017**, *90*, 27–37.

26) Dong, Y.; Wang, R.; Li, G.; Chen, C.; Chi, Y.; Chen, G. Polyamine-Functionalized Carbon Quantum Dots as Fluorescent Probes for Selective and Sensitive Detection of Copper Ions. *Anal. Chem.* **2012**, *84* (14), 6220–6224.

27) Frasco, M. F.; Chaniotakis, N. Semiconductor Quantum Dots in Chemical Sensors and Biosensors. **2009**, No. Figure 1, 7266–7286.

28) Yue, Z.; Lisdat, F.; Parak, W. J.; Hickey, S. G.; Tu, L.; Sabir, N.; Dorfs, D.; Bigall, N. C. Quantum-Dot-Based Photoelectrochemical Sensors for Chemical and Biological Detection. *ACS Appl. Mater. Interfaces* **2013**, *5* (8), 2800–2814.

29) Gao, X.; Yang, L.; Petros, J. A.; Marshall, F. F.; Simons, J. W.; Nie, S. In Vivo Molecular and Cellular Imaging with Quantum Dots. *Curr. Opin. Biotechnol.* **2005**, *16* (1 SPEC. ISS.), 63–72.

30) Shanti Krishna, A.; Radhakumary, C.; Sreenivasan, K. Detection and Imaging of Fatty Plaques in Blood Vessels Using Functionalized Carbon Dots. *Anal. Methods* **2015**, *7* (22), 9482–9488.

31) Jiang, Z. C.; Lin, T. N.; Lin, H. T.; Talite, M. J.; Tzeng, T. T.; Hsu, C. L.; Chiu, K. P.; Lin, C. A. J.; Shen, J. L.; Yuan, C. T. A Facile and Low-Cost Method to Enhance the Internal Quantum Yield and External Light-Extraction Efficiency for Flexible Light-Emitting Carbon-Dot Films. *Sci. Rep.* **2016**, *6* (August 2015), 1–6.

32) Zhou, J.; Sheng, Z.; Han, H.; Zou, M.; Li, C. Facile Synthesis of Fluorescent Carbon Dots Using Watermelon Peel as a Carbon Source. *Mater. Lett.* **2012**, *66* (1), 222–224.

33) Sahu, S.; Behera, B.; Maiti, T. K.; Mohapatra, S. Simple One-Step Synthesis of Highly Luminescent Carbon Dots from Orange Juice: Application as Excellent Bio-Imaging Agents. *Chem. Commun.* **2012**, *48* (70), 8835–8837.

34) Kukreja, D.; Mathew, J.; Lakshmipathy, R.; Sarada, N. C. Synthesis of Fluorescent Carbon Dots from Mango Peels. *Int. J. ChemTech Res.* **2015**, *8* (5), 61–64.

35) Prasannan, A.; Imae, T. One-Pot Synthesis of Fluorescent Carbon Dots from Orange Waste Peels. *Ind. Eng. Chem. Res.* **2013**, *52* (44), 15673–15678.

36) Zheng, J. X.; Liu, X. H.; Yang, Y. Z.; Liu, X. G.; Xu, B. S. Rapid and Green Synthesis of Fluorescent Carbon Dots from Starch for White Light-Emitting Diodes. *Xinxing Tan Cailiao/New Carbon Mater.* **2018**, *33* (3), 276–288.

37) Bandi, R.; Gangapuram, B. R.; Dadigala, R.; Eslavath, R.; Singh, S. S.; Guttena, V. Facile and Green Synthesis of Fluorescent Carbon Dots from Onion Waste and Their

Potential Applications as Sensor and Multicolour Imaging Agents. *RSC Adv.* **2016**, *6* (34), 28633–28639.

38) Wang, Q.; Liu, X.; Zhang, L.; Lv, Y. Microwave-Assisted Synthesis of Carbon Nanodots through an Eggshell Membrane and Their Fluorescent Application. *Analyst* **2012**, *137* (22), 5392–5397.

39) Atchudan, R.; Edison, T. N. J. I.; Lee, Y. R. Nitrogen-Doped Carbon Dots Originating from Unripe Peach for Fluorescent Bioimaging and Electrocatalytic Oxygen Reduction Reaction. *J. Colloid Interface Sci.* **2016**, *482*, 8–18.

40) Shen, J.; Shang, S.; Chen, X.; Wang, D.; Cai, Y. Facile Synthesis of Fluorescence Carbon Dots from Sweet Potato for Fe3 +sensing and Cell Imaging. *Mater. Sci. Eng. C* **2017**, *76*, 856–864.

41) De, B.; Karak, N. A Green and Facile Approach for the Synthesis of Water Soluble Fluorescent Carbon Dots from Banana Juice. *RSC Adv.* **2013**, *3* (22), 8286–8290.

42) Reyes, D.; Camacho, M.; Camacho, M.; Mayorga, M.; Weathers, D.; Salamo, G.; Wang, Z.; Neogi, A. Laser Ablated Carbon Nanodots for Light Emission. *Nanoscale Res. Lett.* **2016**, *11*, 1–11.

43) Li, X.; Zhao, Z.; Pan, C. Ionic Liquid-Assisted Electrochemical Exfoliation of Carbon Dots of Different Size for Fluorescent Imaging of Bacteria by Tuning the Water Fraction in Electrolyte. *Microchim. Acta* **2016**, *183* (9), 2525–2532.

44) Liu, M.; Xu, Y.; Niu, F.; Gooding, J. J.; Liu, J. Carbon Quantum Dots Directly Generated from Electrochemical Oxidation of Graphite Electrodes in Alkaline Alcohols and the Applications for Specific Ferric Ion Detection and Cell Imaging. *Analyst* **2016**, *141* (9), 2657–2664.

45) Yang, H.; He, L.; Long, Y.; Li, H.; Pan, S.; Liu, H.; Hu, X. Fluorescent Carbon Dots Synthesized by Microwave-Assisted Pyrolysis for Chromium(VI) and Ascorbic Acid Sensing and Logic Gate Operation. *Spectrochim. Acta - Part A Mol. Biomol. Spectrosc.* **2018**, *205*, 12–20.

46) Dong, Y.; Pang, H.; Yang, H. Bin; Guo, C.; Shao, J.; Chi, Y.; Li, C. M.; Yu, T. Carbon-Based Dots Co-Doped with Nitrogen and Sulfur for High Quantum Yield and Excitation-Independent Emission. *Angew. Chemie - Int. Ed.* **2013**, *52* (30), 7800–7804.

47) Hu, S.; Tian, R.; Wu, L.; Zhao, Q.; Yang, J.; Liu, J.; Cao, S. Chemical Regulation of Carbon Quantum Dots from Synthesis to Photocatalytic Activity. *Chem. - An Asian J.* **2013**, *8* (5), 1035–1041.

48) Smagulova, S.; Egorova, M.; Tomskaya, A.; Kapitonov, A. Synthesis of Carbon Dots with Tunable Luminescence. *J. Mater. Sci. Eng.* **2017**, *06* (05), 1–6.

49) Zhao, Y.; Liu, X.; Yang, Y.; Kang, L.; Yang, Z.; Chen, L. Carbon Dots : From Intense Absorption in Visible Range to Excitation-Independent and Excitation- Dependent Photoluminescence Carbon Dots : From Intense Absorption in Visible Range to Excitation-Independent and Excitation-Dependent Photoluminescence. **2015**, *23*, 922–929.

50) Sarkar, S.; Banerjee, D.; Ghorai, U. K.; Das, N. S.; Chattopadhyay, K. K. Size Dependent Photoluminescence Property of Hydrothermally Synthesized Crystalline Carbon Quantum Dots. *J. Lumin.* **2016**, *178*, 314–323.

51) Bhattacharya, A.; Chatterjee, S.; Prajapati, R.; Mukherjee, T. K. Size-Dependent Penetration of Carbon Dots inside the Ferritin Nanocages: Evidence for the Quantum Confinement Effect in Carbon Dots. *Phys. Chem. Chem.Phys.* **2015**, *17*, 12833–12840.

52) Bao, L.; Liu, C.; Zhang, Z.; Pang, D. Photoluminescence-Tunable Carbon Nanodots : Surface-State Energy-Gap Tuning. *Adv. Mater.* **2015**, *27*, 1663–1667.

53) Wang, J.; Zhang, P.; Huang, C.; Liu, G.; Leung, K. C.; Wa, J. High Performance Photoluminescent Carbon Dots for In Vitro and In Vivo Bioimaging : E Ff Ect of Nitrogen Doping Ratios. *Am. Chem. Soc.* **2015**, *31*, 8063–8073.

54) Xu, Q.; Kuang, T.; Liu, Y.; Cai, L.; Peng, X.; Sreeprasad, T. S.; Zhao, P.; Yu, Z.; Li, N. Heteroatom-Doped Carbon Dots : Synthesis ,. *J. Mater. Chem. B* **2016**, *4*, 7204–7219.

55) Gu, D.; Zhang, P.; Zhang, L.; Liu, H.; Pu, Z.; Shang, S. Nitrogen and Phosphorus Co-Doped Carbon Dots Derived from Lily Bulbs for Copper Ion Sensing and Cell Imaging. *Opt. Mater. (Amst).* **2018**, *83*, 272–278.

56) Bourlinos, A. B.; Trivizas, G.; Karakassides, M. A.; Baikousi, M.; Kouloumpis, A.; Gournis, D.; Bakandritsos, A.; Hola, K.; Kozak, O.; Zboril, R.; et al. Green and Simple Route toward Boron Doped Carbon Dots with Significantly Enhanced Non-Linear Optical Properties. *Carbon N. Y.* **2015**, *83*, 173–179.

57) Chen, Z.; Wang, S.; Yang, X. Phosphorus-Doped Carbon Dots for Sensing Both Au (III) and L-Methionine. *J. Photochem. Photobiol. A Chem.* **2018**, *365*, 178–184.

58) Zhou, J.; Shan, X.; Ma, J.; Gu, Y.; Qian, Z.; Chen, J.; Feng, H. Facile Synthesis of P-Doped Carbon Quantum Dots with Highly Efficient Photoluminescence. *RSC Adv.* **2014**, *4* (11), 5465–5468.

59) Ashrafi, A. Quantum Confinement : An Ultimate Physics of Nanostructures. *Encycl. semicondutor Nanotechnol.* **2011**, *5*, 1–67.

60) Holmes, J. D.; Ziegler, K. J.; Doty, R. C.; Pell, L. E.; Johnston, K. P.; Korgel, B. A. Highly Luminescent Silicon Nanocrystals with Discrete Optical Transitions. *J. Am. Chem. Soc.* **2001**, *123* (16), 3743–3748.

61) http://www.sigmaaldrich.com/materialsscience/nanomaterials/quantum-dots.html Sigma Aldrich Quantum Dots **(accessed 27 May, 2018**).

62) Su, Y.; Lan, S.; Wei, K. Organic Photovoltaics In the Last Ten Years , the Highest Efficiency Obtained from Organic. *Mater. Today* **2012**, *15* (12), 554–562.

63) Ranabhat, K.; Sofronova, E.; Patrikeev, L.; Revina, A. A.; Andrianov, K.; Lapshinsky, V. AN INTRODUCTION TO SOLAR CELL. *J. Appl. Eng. Sci.* **2016**, *14* (4), 481–491.

64) Hoppe, H.; Sariciftci, N. S. Organic Solar Cells : An Overview. *J. Mater. Res.* **2004**, *19* (7), 1924–1945.

65) Bredas J; J, N.; Cornil, L.; Coropceanu, V. Molecular Understanding of Organic Solar Cells : Introduction. *Acc. Chem. Res.* **2009**, *42* (11), 1691–1699.

66) Yeh, N.; Yeh, P. Organic Solar Cells : Their Developments and Potentials. *Renew. Sustain. Energy Rev.* **2013**, *21*, 421–431.

67) Mazzio, K. A.; Luscombe, C. K. The Future of Organic Photovoltaics. *R. Soc. Chem.* **2014**, (3), 1–13.

68) Bagher, A. M. Introduction to Organic Solar Cells. *Sustain. energy* **2014**, *2* (3), 85–90.

69) Spanggaard, H.; Krebs, F. C. A Brief History of the Development of Organic and Polymeric Photovoltaics. *Sol. Energy Mater. Sol. Cells* **2004**, *83*, 125–146.

70) Yu, G.; Gao, J.; Hummelen, J.; Wudl, F.; Heeger, A. Polymer Photovoltaic Cells : Enhanced Efficiencies via a Network of Internal Donor-Acceptor Heterojunctions. *Science* **1995**, *270*, 1789–1792.

71) Kaushik, M.; Kaushik, B. Organic Solar Cells : Design , Synthesis and Characterization Organic Solar Cells : Design , Synthesis and Characterization. *Int. J. Eng. Sci.* **2013**, *2* (7), 310–319.

72) Gunes, S.; Neugebauer, H.; Sariciftci, N. S. Conjugated Polymer-Based Organic Solar Cells. *Am. Chem. Soc.* **2007**, *107* (4), 1324–1338.

73) Zhang, H.; Zhang, Q.; Li, M.; Kan, B.; Ni, W.; Wang, Y.; Yang, X.; Du, C.; Wan, X.; Chen, Y. Investigation of the Enhanced Performance and Lifetime of Organic Solar Cells Using Solution-Processed Carbon Dots as the Electron Transport Layers. *J. Mater. Chem. C* **2015**, *3* (48), 12403–12409.

CHAPTER 3: CHARACTERIZATION TECHNIQUES

3.1 Introduction

In this section, different characterization techniques used to analyse the as-synthesized carbon dots (Cdots) prepared from different precursors and various reaction conditions are discussed. A careful sample preparation is typically required in almost all characterization techniques prior to analysis. The different characterization techniques below were used to investigate the optical, physical and chemical properties such as the morphology, photoluminescence, absorption, elemental composition, thermal stability, surface functional groups and the crystallinity of the obtained products.

3.1.1. Transmission electron microscopy (TEM)

TEM was used to determine the particle size and the morphology of the as-synthesised Cdots. The Cdots were dispersed in water or ethanol and then ultra-sonicated for about 20 minutes. A drop was then added on a carbon coated copper grid which was then allowed to dry in room temperature for 24 hours before imaging. The TEM images were taken on FEI Tecnai T12 electron microscopy operating at acceleration voltage of 120 kv **(Figure 3.1)**.

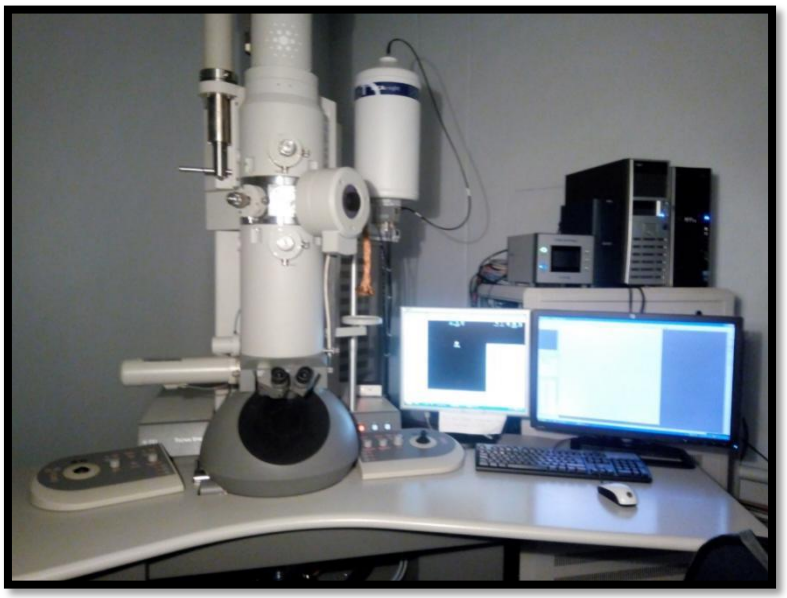

Figure 3.1: FEI Tecnai T12 transmission electron microscope.

3.1.2 Powder X-ray diffraction (PXRD)

The PXRD is a powerful technique that was used for phase identification and determination of the crystallinity of the as-synthesized materials based on their diffraction patterns. In addition, the PXRD can also be used to check the purity of the obtained products. A proper sample preparation is required in order to get valid and accurate results. The samples were ground into powder and packed into a zero-background sample holder. A glass slide was used in order to get a flat and uniform surface. The PXRD patterns were obtained from Bruker D2 PHASER power X-ray diffractometer fitted with a LYNXEYE detector which utilizes co-kα irradiation with a 30 KV x-ray and 10 mA current in 0.0260 º steps for 10 minutes **(Figure 3.2)**. The PXRD patterns were collected at 2Theta = 10 – 90 º range.

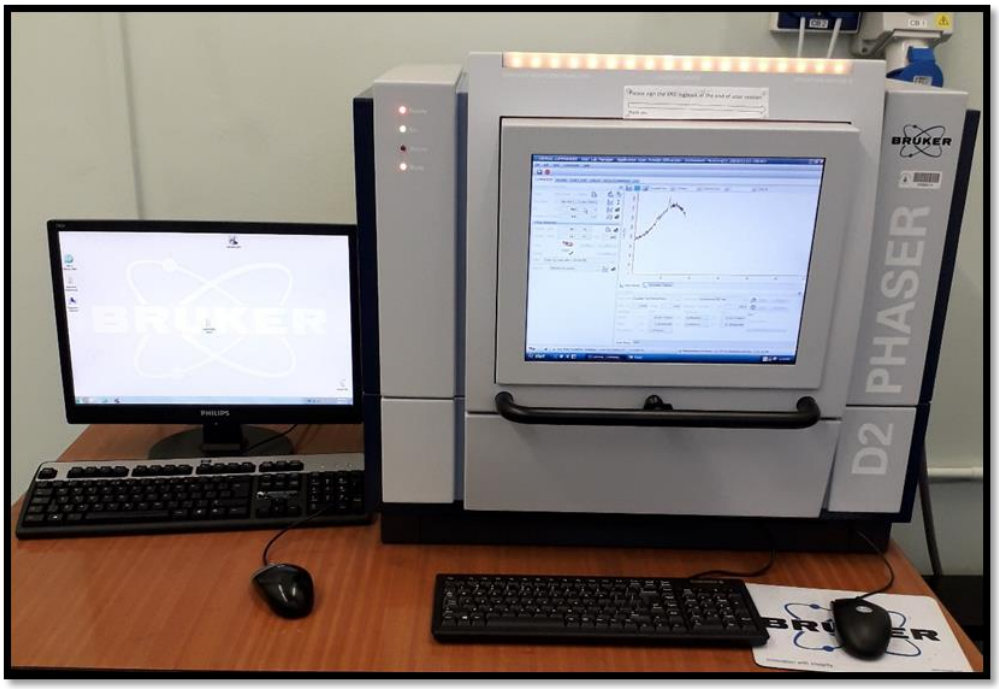

Figure 3.2: Bruker D2 PHASER powder X-ray diffractometer.

3.1.3 Ultra-Violet visible absorption spectroscopy (UV-vis)

Uv-vis absorption measurements NCdots in solution were taken from varian Cary Eclipse (Cary 50) UV-vis absorption spectrophotometer **(Figure 3.3)**. UV-vis absorption spectra were measured in the wavelength range of 200-700 nm.

Figure 3.3: Cary Eclipse (Cary 50) UV-vis absorption spectrophotometer.

3.1.4 Photoluminescence spectroscopy (PL)

PL spectroscopy was used to investigate fluorescence properties of the as-synthesized materials. The emission spectra were measured in the wavelength range of 300-700 nm with a 5 nm slit width in solution. The PL data was obtained from varian Cary Eclipse EL04103870 fluorescence spectrophotometer **(Figure 3.4)**.

Figure 3.4: Varian Cary Eclipse EL04103870 fluorescence spectrophotometer.

3.1.5 Thermogravimetric analysis (TGA)

TGA was used to study the thermal stability of carbon dots (Cdots). The measurements were made on a TA Q50 instrument. Approximately 10.0 mg of Cdots was weighed and heated to 900 °C at the rate of 20 °C/min. The measurements were performed under nitrogen gas. Below is the photograph of the instrument.

Figure 3.5: Perkin Elmer STA 4000 simultaneous thermal analyser/thermogravimetric analysis.

3.1.6 Laser Raman spectroscopy

The laser Raman spectroscopy was used to determine the degree of graphitization of the as-synthesized samples. A powdered sample was placed on a glass slide and the spectra were collected in the dark field mode. The Raman spectra were obtained from a Bruker Senterra Laser Raman spectrophotometer equipped with a laser wavelength of 514.5 nm **(Figure 3.6).** The laser Raman spectrophotometer utilizes the opus software.

Figure 3.6: Bruker Senterra Raman spectrophotometer.

3.1.7 Fourier transmission infrared (FTIR)

The functional groups of the Cdots were determined using a Bruker Tensor 27 FTIR analyser (**Figure 3.7**). The measurements were performed on solid samples using a transmission mode in the range of 400-4000 cm^{-1} with an accumulation of 64 scans and 4.0 cm^{-1} resolution.

Figure 3.7: Bruker Tensor 27 FTIR analyser.

3.1.8. X-ray photoelectron spectroscopy (XPS)

XPS was used to determine the surface composition of the as-synthesized Cdots. In this technique, the surface of the materials is irradiated with x-rays in order to extract the photo-electrons. The spectra were obtained using quantum 2000 scanning ESCAlab 250Xi microprobe system operated at 300 W with monochromatic Al kα (1486.7 eV). The sample preparation and analysis were done at CSIR. The deconvolution processing of the XPS spectra of the obtained Cdots were performed using CasaXPS software.

CHAPTER 4: SYNTHESIS OF NITROGEN-DOPED CARBON DOTS FROM DIFFERENT PRECURSORS

4.1. Introduction

Since their discovery in 2004, carbon dots (Cdots) have received a tremendous amount of attention due to their optical, physical and chemical properties[1]. Cdots can be prepared from an unlimited number of carbon precursors, including: glucose[2,3], ascorbic acid[4], polyethylene glycol (PEG)[5], chitosan[6-8], fumaronitrile (FN)[9], sucrose[10], citric acid (CA)[11-17] and many other precursors using the bottom-up approach as it involves easy operations as compared to a top-down approach. Among these carbon precursors, CA has been well-studied and when combined with ethylenediamine (EDA), it produces Cdots with high quantum yield (QY)[13,14,17]. The highest QY was obtained when Cdots were prepared from CA and EDA via the hydrothermal method as compared to other methods. Qu *et al.* produced nitrogen-doped (N-doped) Cdots with 94 % QY from CA and EDA as carbon and nitrogen precursors, respectively, via a hydrothermal treatment method[17]. However, the hydrothermal treatment method involved long reaction times, low production yields and expensive Teflon-lined stainless-steel apparatus that are used as reactors. In addition, the hydrothermal treatment method involves high temperatures and pressures. Therefore, the synthesis of Cdots with high QY using a more cost-effective method is essential. In comparison with a hydrothermal treatment method, a microwave-irradiation method is cost-effective and involves shorter reaction times and higher production yields[12,13].

For this study, N-doped carbon dots (NCdots) were prepared from different precursors such as; citric acid plus ethylenediamine (CAEDA) and FN using a microwave-irradiation method and the structures of the precursors are shown in **Figure 4.1**.

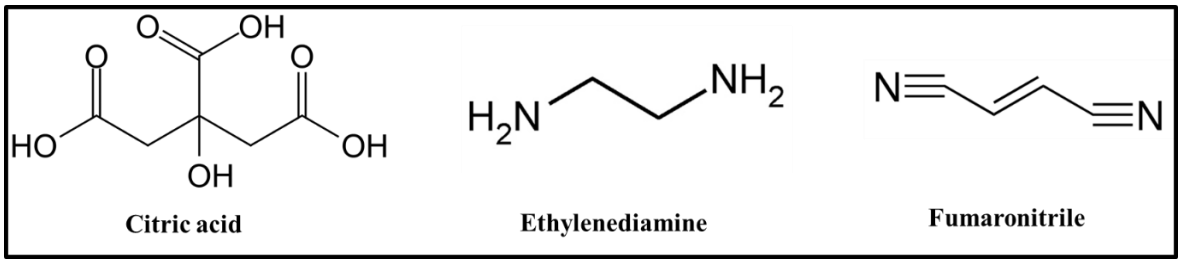

Figure 4.1: The structures of precursors used to prepare NCdots.

CA is a nontoxic small molecule that is readily available and normally used as a carbon precursor for the synthesis of Cdots. It contains three carboxylic acid groups that help in facilitating the dehydration and carbonization processes during the formation of Cdots[13]. As mentioned before, a combination of CA and EDA in the synthesis of Cdots results in Cdots with high QY. Previous studies showed that doping Cdots with nitrogen atom enhanced their fluorescence which is beneficial for optoelectronic applications[16]. EDA is a primary amine molecule that is commonly used as a surface passivation agent or/and nitrogen precursor[13]. When EDA is reacted with CA, it forms amide groups with carboxylic groups from CA and therefore enhances the fluorescence properties of the resultant Cdots. So *et al.* showed that adding EDA not only enhanced fluorescence of Cdots, but also shortened the carbonization time[12]. The formation mechanism of NCdots-CAEDA involves several steps: dehydration, condensation, polymerization and carbonization, as shown in **Scheme 4.1**[19]. The other type of Cdots were prepared from FN which was used as both carbon and nitrogen precursor. FN contains two nitrile groups that also help in facilitating the carbonization process. To the best of our knowledge, FN has never been used to prepare Cdots via microwave-irradiation method. The mechanism formation of NCdots-FN is speculated to follow the same steps as NCdots-CAEDA.

It has been suggested that different starting materials produce Cdots with different properties[20]. In this chapter, the properties of NCdots-CAEDA and NCdots-FN were investigated and compared using various characterization techniques.

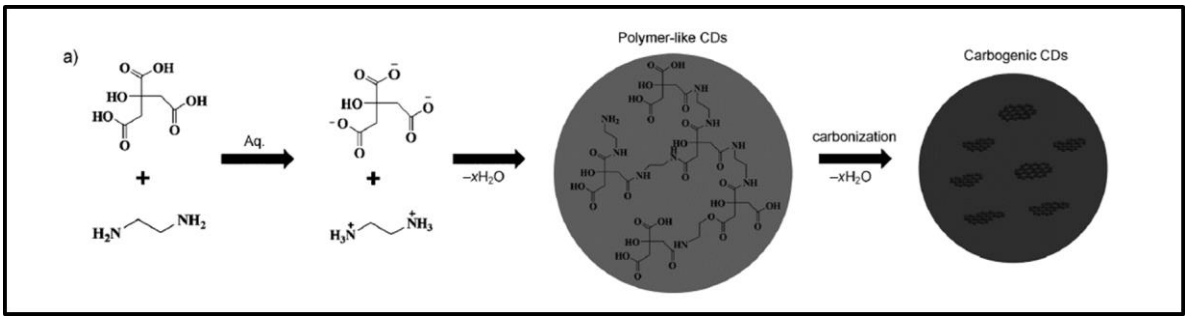

Scheme 4.1: The plausible mechanism for the formation of NCdots-CAEDA[19].

4.2 Synthesis procedures

4.2.1 Materials

Citric acid (CA, ACS reagent, ≥ 99.5 %), ethylenediamine (EDA, absolute, ≥ 99.5 %), fumaronitrile (FN, purum, ≥ 98.0 %), quinine sulfate (QS, Bioreagent, ≥ 98.0 %) and a dialysis membrane with a molecular weight cut-off of 14 000 Da, were purchased from sigma Aldrich. All chemicals were used as received, without further purification. Distilled water was used throughout the experimental methods.

4.2.2 Synthesis of NCdots from citric acid with ethylenediamine, and fumaronitrile

Both types of NCdots were prepared via a microwave-irradiation method using the same conditions. NCdots-CAEDA were prepared by adopting the synthetic method reported by Zhai *et al.*[13] and NCdots-FN by Moon *et al*[9]. Moon *et al*. prepared NCdots from fumaronitrile via the hotplate method.

In a standard procedure, 1.0 g citric acid and 1.0 g ethylenediamine were dissolved in 10.0 ml distilled water in a 100 ml beaker. The mixture was then transferred to a microwave tube and heated at 700 W for 10 min. After completion of the reaction, the solution changed from colorless to dark brown in color, indicating carbonization of the starting material. The microwave oven was allowed to cool to room temperature. The aqueous Cdots dispersion was purified by centrifugation at 15000 rpm for 15 min to remove large particles or unreacted starting materials. The collected supernatant was then filtered using a 0.22 µm filter membrane. The supernatant was further purified using a dialysis membrane with molecular weight cut-off of 14 000 Da for 72 h, changing the distilled water every 24 h. Upon completion of the dialysis, a rotary evaporator was then used to evaporate off the water from the Cdots solution. The obtained product was allowed to dry in a vacuum oven at 70 ºC. NCdots-FN were prepared the same way. The only difference is that, FN was used as both carbon and nitrogen precursor. The product yield of NCdots-CAEDA and NCdots-FN was found to be 52 % and 38 %, respectively. The properties of the obtained products were investigated and evaluated by TEM, PXRD, UV-vis absorption spectroscopy. PL spectroscopy, TGA, FTIR, XPS and CHNS analysis. **Scheme 4.2 and 4.3** depicts the synthesis of NCdots-CAEDA and NCdots-FN via the microwave-irradiation method, respectively. The synthesis and purification steps carried out to obtain pure NCdots-CAEDA and NCdots-FN from CA and EDA, and FN as starting materials are displayed in **Scheme 4.4**

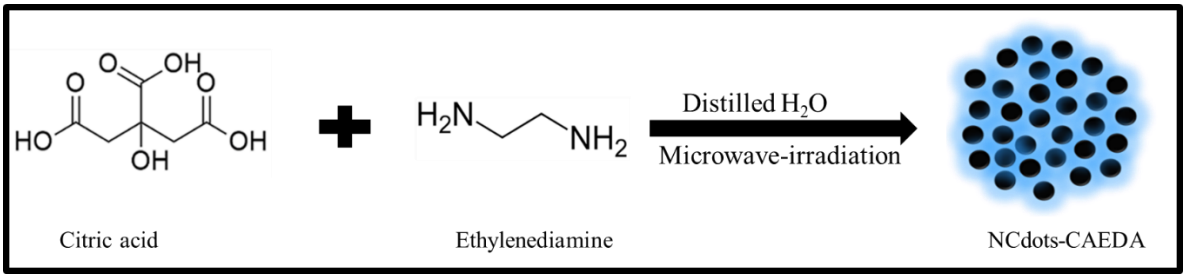

Scheme 4.2: Schematic illustration for the synthesis of NCdots-CAEDA from citric acid and ethylenediamine as carbon and nitrogen precursors, respectively, via a microwave-irradiation method**.**

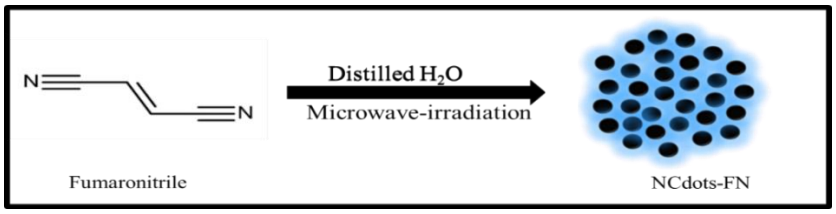

Scheme 4.3: Schematic illustration for the synthesis of NCdots-FN from fumaronitrile as both carbon and nitrogen precursor via a microwave-irradiation method.

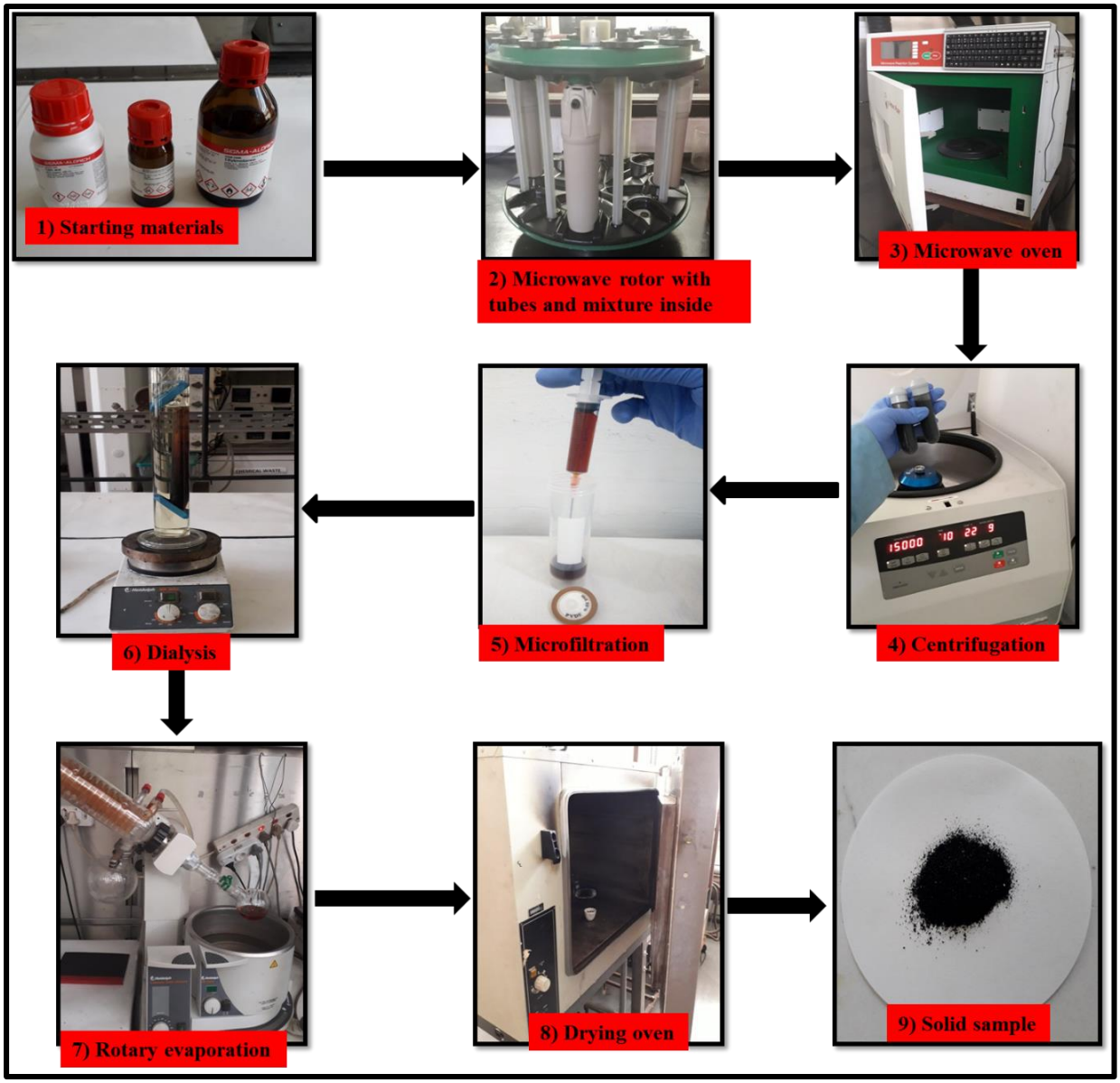

Scheme 4.4: Photographs of the synthesis and purification steps carried out to obtain pure NCdots from CA plus EDA and FN as starting materials.

4.3. Results and discussion

4.3.1. Transmission electron microscopy (TEM) analysis

From TEM analysis, the particle size and morphology of the as-synthesized NCdots were determined. The results revealed that both NCdots-CAEDA and NCdots-FN are quasi-spherical and monodispersed with sizes less than 10 nm. **Figure 4.2.a and 4.2.b** depicts TEM images of both NCdots-CAEDA and NCdots-FN with their corresponding particle size distribution histograms, respectively, which were obtained by measuring approximately 100 particles using imageJ software.

The particle size distributions of the as-synthesized NCdots-CAEDA and NCdots-FN were 1.5-5.5 nm and 1.0-8.0 nm with the average size of 3.28 ± 0.60 nm and 4.50 ± 1.42 nm, respectively. The NCdots-FN were determined to be larger than the NCdots-CAEDA. These results are similar to the results obtained by Moon *at al.* for NCdots-FN[9] and Wang *et al.* for NCdots-CAEDA[21]. Moreover, a histogram of NCdots-FN demonstrated a broader size distribution as compared to NCdots-CAEDA. This can be due to the inhomogeneous sizes of Cdots present in NCdots-FN. The insets demonstrate HRTEM images of both NCdots-CAEDA and NCdots-FN. The lattice spacing of NCdots-CAEDA was measured to be 0.28 nm which correspond to the (020) diffraction plane of graphite carbon[3]. The lattice spacing for the NCdots-FN was determined to be 0.24 nm which is similar to the (112) lattice fringe of graphene[9].

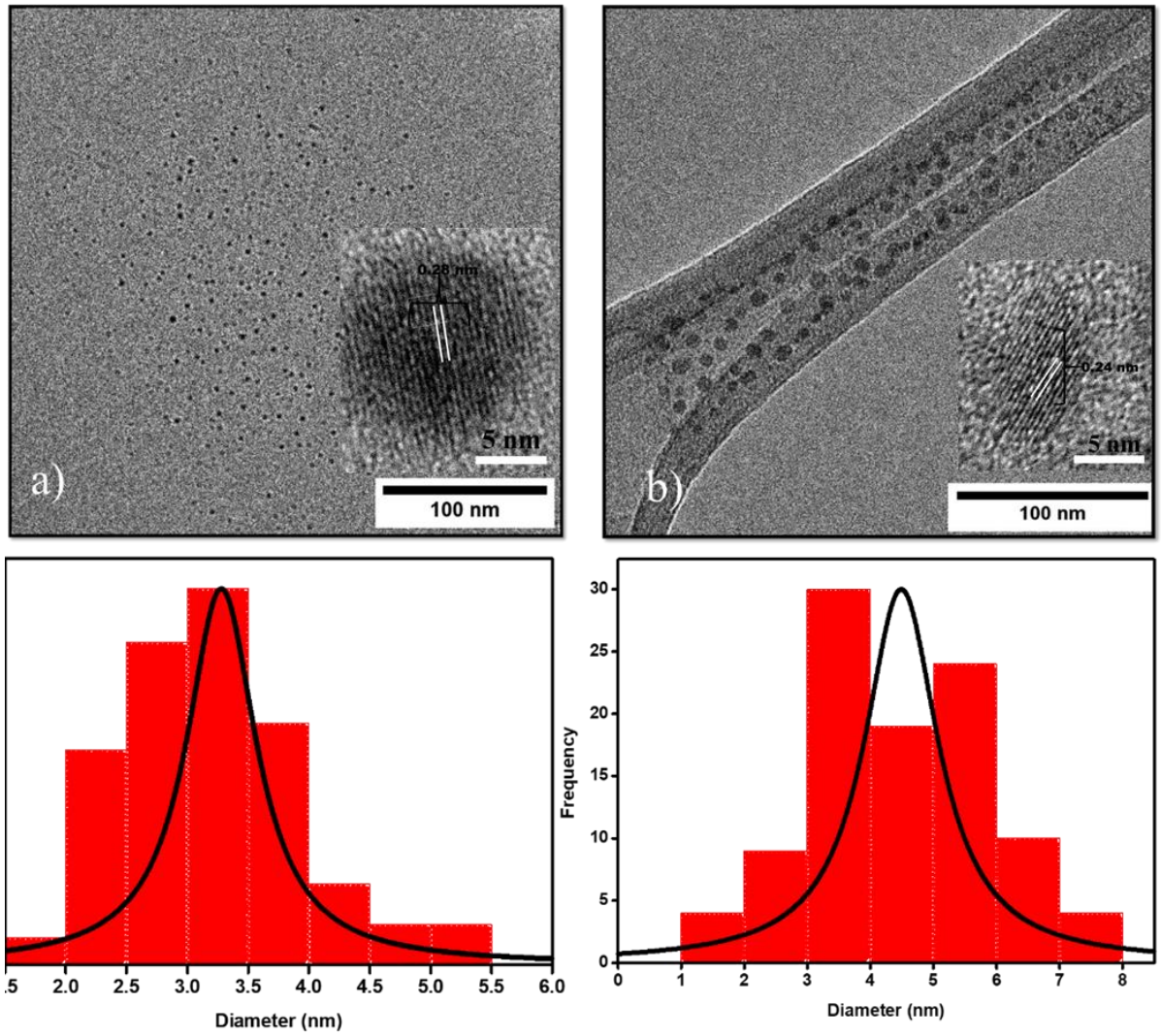

Figure 4.2: TEM images and their corresponding size distribution histograms of a) NCdots-CAEDA and b) NCdots-FN. The insets depict the HRTEM images.

4.3.2 Powder X-ray diffraction (PXRD) analysis

Carbonization of the as-synthesized NCdots-CAEDA and NCdots-FN was confirmed by comparing their PXRD patterns with their starting materials; CA and FN, respectively. PXRD was also used to determine the degree of crystallinity of both types of NCdots. **Figure 4.3.a** depicts the PXRD patterns of both CA and NCdots-CAEDA. The CA shows a complete pattern (as expected) which shows a complete conversion to a graphite-like material with a broad carbon peak for NCdots-CAEDA. The PXRD pattern of NCdots-CAEDA demonstrated one broad peak centered at 2theta = 23.1 ˚ (002) and a small peak at 2theta = 40.0 ˚ (100) which are attributed to the highly disordered carbon atom with amorphous structure and a graphitic characteristic, respectively[22-25]. On the other hand, the PXRD pattern of NCdots-FN

demonstrated a narrow peak centered at 2theta = 27.2 ˚ which is attributed to the highly disordered carbon atoms with crystallization characteristic[26] (**Figure 4.3.b**).

The PXRD pattern of a graphitic carbon typically shows a diffraction peak at around 2theta = 25.0 ˚ or higher[27-29]. Therefore, both NCdots-CAEDA and NCdots-FN consist of both amorphous and graphitic carbon structures and these results are similar to those reported by other researchers[8,12,14]. In addition, the PXRD pattern of NCdots-FN demonstrated a sharper peak as compared to the diffraction peak of NCdots-CAEDA, implying that NCdots-FN might have a higher degree of graphitization than NCdots-CAEDA[30]. The broader 002 peak of NCdots-CAEDA is a characteristic of Cdots with smaller sizes[14,21]. These results are in agreement with the TEM analysis which demonstrated that the average particle sizes of NCdots-CAEDA were smaller than that of NCdots-FN.

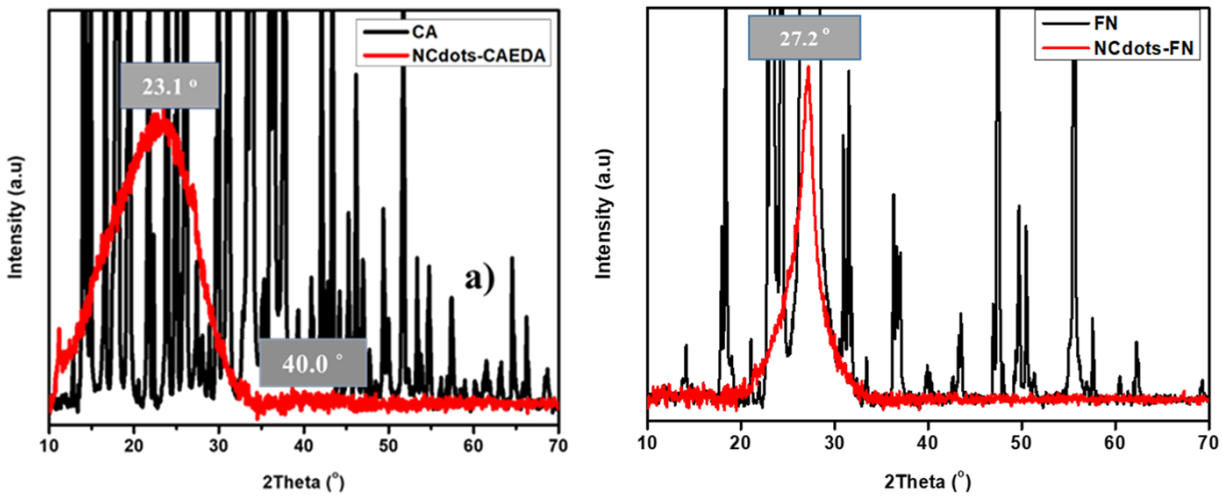

Figure 4.3: PXRD patterns of the as-synthesized a) NCdots-CAEDA and b) NCdots-FN, with their corresponding starting materials.

4.3.3 Optical properties

The optical properties of both as-synthesized NCdots-CAEDA and NCdots-FN were investigated using ultraviolet-visible (Uv-vis) absorption and photoluminescence (PL) spectrophotometry. It has been suggested that different precursors produce Cdots with different optical properties[20]. Therefore, different types of precursors; citric acid with ethylenediamine (CAEDA), and FN, were used for the preparation of NCdots and their optical properties were investigated in this section. **Figure 4.4** depicts the UV-vis absorption and PL spectra of NCdots-CAEDA and NCdots-FN prepared via microwave-irradiation method at 700 W for 10 minutes.

The UV-vis absorption spectrum of NCdots-CAEDA (**Figure 4.4.a**) showed two absorption peaks at 235 nm and 340 nm. On the other hand, the UV-vis absorption spectrum of NCdots-FN (**Figure 4.4.b**) demonstrated two absorption peaks at 237 nm and 280 nm. The absorption peak at 235 nm for NCdots-CAEDA and 237 for NCdots-FN, are typically attributed to the π—π* transition of C=C or C=N from the carbon core, whereas the absorption peaks at 340 nm for NCdots-CAEDA and 280 nm for NCdots-FN, could be assigned to the n—π* transition of C=O or amine groups on the surface of Cdots[12,21,31].

The insets are photographs of NCdots-CAEDA and NCdots-FN in aqueous solution under visible light (brown solutions) and under a hand-held UV lamp (blue solutions) at 365 nm excitation wavelength. The majority of the Cdots prepared via the microwave-irradiation method emit blue fluorescence emissions under a UV lamp and it is easy to see with a naked eye[13,20,32]. CA, EDA and FN as the starting materials, do not fluorescence and absorb in the UV-vis region, therefore, these PL and UV-vis absorption data are an indicative of the successful synthesis of NCdots. The energy band gaps of both NCdots were determined using Tauc plots[33,34] (**Figure 4.5**). The energy band gap of NCdots-CAEDA was found to be 4.44 eV which was higher than that of NCdots-FN (3.11 eV). The difference in energy band gaps between the two types of NCdots is due to the quantum confinement effects. The smaller the particle size the larger the band gap[35]. These results were supported by TEM results which revealed that the average particle size of NCdots-CAEDA was smaller (3.28 nm) than that of NCdots-FN (4.50 nm). The PL spectra of NCdots-CAEDA and NCdots-FN demonstrated maximum emission peaks at 470 nm and 468 nm, respectively, at excitation wavelength of 365 nm which indicates that these materials exhibit excellent photoluminescence properties (**Figure 4.4a and 4.4b**). The emission peaks of both types of NCdots were found to be broad, and this is a typical characteristic of fluorescent NCdots[3,11,21].

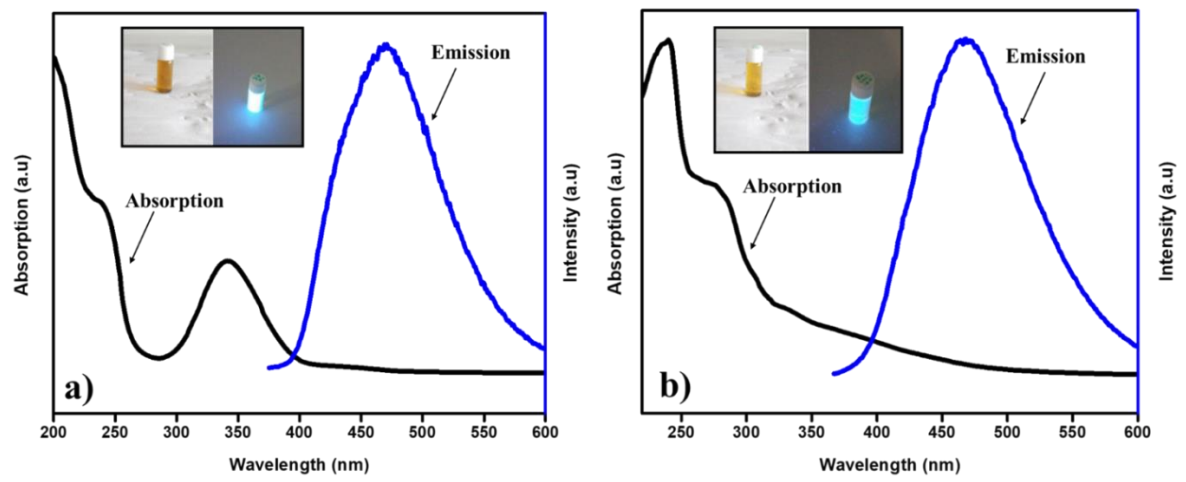

Figure 4.4: UV-vis absorption spectrum and PL emission spectrum of a) NCdots-CAEDA, and b) NCdots-FN in aqueous solution. The insets are the photographs of NCdots-CAEDA and NCdots-FN in solution under visible light (brown solutions) and under UV lamp (blue solutions) at 365 nm excitation wavelength.

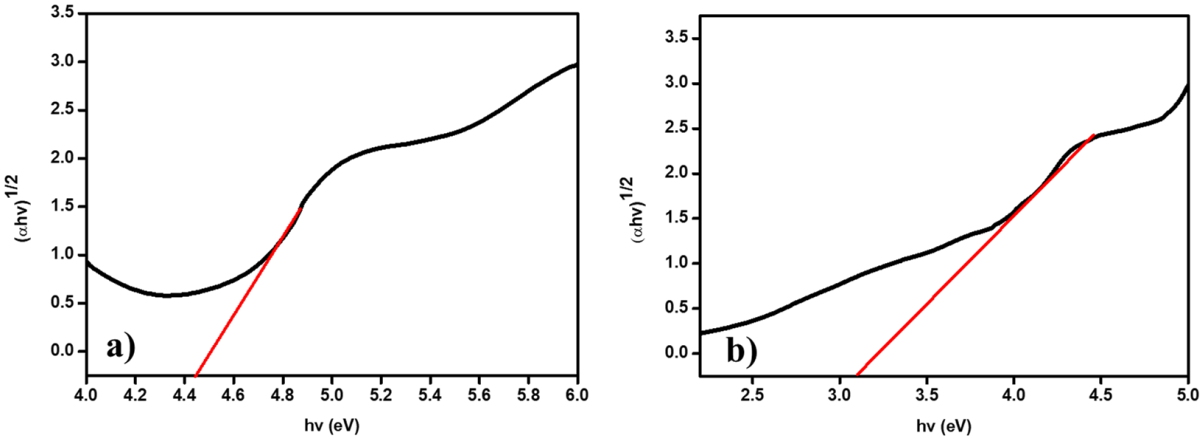

Figure 4.5: Determination of band gap energy of a) NCdots-CAEDA and b) NCdots-FN using Tauc plots.

The optical properties of both the as-synthesized NCdots-CAEDA and NCdots-FN were further explored and investigated by varying the excitation wavelengths ranging from 360 nm to 470 nm in increments of 10 nm (**Figure 4.6.a and 4.6.b**). Both the aqueous solutions of NCdots-CAEDA and NCdots-FN demonstrated excitation-dependent fluorescence behavior. However, it was discovered that upon increasing the excitation wavelength from 360 nm to 390 nm in NCdots-CAEDA, the PL emissions remained constant with the peak position at around 467 nm. The excitation-dependent fluorescence behavior of NCdots-CAEDA was only observed when the sample was excited with excitation wavelengths that are greater than 390

nm. Therefore, a red-shift was observed when the sample was excited with excitation wavelength ranging from 400 nm to 470 nm with emission peaks shifting from 478 nm to 515 nm as shown in **Figure 4.6.a and 4.6.c**. The excitation-independent fluorescence behavior of NCdots-CAEDA at excitation wavelengths ranging from 360 nm to 390 nm is a typical characteristic of NCdots that are uniform in size[13]. These results are in agreement with TEM results which demonstrated that the size distribution of NCdots-CAEDA was narrower than that of NCdots-FN. In addition, the PL intensities of NCdots-CAEDA increased with an increasing excitation wavelength from 360 nm to 450 nm and decreased significantly from 460 nm.

As compared to NCdots-CAEDA, the PL emissions of NCdots-FN demonstrated a continuous red-shift upon increasing the excitation wavelengths from 360 nm to 470 nm with emission peaks shifting from 447 nm to 532 nm (**Figure 4.6.b and 4.6.c**). The PL intensities also increased with an increasing excitation wavelength from 360 nm to 390 nm and started to decrease from 400 nm. The maximum emission PL peaks for NCdots-CAEDA and NCdots-FN were located at 506 nm and 460 nm upon excitation wavelengths of 450 nm and 390 nm, respectively. As mentioned before, the PL properties of Cdots can be influenced by excitation wavelength, doping with heteroatoms, functional groups, quantum confinement effect which is due to smaller sizes, and defects that result in emission traps on the surface of Cdots. However, the specific mechanism of PL emission is still not understood, therefore, more research will need to be done in this specific area in the future.

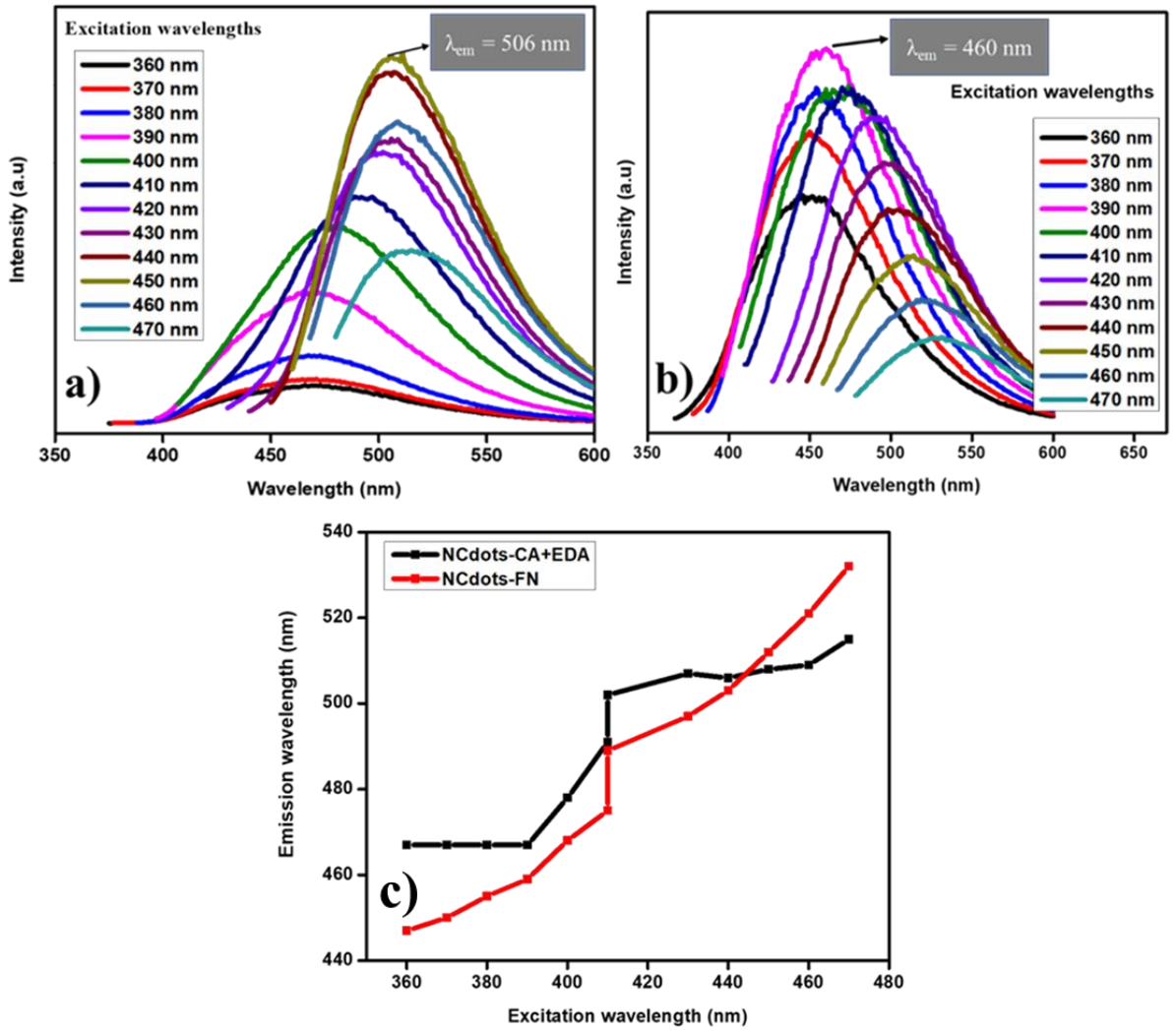

Figure 4.6: PL spectra of the aqueous solution of a) NCdots-CAEDA and b) NCdots-FN at different excitation wavelengths c) with their corresponding plot of excitation wavelength against emission wavelength.

4.3.4 Thermogravimetric analysis (TGA)

The thermal stability of NCdots-CAEDA and NCdots-FN were investigated by TGA and their TGA-DTGA profiles recorded under ambient conditions are depicted in **Figure 4.7a and 4.7.b** respectively. Both NCdots-CAEDA and NCdots-FN showed small decomposition peaks at temperatures around 100 ˚C which are due to moisture or adsorbed water by the NCdots[21,28]. Both types of NCdots also showed different decomposition peaks at temperatures between 200 and 500 ˚C which are attributed to different functional groups on the surface of the two types of the NCdots[21]. These results are in agreement with FTIR and XPS results which demonstrated that both NCdots-CAEDA and NCdots-FN contain different functional groups on their surface.

The TGA-DTGA profiles for both NCdots-CAEDA and NCdots-FN also demonstrated similar gradual weight loss at temperatures above 500 ˚C which is due to decomposition of graphitic carbon core of Cdots[21]. The decomposition peaks of graphitic carbon in NCdots-CAEDA and NCdots-FN occurred at around 671˚C and 648 ˚C, respectively. This indicate that NCdots-CAEDA have a similar thermal stability to NCdots-FN.

In addition, the decomposition peak of NCdots-FN at 648 ˚C was found to be broader than that of NCdots-CAEDA at 671˚C. We can suggest that the broader peak for NCdots-FN relative to NCdots-CAEDA is due to the incorporation of more nitrogen. This could be supported by Raman data but, we found out that the fluorescence properties of both types of NCdots disturb the Raman characterization as there were no defined peaks observed from the Raman data.

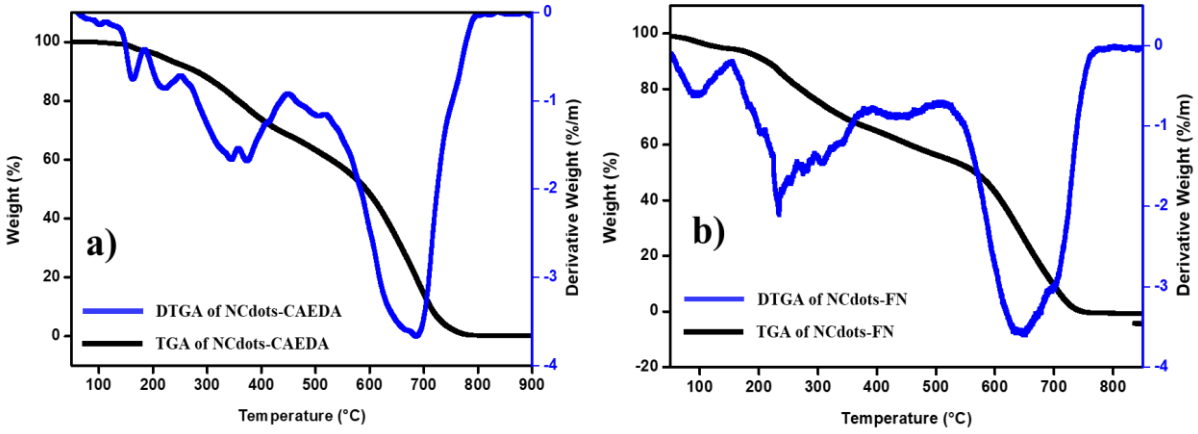

Figure 4.7: TGA-DTGA curves of a) NCdots-CAEDA and b) NCdots-FN heated under ambient conditions.

4.3.5 Fourier transmission infrared spectroscopy (FTIR) analysis

Determining the types of the functional groups that are present on the surface of Cdots is a crucial step because they can have a strong impact on the chemical, physical and optical properties of the Cdots. The functional groups of the as-synthesized NCdots-CAEDA and NCdots-FN were determined using FTIR spectroscopy. It has been reported that the functional groups of the starting materials are retained on the surface during the synthesis of Cdots[20]. To confirm that statement, the functional groups of both citric acid (CA) and fumaronitrile (FN) as the starting materials, were determined by FTIR spectroscopy and their spectra are depicted on **Figure 4.8.a and 4.8.b** together with their resultant NCdots. The FTIR spectrum NCdots-CAEDA (**Figure 4.8.a**) demonstrated a broad absorption peak centered at approximately 3275 cm^{-1} which was assigned to O-H or/and N-H groups. The characteristic stretching vibrations at

approximately 2922 cm^{-1} and 1697 cm^{-1} were attributed to C-H and C=O, respectively. Other vibrations were observed at approximately 1536 cm^{-1}, 1351 cm^{-1} and 1129 cm^{-1} which were assigned to C=C/C=N, C-N and C-O, respectively[36].

Compared to the FTIR spectrum of NCdots-CAEDA, NCdots-FN spectrum (**Figure 4.8.b**) demonstrated absorption bands at around 3222 cm^{-1}, 2857 cm^{-1}, 2241 cm^{-1}, 1667 cm^{-1}, 1548 cm^{-1}, 1398 cm^{-1}, 1261 cm^{-1} and 1177 cm^{-1} which were attributed to vibrations of O-H or/and N-H, C-H, C≡N, C=O, C=C/C=N, C-N, C-H and C-O, respectively[9]. In addition, it was observed that the peaks of both as-synthesized NCdots were less intense as compared to their respective starting materials. It has been suggested that the functional groups on the surface of NCdots are essential for their fluorescence and this will be discussed in more details in **chapter 5.**

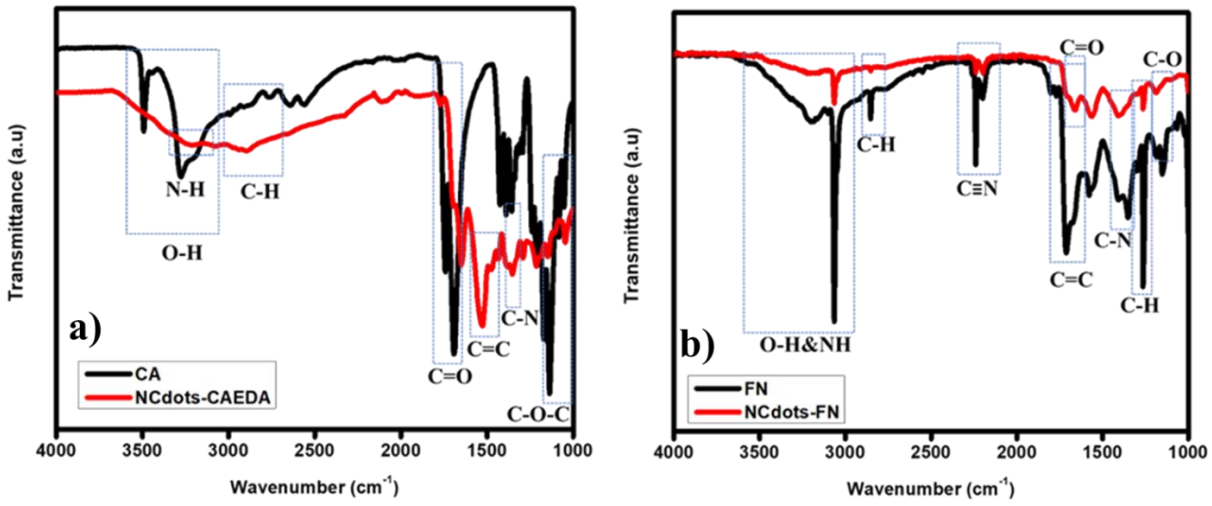

Figure 4.8: FTIR spectra of a) NCdots-CAEDA and b) NCdots-FN with their respective carbon precursors.

4.3.6 X-ray photoelectron spectroscopy (XPS)

XPS is a powerful technique that was used to investigate the surface functional groups and elemental composition of both the as-synthesized NCdots-CAEDA and NCdots-FN. It was used to further confirm the composition and functional groups on the surface of both types of NCdots determined by FTIR analysis. The XPS spectra of both NCdots-CAEDA and NCdots-FN (**Figure 4.9 and 4.10**) revealed that both the NCdots are mainly composed of carbon, nitrogen and oxygen. **Figure 4.9.a** shows the XPS full scan spectrum of NCdots-CAEDA with three predominant peaks at 285.1 eV, 399.9 eV and 531.2 eV which are attributed to the first orbital of the carbon (C1s), nitrogen (N1s) and oxygen (O1s) with atomic percentages of 68.6

%, 12.4 % and 18.1 %, respectively, as shown in **Table 4.1**. Feng *et al.* produced similar results[37].

The high resolution spectra of C1s, N1s and O1s were deconvoluted separately into different peaks. The high-resolution spectrum of C1s (**Figure 4.9.b**) revealed five different peaks at 284.0 eV, 284.6 eV, 285.9 eV, 287.6 eV and 288.7 eV which were assigned to C-C sp^2 hybridization, C-C sp^3 hybridization, C-O, C=O/C=N and C-N respectively[38,39]. The high-resolution spectrum of N1s (**Figure 4.9.c**) was deconvoluted into three peaks located at 399.5 eV, 400.3 eV and 401.5 eV which are assigned to pyridinic, pyrrolic and graphitic nitrogen, respectively[39]. From these results, it was observed that the dominant nitrogen doping configuration on the surface of NCdots-CAEDA was pyridinic N followed closely by pyrrolic N and a small amount of graphitic N. These results are similar to those reported previously[13,39]. In addition, deconvolution of the high-resolution spectrum of O1s (**Figure 4.9.d**) revealed two signals at 531.0 eV and 532.5 eV which are associated with C=O and C-OH/C-O-C respectively[40]. The O/C and N/C ratios of NCdots-CAEDA were determined to be 26.4 % and 18.1 %, respectively.

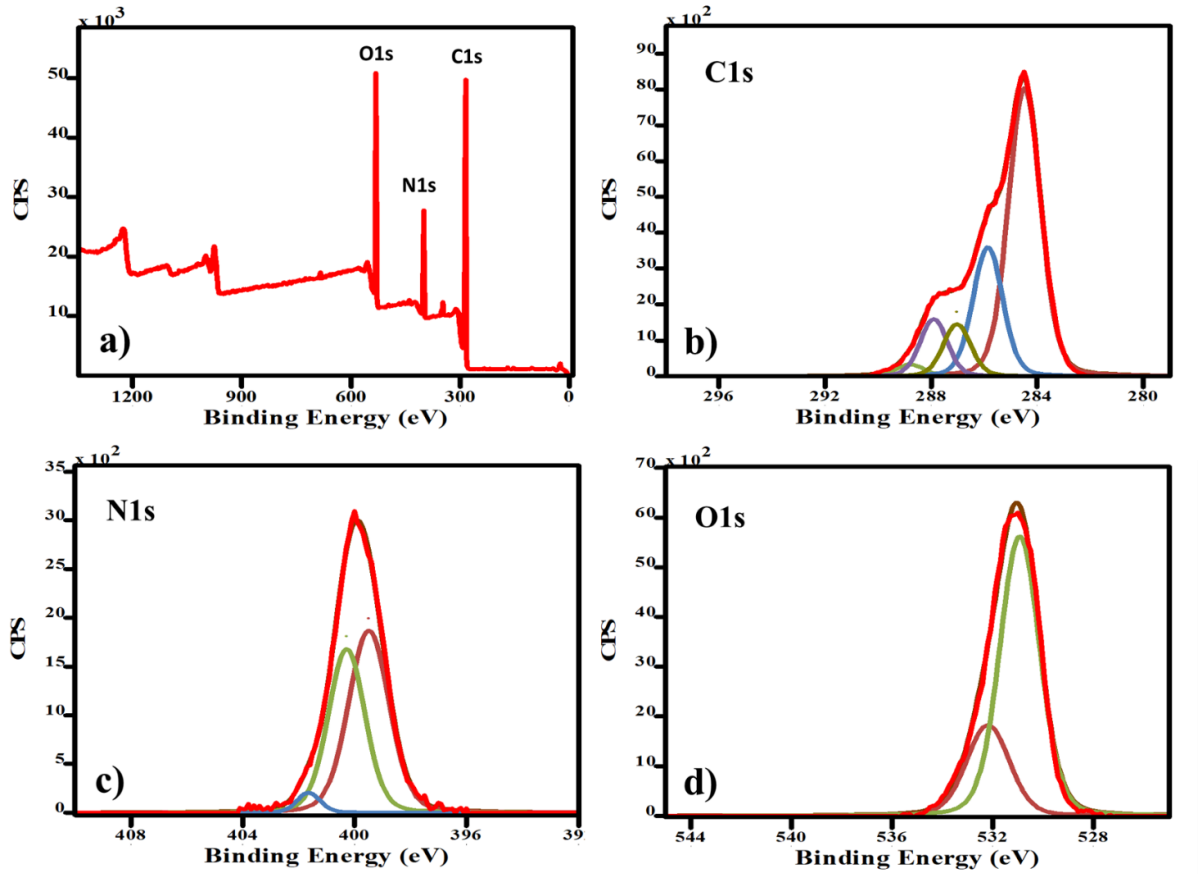

Figure 4.9: a) XPS full scan spectrum, and the corresponding high-resolution spectra of b) C1s, c) N1s, and d) O1s of the as-synthesized NCdots-CAEDA.

NCdots-FN contain a similar elemental composition as do the NCdots-CAEDA, but the atomic percentages differ. As compared to the NCdots-CAEDA, the XPS full scan spectrum of NCdots-FN (**Figure 4.10.a**) revealed the three main peaks at 284.9 eV, 399.2 eV and 531.4 eV which are attributed to the C1s, N1s and O1s respectively. As shown in **Table 4.1**, the atomic percentages of C1s, N1s and O1s in NCdots-FN were 71.4 %, 14.1 % and 14.1 %, respectively. The high-resolution C1s (**Figure 4.10.b**) also showed five different types of carbon at 284.2 eV, 284.6 eV, 285.2 eV, 286.2 eV and 288.1 eV which were assigned to C-C Sp^2 hybridization, C-C Sp^3 hybridization, C-O, C=O/C=N and C-N, respectively[9]. The deconvolution of high-resolution spectrum of N1s (**Figure 4.10.c**) resulted in three different types of nitrogen atoms located at 398.5 eV, 399.8 eV and 401.1 eV associated with pyridinic, pyrrolic and graphitic nitrogen, respectively. For NCdots-FN, the most dominant nitrogen-doping configuration was found to be pyrrolic N and these results are similar to those reported previously[9,41]. The high-resolution spectrum of O1s (**Figure 4.10.d**) revealed two peaks at 531.5 eV and 533.1 eV which are attributed to C=O and C-OH/C-O-C. Both O/C and N/C ratios of NCdots-FN were

measured to be 19.7 %. Even though FN as the starting material for NCdots-FN has no oxygen-containing groups, O1s signals were observed. This is because oxygen from the air can react with the samples as the measurements were done under ambient conditions.

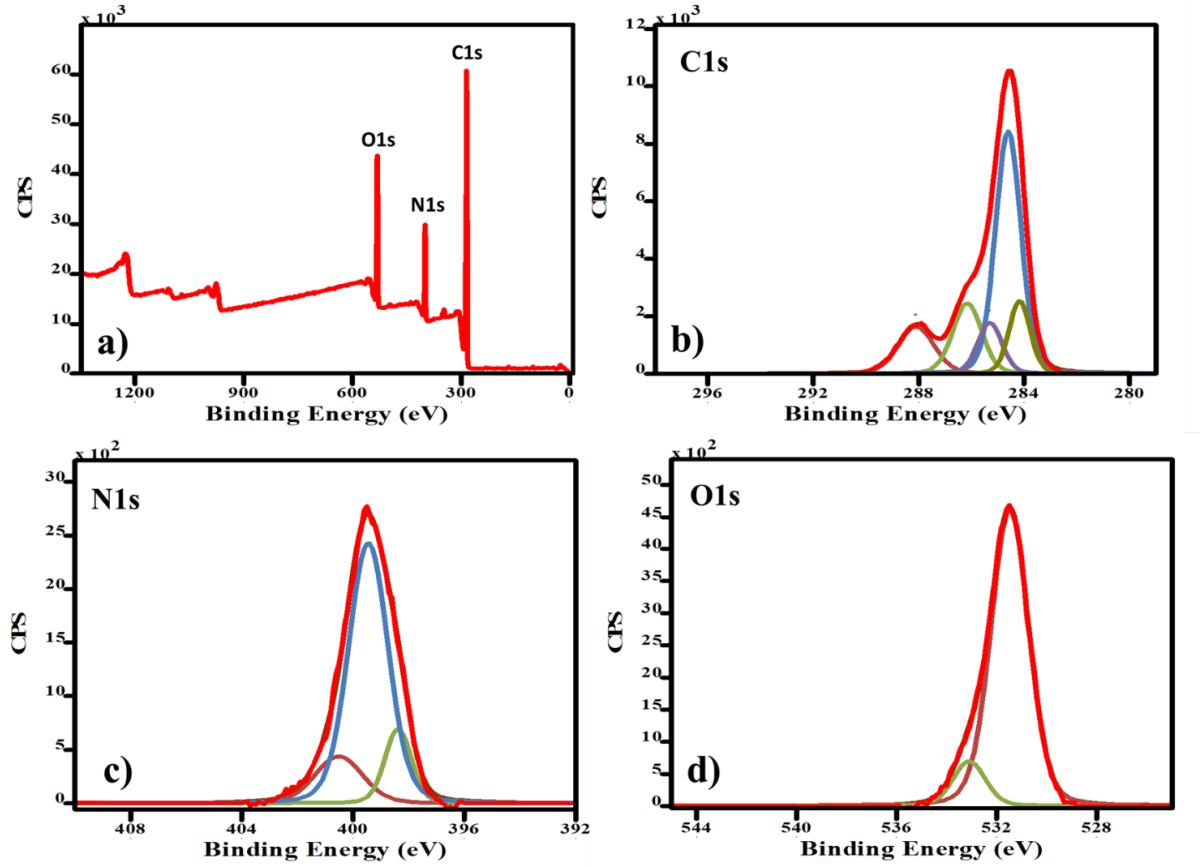

Figure 4.10: a) XPS full scan spectrum, and the corresponding high-resolution spectra of b) C1s, c) N1s, and d) O1s of the as-synthesized NCdots-FN.

Table 4.1: The relative percentage composition of the as-synthesized NCdots-CAEDA and NCdots-FN from XPS spectroscopy.

Sample name	**Atomic percentage**		
	C (%)	**N (%)**	**O (%)**
NCdots-CAEDA	68.6	12.4	18.1
NCdots-FN	71.4	14.1	14.1
NCdots (Literature)[37]	60.1	13.6	26.4

The XPS results of both types of NCdots demonstrated a successful doping of nitrogen on the surface of NCdots during the microwave synthesis. The XPS full scan of both types of NCdots showed trace quantities of calcium at binding energy of approximately 326 eV, assigned to Ca2p. The samples might have been contaminated during sample preparation. The nitrogen content in NCdots-FN was higher than in NCdots-CAEDA by approximately 2.0 %. Both NCdots-CAEDA and NCdots-FN demonstrated three types of nitrogen: pyridinic, pyrrolic and graphitic nitrogen and **Figure 4.11** shows how these types of nitrogen configurations are bonded. The most dominant nitrogen configuration in NCdots-CAEDA was pyridinic and in NCdots-FN was pyrrolic nitrogen. The XPS results are in agreement with TEM, TGA and XRD results as both types of NCdots showed the presence of crystalline cores of graphitic sp^2 carbon hybridization represented by C=C located at binding energies around 284.0-284.9 eV.

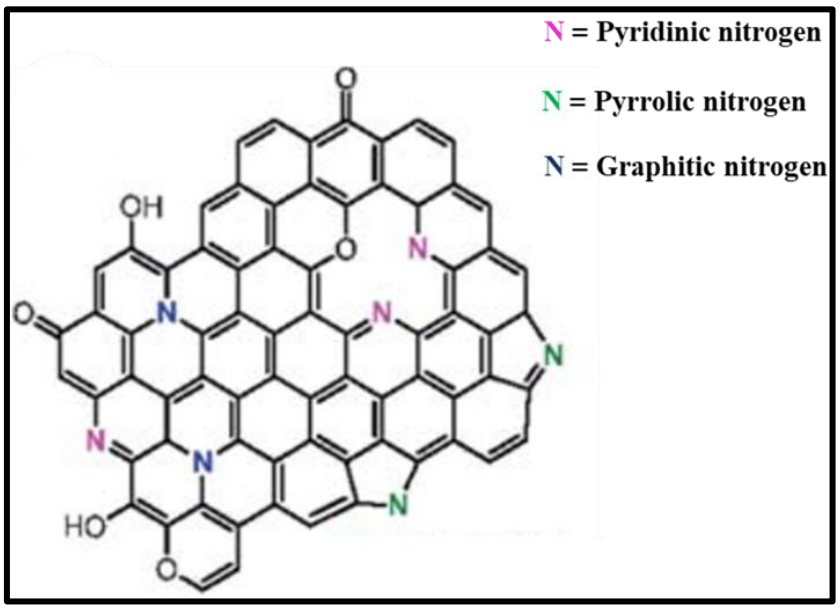

Figure 4.11: A structure representing three types of nitrogen configurations present in both NCdots-CAEDA and NCdots-FN[39].

4.4 Conclusions

In conclusion, we successfully synthesized NCdots from different precursors: CAEDA and FN using a microwave-irradiation method at the same reaction conditions. A microwave-irradiation method offers a great promise to prepare NCdots with good yield and high fluorescence. Furthermore, this method was found to be simple, fast and environmentally friendly. Both the aqueous solutions of NCdots-CAEDA and NCdots-FN showed a bright-blue colour when illuminated with a hand-held UV lamp at 365 nm excitation wavelength and demonstrated excellent fluorescence properties with excitation-dependent fluorescence behaviours. Both the as-synthesized NCdots have the ability to absorb light in the UV-vis region, which makes them to be potential candidates for solar cell applications. The results showed that although we used the same reaction conditions for the preparation of NCdots, the final products demonstrated different optical properties. The obtained results also confirmed that using different starting materials on the preparation of NCdots results in NCdots with different optical properties. TEM analysis showed that both NCdots-CAEDA and NCdots-FN are quasi-spherical carbon nanoparticles with diameters less than 10 nm. The particle size of NCdots-FN were larger than those of NCdots-CAEDA. The FTIR and XPS results confirmed the successful of nitrogen-doping in both samples.

References

1) Blau, W.; Ji, W. Feature Issue Introduction : Nanocarbon for Photonics and Optoelectronics. *Opt. Mater. express* **2012**, *2*, 891–892.
2) Yang, Z.; Wang, M.; Yong, M.; Wong, Y.; Zhang, X. Intrinsically Fluorescent Carbon Dots with Tunable Emission Derived from Hydrothermal Treatment of Glucose in the Presence of Monopotassium Phosphate W. *Chem. Commun.* **2011**, *47*, 11615–11617.
3) Wang, Z.; Long, P.; Feng, Y.; Qin, C.; Feng, W. Surface Passivation of Carbon Dots with Ethylene Glycon and Their High-Sensitivity to Fe^{3+}. *R. Soc. Chem. Adv.* **2017**, *7*, 2810–2816.
4) Cailotto, S.; Amadio, E.; Facchin, M.; Selva, M.; Pontoglio, E.; Rizzolio, F.; Riello, P.; To, G.; Benedetti, A.; Perosa, A. Carbon Dots from Sugars and Ascorbic Acid: Role of the Precursors on Morphology, Properties, Toxicity, and Drug Uptake. *ACS Med. Chem.* **2018**, *9*, 832–837.
5) Li, H.; Liu, J.; Guo, S.; Zhang, Y.; Huang, H.; Liu, Y.; Kang, Z. Carbon Dots from PEG for Highly Sensitive Detection of Levodopa †. *J. Mater. Chem. B* **2015**, *3*, 2378–2387.
6) Xiao, D.; Yuan, D.; He, H.; Lu, J. Microwave-Assisted One-Step Green Synthesis of Amino-Functionalized Fluorescent Carbon Nitride Dots from Chitosan. *Luminescence* **2013**, *28*, 612–615.
7) Chowdhury, D.; Gogoi, N.; Majumdar, G. Fluorescent Carbon Dots Obtained from Chitosan Gel. *RSC Adv.* **2012**, *2*, 12156–12159.
8) Liu, X.; Pang, J.; Xu, F.; Zhang, X. Simple Approach to Synthesize Amino-Functionalized Carbon Dots by Carbonization of Chitosan. *Sci. Rep.* **2016**, *6*, 1–9.
9) Moon, B. J.; Oh, Y.; Shin, D. H.; Kim, S. J.; Lee, S. H. Facile and Purification-Free Synthesis of Nitrogenated Amphiphilic Graphitic Carbon Dots. *Chem. Mater.* **2016**, *28*, 1481–1488.
10) Naik, V. M.; Gunjal, D. B.; Gore, A. H.; Pawar, S. P. Quick and Low Cost Synthesis of Sulphur Doped Carbon Dots by Simple Acidic Carbonization of Sucrose for the Detection of Fe^{3+} Ions in Highly Acidic Environment. *Diam. Relat. Mater.* **2018**, *88*, 262–268.
11) Kasprzyk, W.; Swiergosz, T.; Bednarz, S.; Walas, K.; Bashmakova, N. V. From Citric Acid and Urea – a Molecular Insight. *Nanoscale* **2018**, *10*, 13889–13894.

12) So, R. C.; Sanggo, J. E.; Jin, L.; Diaz, J. M. A.; Guerrero, R. A.; He, J. Gram-Scale Synthesis and Kinetic Study of Bright Carbon Dots from Citric Acid and Citrus Japonica via a Microwave-Assisted Method. *ACS Omega* **2017**, *2*, 5196–5208.
13) Zhai, X.; Zhang, P.; Liu, C.; Bai, T.; Li, W.; Dai, L.; Liu, W. Highly Luminescent Carbon Nanodots by Microwave-Assisted Pyrolysis W. *Chem. Commun.* **2012**, *48*, 7955–7957.
14) Rao, L.; Tang, Y.; Lu, H.; Yu, S.; Ding, X.; Xu, K.; Li, Z.; Zhang, J. Z. Highly Photoluminescent and Stable N-Doped Carbon Dots as Nanoprobes for Hg^{2+} Detection. *Nanomaterials* **2018**, *8*, 1–18.
15) Karakoçak, B. B.; Liang, J.; Kavadiya, S.; Berezin, M. Y.; Biswas, P.; Ravi, N. Optimizing the Synthesis of Red-Emissive Nitrogen-Doped Carbon Dots for Use in Bioimaging. *ACS Appl. Nano Mater.* **2018**, *1*, 3682–3692.
16) Zhang, X.; Li, Z.; Zhang, Z.; Liu, C.; Li, J.; Guo, W.; Shen, L.; Qu, S. Preparation and Employment of Carbon Nanodots to Improve Electron Extraction Capacity of Polyethylenimine Interfacial Layer for Polymer Solar Cells. *Org. Electron.* **2016**, *33*, 62–70.
17) Qu, D.; Zheng, M.; Zhang, L.; Zhao, H.; Xie, Z.; Jing, X.; Haddad, R. E.; Fan, H.; Sun, Z. Formation Mechanism and Optimization of Highly Luminescent N-Doped Graphene Quantum Dots. *Sci. Rep.* **2014**, *4*, 1–11.
18) Devaraju, M. K.; Honma, I. Hydrothermal and Solvothermal Process Towards Development of LiMPO 4 (M = Fe, Mn) Nanomaterials for Lithium-Ion Batteries. *Adv. energy Mater.* **2012**, *2*, 284–297.
19) Zhu, S.; Meng, Q.; Wang, L.; Zhang, J.; Song, Y.; Jin, H.; Zhang, K.; Sun, H.; Wang, H.; Yang, B. Highly Photoluminescent Carbon Dots for Multicolor Patterning , Sensors , and Bioimaging. Angewandte. *Angew. Chemie* **2013**, *125*, 4045–4049.
20) Sugiarti, S.; Darmawan, N. Synthesis of Fluorescence Carbon Nanoparticles from Ascorbic Acid. *Indones. J. Chem* **2015**, *15*, 141–145.
21) Wang, D.; Wang, Z.; Zhan, Q.; Pu, Y.; Wang, J.; Foster, N. R.; Dai, L. Facile and Scalable Preparation of Fluorescent Carbon Dots for Multifunctional Applications. *Engineering* **2017**, *3*, 402–408.
22) Peng, S.; Fan, X.; Li, S.; Zhang, J. U. N. Green Synthesis and Characterization of Graphite Oxide By Orthogonal Experiment. *J. Chil. Chem. Sco.* **2013**, *4*, 2213–2217.

23) Qian, W.; Sun, F.; Xu, Y.; Qiu, L.; Liu, C.; Wang, S.; Yan, F. Human Hair-Derived Carbon Flakes for Electrochemical Supercapacitors. *Energy Environ. Sci.* **2014**, *7*, 379–386.

24) Puvvada, N.; Kumar, B. N. P.; Konar, S.; Kalita, H.; Mandal, M.; Pathak, A. Synthesis of Biocompatible Multicolor Luminescent Carbon Dots for Bioimaging Applications. *Sci. Technol. Adv. Mater.* **2012**, *13*, 1–7.

25) Gao, T.; Du, Y.; Li, H. Preparation of Nitrogen-Doped Graphitic Porous Carbon towards Capacitive Deionization with High Adsorption Capacity and Rate Capability. *Sep. Purif. Technol.* **2019**, *211*, 233–241.

26) Papaioannou, N.; Marinovic, A.; Yoshizawa, N.; Goode, A. E.; Fay, M.; Khlobystov, A.; Titirici, M. M.; Sapelkin, A. Structure and Solvents Effects on the Optical Properties of Sugar-Derived Carbon Nanodots. *Sci. Rep.* **2018**, *8*, 1–10.

27) Atchudan, R.; Edison, T. N. J. I.; Lee, Y. R. Nitrogen-Doped Carbon Dots Originating from Unripe Peach for Fluorescent Bioimaging and Electrocatalytic Oxygen Reduction Reaction. *J. Colloid Interface Sci.* **2016**, *482*, 8–18.

28) Safardoust-Hojaghan, H.; Salavati-Niasari, M.; Amiri, O.; Hassanpour, M. Preparation of Highly Luminescent Nitrogen Doped Graphene Quantum Dots and Their Application as a Probe for Detection of Staphylococcus Aureus and E. Coli. *J. Mol. Liq.* **2017**, *241*, 1114–1119.

29) Yang, Z.; Xu, M.; Liu, Y.; He, F.; Gao, F.; Su, Y.; Wei, H.; Zhang, Y. Nitrogen-Doped, Carbon-Rich, Highly Photoluminescent Carbon Dots from Ammonium Citrate . *Nanoscale* **2014**, *6*, 1890–1895.

30) Li, W.; Li, M.; Liu, Y.; Pan, D.; Li, Z.; Wang, L.; Wu, M. Three Minute Ultrarapid Microwave-Assisted Synthesis of Bright Fluorescent Graphene Quantum Dots for Live Cell Staining and White LEDs. *ACS Appl. NANO Mater.* **2018**, *1*, 1623–1630.

31) Liao, J.; Cheng, Z.; Zhou, L. Nitrogen-Doping Enhanced Fluorescent Carbon Dots: Green Synthesis and Their Applications for Bioimaging and Label-Free Detection of Au 3+ Ions. *ACS Sustain. Chem. Eng.* **2016**, *4*, 3053–3061.

32) Liu, Q.; Zhang, N.; Shi, H.; Ji, W.; Guo, X.; Yuan, W.; Hu, Q. Highly Sensitive and Selective Detection of Copper. *New J. Chem.* **2018**, *42*, 3097–3101.

33) Suzuki, T.; Watanabe, H.; Ueno, T.; Oaki, Y.; Imai, H. Significant Increase in Band Gap and Emission Efficiency of In2O3 Quantum Dots by Size-Tuning around 1 Nm in Supermicroporous Silicas. *Langmuir* **2017**, *33*, 3014–3017.

34) Umrao, S.; Sharma, P.; Bansal, A.; Sinha, R.; Singh, R. K.; Srivastava, A. Multi-Layered Graphene Quantum Dots Derived Photodegradation Mechanism of Methylene Blue. *RSC Adv.* **2015**, *5* (64), 51790–51798.

35) Bhattacharya, A.; Chatterjee, S.; Prajapati, R.; Mukherjee, T. K. Size-Dependent Penetration of Carbon Dots inside the Ferritin Nanocages: Evidence for the Quantum Confinement Effect in Carbon Dots. *Phys. Chem. Chem.Phys.* **2015**, *17*, 12833–12840.

36) Du, Q.; Zheng, J.; Wang, J.; Yang, Y.; Liu, X. The Synthesis of Green Fluorescent Carbon Dots for Warm White LEDs. *RSC Adv.* **2018**, *8*, 19585–19595.

37) Feng, Z.; Li, Z.; Zhang, X.; Shi, Y.; Zhou, N. Nitrogen-Doped Carbon Quantum Dots as Fluorescent Probes for Sensitive and Selective Detection of Nitrite. *Molecules* **2017**, *22*, 2061–2069.

38) Wang, H.; Gao, P.; Wang, Y.; Guo, J.; Zhang, K. Q.; Du, D.; Dai, X.; Zou, G. Fluorescently Tuned Nitrogen-Doped Carbon Dots from Carbon Source with Different Content of Carboxyl Groups. *APL Mater.* **2015**, *3*, 1–8.

39) Tang, L.; Ji, R.; Li, X.; Teng, K. S.; Lau, S. P. Energy-Level Structure of Nitrogen-Doped Graphene Quantum Dots. *J. Mater. Chem. C* **2013**, *1*, 4908–4915.

40) Wang, H.; Sun, P.; Cong, S.; Wu, J.; Gao, L.; Wang, Y.; Dai, X.; Yi, Q.; Zou, G. Nitrogen-Doped Carbon Dots for "Green" Quantum Dot Solar Cells. *Nanoscale Res. Lett.* **2016**, *11*, 1–6.

41) Du, F.; Li, J.; Hua, Y.; Zhang, M.; Zhou, Z.; Yuan, J.; Wang, J.; Peng, W.; Zhang, L.; Xia, S.; et al. Multicolor Nitrogen-Doped Carbon Dots for Live Cell Imaging. *J. Biomed. Nanotechnol.* **2014**, *10*, 1–9.

CHAPTER 5: INCORPORATION OF NITROGEN-DOPED CARBON DOTS IN ORGANIC SOLAR CELL

5.1 Introduction

Since the discovery of the photovoltaic effect by Alexandre-Edmund Becquerel in 1839, organic solar cells (OSCs) have received tremendous attention from researchers[1]. This is because of its advantages such as great mechanical flexibility, low light-weight, ease of fabrication and cost-effectiveness[2-5]. OSCs are a promising sustainable energy technology for the future. However, they are still suffering from low efficiency and limited stability as compared to inorganic-based solar cells (ISCs)[2,4,6]. Therefore, the primary concern in organic solar cell is to improve the power conversion efficiency (PCE) for application in consumer electronics. As mentioned in Chapter 2, there are three types of device architectures of organic solar cells: the single layer, bilayer and bulk heterojunction (BHJ). The PCE of the single and bilayer are extremely low due to the fact that the exciton diffusion length is shorter than the absorption length and they are prone to high recombination rates[7]. The introduction of the BHJ was to solve this problem and therefore enhance the PCE. The PCE depends on various factors such as the nanoscale morphology of the film, the type of the electrodes (work function) used, the thickness of the photoactive layer, charge mobility, energy band gap, dielectric constant and molecular energy levels[4]. All these factors need to be controlled for better device performance.

The performance of the BHJ cell is evaluated from current density-voltage characteristics. **Figure 5.1.a and b** depict the basic energy diagram of the donor and acceptor materials used in a BHJ organic solar cell and a typical current-voltage curve under dark and light conditions, respectively[8]. The current-voltage characteristic is used to determine the important operational parameters of the solar cell. These parameters include:

- short circuit current (J_{sc}),
- open circuit voltage (V_{oc}),
- fill factor (FF) and
- the power conversion efficiency (PCE).

The J_{sc} is defined as the current density generated by the solar cell under illumination in the absence of the voltage whereas the V_{oc} is the voltage that the device provides when the terminals are not connected to any load and their values can be determined directly from the current density-voltage curve[9]. The fill factor is defined as the ratio of the maximum power that the array can actually provide under normal operating conditions to the product of the open-circuit voltage times the short-circuit current, and it can be determined using **Equation 5.1**. This fill factor value determines the quality of the device and the closer the fill factor is to one (unity), the more power the device can provide. PCE is the percentage of the incident light that is converted into electrical power. The device with higher fill factor is expected to produce more power, thus high efficiency. Therefore, the power conversion efficiency of the cell is dependent on the V_{oc}, I_{sc} and FF, and it can be determined using **Equation 5.2**.

$$FF = \frac{J_{max} \times V_{max}}{J_{sc} \times V_{oc}} \quad \text{.....(5.1)}$$

$$PCE = \eta = \frac{P_{max}}{P_{in}} = \frac{FF \times V_{OC} \times J_{SC}}{P_{in}} \quad \text{.....(5.2)}$$

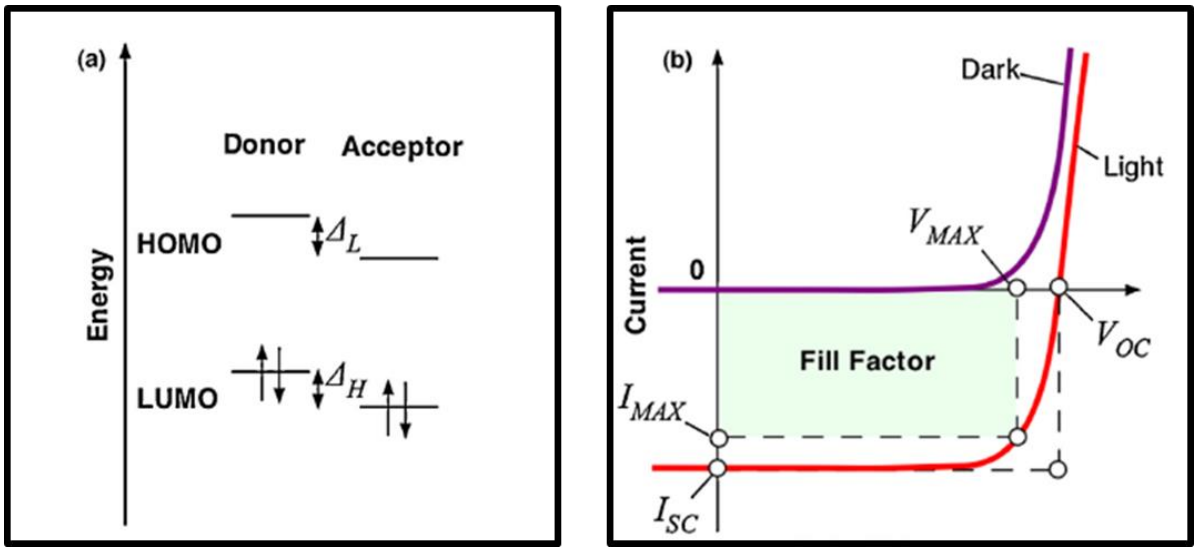

Figure 5.1: a) The LUMO and HOMO energy levels of the donor and acceptor materials used in BHJ organic solar cell. b) A typical current-voltage curve under dark (purple) and light (red) conditions[8].

In this chapter, we aim to enhance or improve the efficiency of the organic solar cell by incorporating nitrogen-doped carbon dots (N-Cdots) in the active layer of an organic BHJ solar cell. N-Cdots have the potential to improve the performance of the cell by enhancing the light harvesting active layer.

5.2 Device fabrication

5.2.1 Materials

Acetone (99.5 %), Ethanol (99.8 %), hydrochloric acid (HCl), chlorobenzene, Indium tin oxide (ITO, side dimension: 2.50 cm, surface resistivity ρ: 30-60 Ω/square slide), zinc dust (< 10 μm ≥ 98%) Poly(3,4-ethylenedioxythiophene)-polystyrenesulphonate (PEDOT:PSS, 3-4% in water), poly(3-hexylthiophene-2,5-diyl) (P3HT, 99.99 %), [6,6]-phenyl C_{61} butyric acid methyl ester (PCBM, 99.5 %). Detergent was obtained from a local supermarket. All chemicals were used as received, without further purification.

5.2.2 Fabrication method

In BHJ device, the polymers that are commonly used are P3HT:PCBM (as the active layer) and PEDOT:PSS (as the hole transport layer) and their structures are shown in **Figure 5.2**. In this study, ITO coated glass was used as a transparent conducting oxide substrate for device fabrication. In order to prevent the short circuiting of the cell, one third distance ITO was etched with zinc dust and 2M HCl. ITO coated glass was then cleaned with detergent solution, distilled water, acetone, ethanol and then a mixture of distilled water and ethanol (1:1 ratio), sequentially in an ultrasonic bath under fume hood for 10 minutes in each step. The samples were then blown dry with nitrogen gas (5N). PEDOT:PSS solution as the hole transport layer was then spin-coated using a spin coater shown in **Figure 5.3.a**, on the cleaned ITO coated glass at a speed of 2000 rpm for 1 min. The resultant film was then baked on a hot plate at 110 ℃ for 15 minutes in order to remove water from the PEDOT:PSS solution. To prepare the active layer for the reference cell (without N-Cdots), 8 mg of P3HT and 8 mg of PCBM (1:1 ratio) were dissolved in 0.5 ml of chlorobenzene separately and stirred for 3 hours under ambient conditions. The P3HT and PCBM solutions were then mixed together and stirred for 2 hours under ambient conditions. The active layer (P3HT:PCBM) was spin coated on top of the dried PEDOT:PSS film at a speed of 2000 rpm for 1 min, followed by deposition of aluminum (Al) as the cathode by thermal evaporation under vacuum of 1.5 $\times 10^{-6}$ mbar (shown in **Figure 5.3.b**). The performance of the fabricated devices were then tested using current density-voltage measurements interfaced with a Solar Simulator at Air Mass 1.5. The two types of N-

Cdots prepared from citric acid plus ethylenediamine (NCdots-CAEDA) and fumaronitrile (NCdots-FN) prepared in Chapter 4 were used to modify the active layer. The modified active layers were prepared the same way as the reference with P3HT:PCBM+NCdots-CAEDA (1:1 ratio) and P3HT:PCBM+NCdots-FN (1:1 ratio) as the active layer. All the three devices were annealed at 50 °C for 5 min prior to characterization.

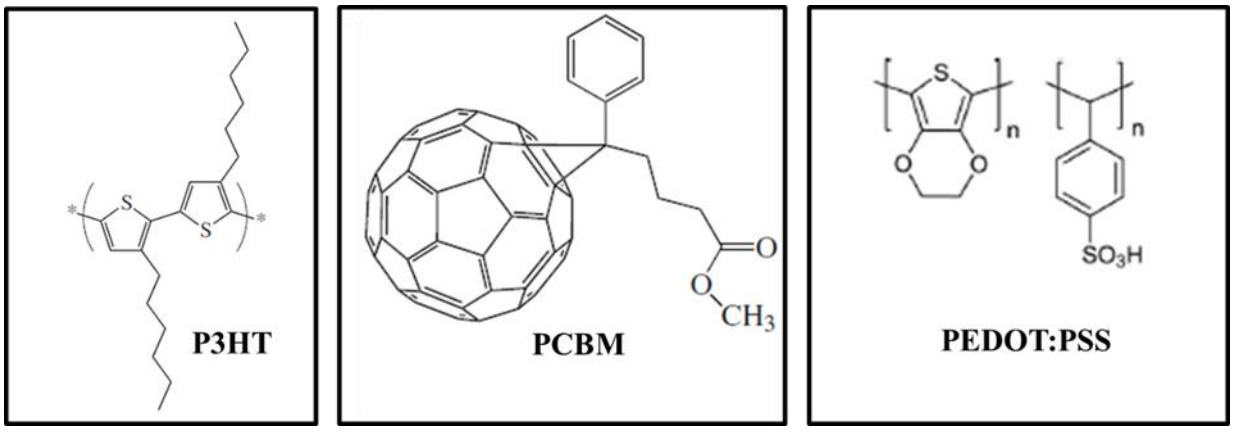

Figure 5.2: The chemical structures of the polymers used in the BHJ organic solar cells[10,11].

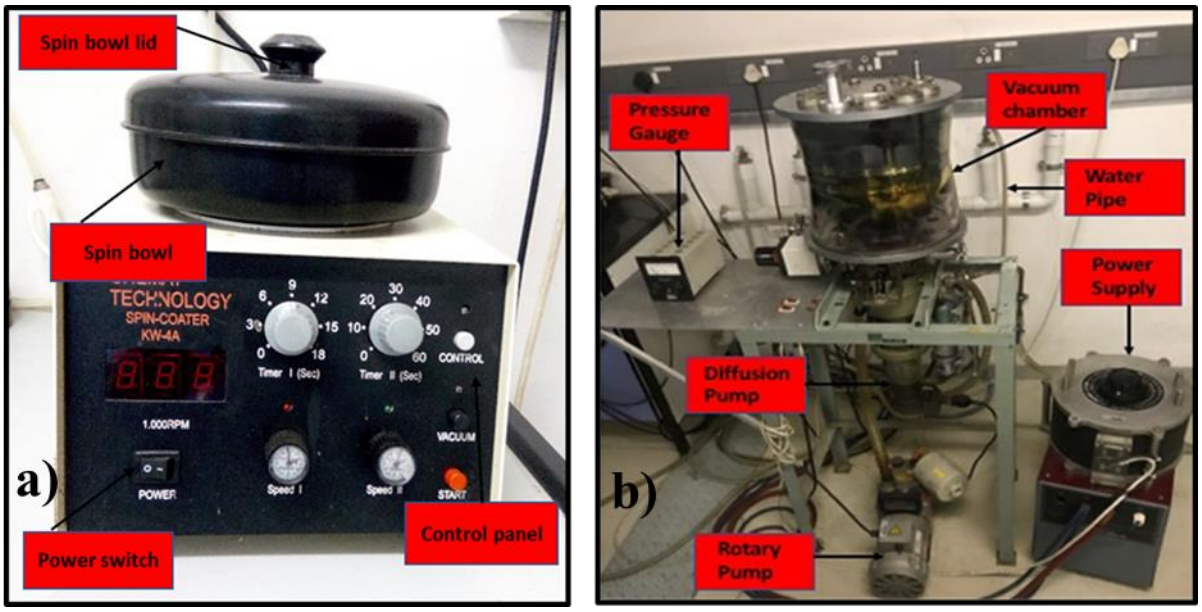

Figure 5.3: a) The spin-coater used to spin coat the active and the hole transport layers. b) The thermal evaporator used to deposit Al.

5.3 Characterization of the fabricated devices

In this section, three different architectures of BHJ solar cells were fabricated and tested using a HP 4141B DC system under AM 1.5 G irradiation at 100 mW/cm^2 to measure their I-V characteristics. The IVplot software[12] was used to draw the J-V curves and extract the device parameters. The following architectures were fabricated and characterized (**Figure 5.4**).

- ITO/PEDOT:PSS/P3HT:PCBM/Al, (reference cell),
- ITO/PEDOT:PSS/P3HT:PCBM+NCdots-CAEDA/Al
- ITO/PEDOT:PSS/P3HT:PCBM-NCdots-FN/Al

The difference among these three fabricated devices were in the constituent of their photo-active layers. The J-V curves and the important operational parameters of the fabricated cells are reported in **Figure 5.5** and **Table 5.1**, respectively. The parameters give an important information about the fabricated devices. The area of the fabricated device was 0.07 cm^2.

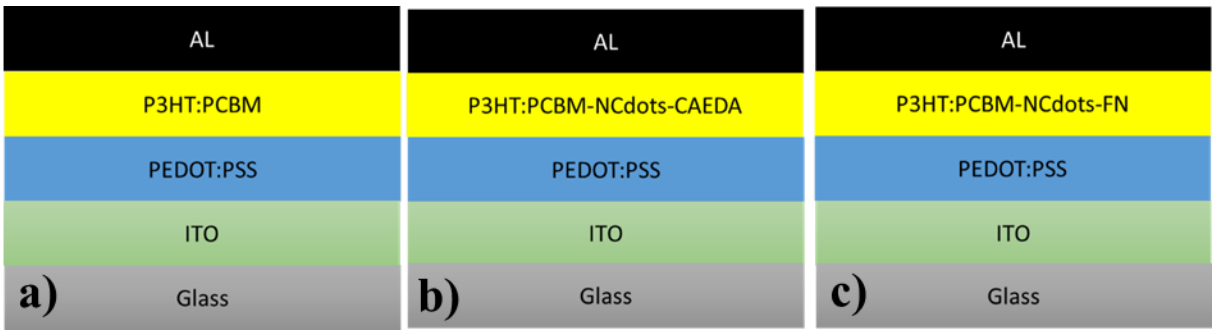

Figure 5.4: The architectures of the fabricated BHJ devices:
a) ITO/PEDOT:PSS/P3HT:PCBM/Al (reference cell without N-Cdots),
b) ITO/PEDOT:PSS/P3HT:PCBM+NCdots-CAEDA/Al and
c) ITO/PEDOT:PSS/P3HT:PCBM-NCdots-FN/Al.

Figure 5.5.a shows the J-V curves of the reference cell (P3HT:PCBM active layer) in the dark and under illumination. The values of the V_{oc}, J_{sc}, FF and PCE of the reference cell were determined to be 0.47 V, 0.06 mA/ cm^2, 24.7 % and 0.01 %, respectively. According to literature review[13], the V_{oc} of the reference cell (ITO/PEDOT:PSS/P3HT:PCBM/Al) is typically around 0.60 V and this is much higher that what we obtained with our reference. This could be due to the fact that P3HT-PCBM as the active layer, oxidises very fast, resulting in lower V_{oc}. Incorporation of NCdots-CAEDA and NCdots-FN into the active layer demonstrated a positive effect as shown by the J-V curves (**Figure 5.5.b and c**, respectively).

Incorporation of NCdots-CAEDA into P3HT:PCBM increased the efficiency of the cell from 0.01 (of the reference cell) to 0.03 %. However, the V_{oc} of the cell modified with NCdots-CAEDA was smaller (0.45 V) than that of the reference cell. The V_{oc} alone cannot determine the performance of the cell. We need all the other parameters in order to determine the PCE of the device. Hence a smaller V_{oc} does not mean poor performance of the device or lower PCE. For example, silicon-based solar cells have relatively low V_{oc} (0.5 V)[14] as compared to organic solar cells (0.6 V), but their PCE is much higher. The V_{oc} of the organic BHJ cell is highly dependent on the difference between the highest occupied molecular orbital (HOMO) of the donor and the lowest unoccupied molecular orbital (LUMO) of the acceptor material[14,15]. The maximum open circuit voltage increases with an increasing energy band gap.

We also noticed that even though NCdots-CAEDA and NCdots-FN were prepared using the same methods under same conditions, their incorporation into the active layer yielded different results. As compared to NCdots-CAEDA, incorporation of NCdots-FN into the active layer increased the efficiency of the cell significantly (0.13%). We speculated that perhaps the different behavior have been caused by the presence of different nitrogen configurations in both samples. In **Chapter 4**, XPS data demonstrated that even though the NCdots-CAEDA and NCdots-FN contained similar nitrogen contents, the configurations differed. The most dominant nitrogen configuration in NCdots-CAEDA was pyridinic and in NCdots-FN was pyrrolic nitrogen. This might have contributed to the difference in the performance of the devices.

The V_{oc}, FF and J_{sc} of the device incorporated with NCdots-FN were also improved significantly as compared to the device incorporated with NCdots-CAEDA. It was also observed that the operational parameters values of the three fabricated devices were very low as compared to the literature values where P3HT:PCBM was used as the active layer[13]. Zhen-boo *et. al.* further improved their device by modifying PEDOT:PSS (hole transport layer) with different percentages of dimethyl sulfoxide (DMSO)[13]. Their results demonstrated that 4 % of DMSO produced a device with the best PCE (3.34 %). These results show that there is still a room for organic solar cells research to improve the efficiency before it reaches the market demand (commercially scalable).

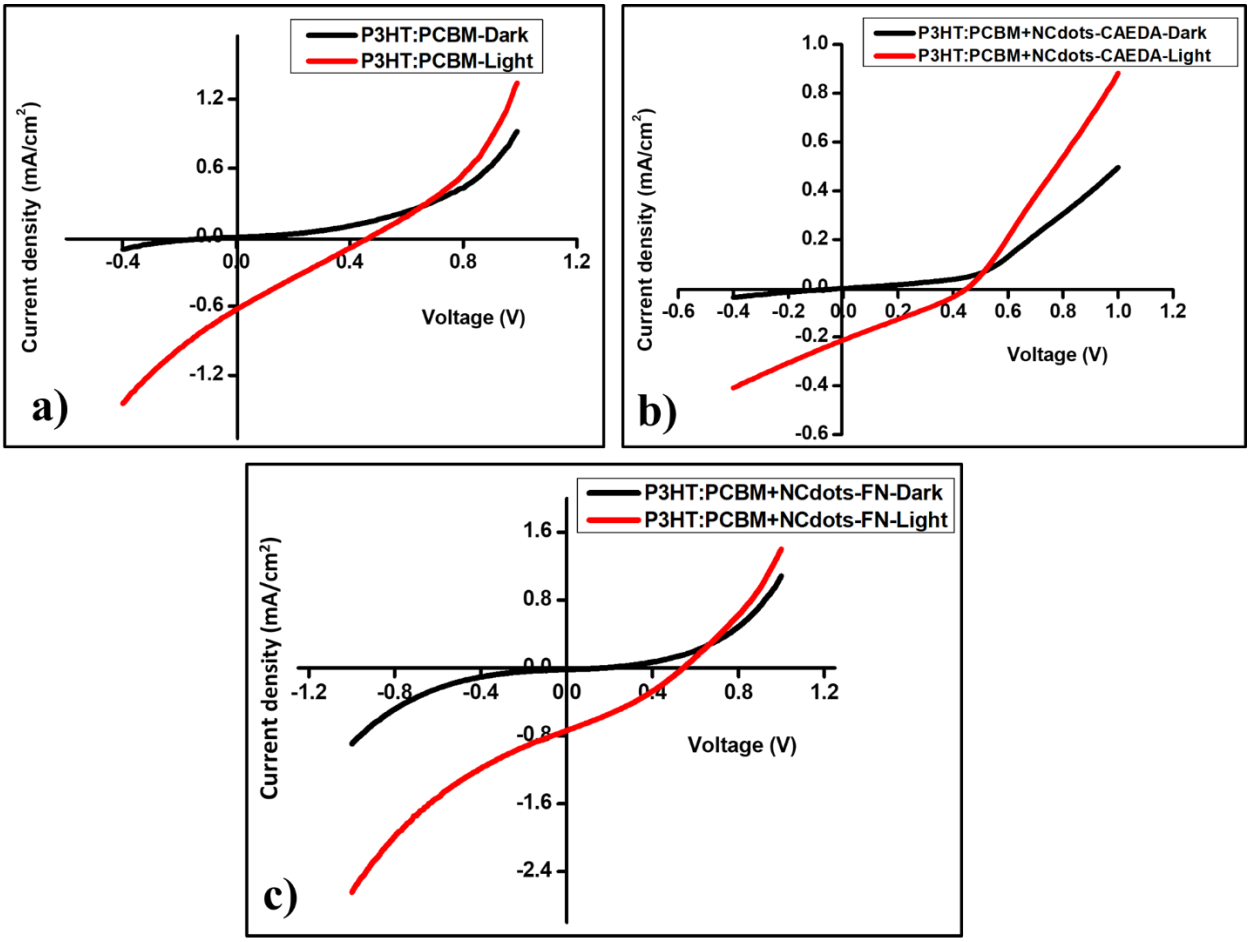

Figure 5.5: The current density-voltage curves of the organic BHJ devices with different active layers under dark and light conditions: a) P3HT:PCBM, b) P3HT:PCBM+NCdots-CAEDA and c) P3HT:PCBM+NCdots-FN.

Table 5.1: Summary of the operational parameters of the fabricated organic BHJ devices with different active layers.

Device architecture	V_{oc} (V)	J_{sc} (mA/cm^2)	FF (%)	PCE (%)
ITO/PEDOT:PSS/P3HT:PCBM/Al (Literature review)[13]	0.60	9.94	45.74	2.73
ITO/PEDOT:PSS/P3HT:PCBM/Al (reference cell)	0.47	0.06	24.7	0.01
ITO/PEDOT:PSS/P3HT:PCBM+NCdots-CAEDA/Al	0.45	0.21	27.7	0.03
ITO/PEDOT:PSS/P3HT:PCBM+NCdots-FN/Al	0.57	0.74	31.7	0.13

In order to optimize the efficiency of the organic BHJ cell, different percentages of N-Cdots (1 and 10 %) were incorporated into the active layer, while retaining the constant mass ratios of 1:1 for the donor and acceptor, respectively. The current density-voltage curves of the BHJ devices with different percentages of N-Cdots in the active layer are depicted in **Figure 5.6**. The values of the V_{oc}, J_{sc}, FF and PCE of the cell incorporated with 1 % NCdots-FN were measured to be 0.42 V, 0.17 mA/ cm^2, 28.0 % and 0.020 %, respectively (**Table 5.2 and Figure 5.6.a**). Upon increasing the percentage to 10 %, the J_{sc}, FF and PCE dropped to 0.14 mA/ cm^2, 25.2 % and 0.015 %, respectively, but the V_{oc} increased to 0.52 V. It was interesting to notice that under dark conditions, the J_{sc} was not zero for a device incorporated with 10 % NCdots-FN (**Figure 5.6.b**). This can be due to the strong and persistent fluorescence emissions of NCdots. We also fabricated a device with 5 % NCdots-FN and the current density-voltage curve is shown in **Appendix I**.

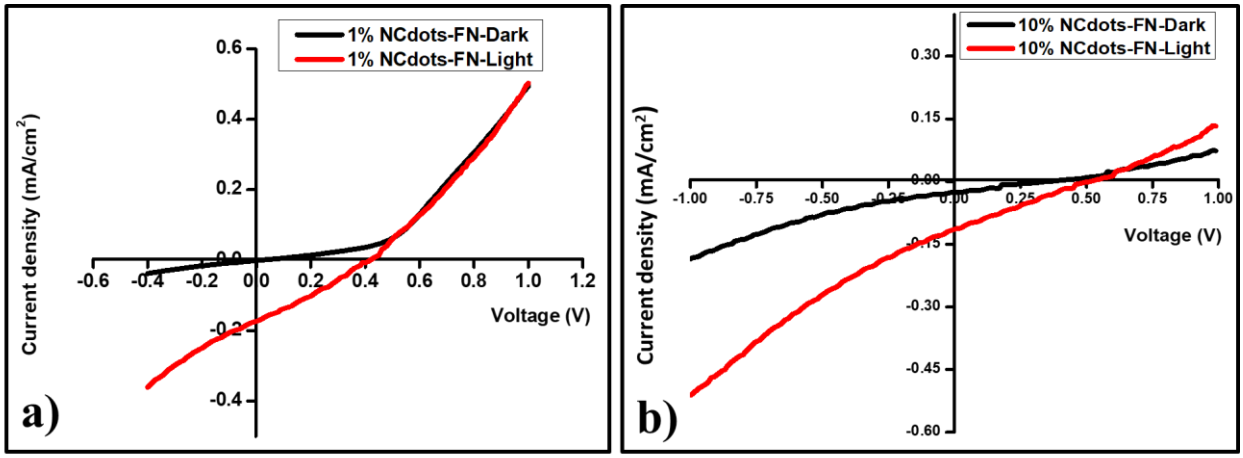

Figure 5.6: The current density-voltage curves of the organic BHJ devices with different percentage of NCdots-CAEDA in the active layers under dark and light conditions: a) 1 % and b) 10 %.

Table 5.2: Summary of the operational parameters of the fabricated organic BHJ devices with different percentage of NCdots-CAEDA in the active layers.

Device architecture	V_{oc} (V)	J_{sc} (mA/cm^2)	FF (%)	PCE (%)
ITO/PEDOT:PSS/P3HT:PCBM(1% NCdots-FN)/Al	0.42	0.17	28.0	0.020
ITO/PEDOT:PSS/P3HT:PCBM(10% NCdots-FN)/Al	0.52	0.14	25.2	0.015

5.4 Conclusions

In conclusion, we fabricated the organic BHJ device using P3HT:PCBM as the active layer (reference cell) and the devices modified with different types of N-Cdots. The results demonstrated that the modified devices outperformed the reference cell (without N-Cdots). In addition, devices modified with different percentages of NCdots-FN were fabricated and the device modified with 1 % NCdots-FN demonstrated better results. Future research efforts should focus on developing and designing materials with sufficient light absorption. The results showed that there is still a chance to significantly improve the PCE of the OSCs through introducing other materials with good properties for an efficient device.

References

1) Becquerel, A.E Comt. Rend. Acad. Sci. **1839**, 9, 561.
2) Lin, X.; Yang, Y.; Nian, L.; Su, H.; Ou, J.; Yuan, Z.; Xie, F.; Hong, W.; Yu, D.; Zhang, M.; et al. Interfacial Modi Fi Cation Layers Based on Carbon Dots for Efficient Inverted Polymer Solar Cells Exceeding 10 % Power Conversion Efficiency. *Nano Energy* **2016**, *26*, 216–223.
3) Thompson, B. C.; Frechet, J. M. J. Polymer – Fullerene Composite Solar Cells. *Angew. Chemie* **2008**, *47*, 58–77.
4) Bagher, A. M. Introduction to Organic Solar Cells. *Sustain. energy* **2014**, *2*, 85–90.
5) Qi, X.; Lo, Y.; Zhao, Y.; Xuan, L.; Ting, H.; Wong, K.; Rahaman, M.; Chen, Z.; Xiao, L.; Qu, B. Two Novel Small Molecule Donors and the Applications in Bulk-Heterojunction Solar Cells. *Front. Chem.* **2018**, *6*, 1–8.
6) Ranabhat, K.; Patrikeev, L.; Revina, A. A.; Andrianov, K.; Sofronova, E.; Lapshinsky, V. AN INTRODUCTION TO SOLAR CELL. *J. Appl. Eng. Sci.* **2016**, *14* (4), 481–491.
7) Mazzio, K. A.; Luscombe, C. K. The Future of Organic Photovoltaics. *R. Soc. Chem.* **2014**, (3), 1–13.
8) Chiechi, R. C.; Havenith, R. W. A.; Hummelen, J. C.; Koster, L. J. A.; Loi, M. A. Modern Plastic Solar Cells : Materials , Mechanisms and Modeling. *Mater. Today* **2013**, *16*, 281–289.
9) Elumalai, N. K.; Uddin, A. Open Circuit Voltage of Organic Solar Cells: An in-Depth Review. *Energy Environ. Sci.* **2016**, *9*, 391–410.
10) Troshin, P. A.; Lyubovskaya, R. N.; Razumov, V. F. Organic Solar Cells : Structure , Materials , Critical Characteristics , and Outlook. *Nanotechnologies Russ.* **2008**, *3*, 242–271.
11) Li, Z.; Liang, Y.; Zhong, Z.; Qian, J.; Liang, G.; Zhao, K.; Shi, H.; Zhong, S.; Yin, Y.; Tian, W. A Low-Work-Function , High-Conductivity PEDOT : PSS Electrode for Organic Solar Cells with a Simple Structure. *Synth. Met.* **2015**, *210*, 363–366.
12) Shnier, A. IVplot software, **2017**, 5.4.
13) Zhen-bo, D.; Zheng, C.; Hui, W.; Zhao-yue, L.; Hai-liang, D.; Ye, Z.; Guo-liang, Z.; Mao-yang, Z. High Efficiency Bulk Heterojunction Organic Solar Cell by Using High Conductivity Modified PEDOT : PSS as a Buffer Layer. *Optoelectron Lett.* **2012**, *8*, 1–4.

14) Abdulrazzaq, O. A.; Saini, V.; Bourdo, S.; Dervishi, E.; Biris, A. S. Organic Solar Cells: A Review of Materials, Limitations, and Possibilities for Improvement. *Part. Sci. Technol.* **2013**, *31*, 427–442.
15) Dennler, G.; Scharber, M. C.; Brabec, C. J. Polymer-Fullerene Bulk-Heterojunction Solar Cells. *Adv. Mater.* **2009**, *21*, 1323–1338.

CHAPTER 6: THE EFFECTS OF SYNTHESIS CONDITIONS ON THE FLUORESCENCE PROPERTIES OF NITROGEN-DOPED CARBON DOTS

6.1 Introduction

The synthesis, properties and applications of carbon dots (Cdots) have been studied intensively[1-5] because carbon nanomaterials are highly fluorescent. However, the actual photoluminescence (PL) mechanism of Cdots is still not understood. There are only few reports on the effect of reaction conditions on the fluorescence properties of Cdots[6-9]. Tuning the reaction conditions such as reaction temperature, microwave power, reaction time, reaction solvent, carbon precursor and surface passivation agent/ nitrogen precursor can have an impact on the fluorescence properties of Cdots. In terms of carbon precursors, citric acid (CA), as compared to other carbon precursors, has produced Cdots with good fluorescence properties. This is especially true when combined with amine molecules a surface passivation agent and/or nitrogen precursor[6,10,11]. This effect can be due to its carboxyl groups that tend to facilitate the dehydration and carbonization processes[12]. Zhai *et al.* investigated the effect of nitrogen precursors on the fluorescence properties of Cdots by using various amine molecules such as ethylenediamine (EDA), diethylamine (DEA), triethylamine (TEA) and butanediamine (BDA)[10]. Among these amine molecules, EDA as a primary amine molecule, produced the Cdots with the highest fluorescence. Their results demonstrated that different amine molecules as surface passivation agent and/or nitrogen precursor in preparation of Cdots, results in Cdots with different fluorescence properties.

Zhu *et al.* used a hydrothermal method to produce highly photoluminescent Cdots at various reaction temperatures[13]. At low and high temperatures they produced two different types of Cdots. Polymer-like Cdots were produced at low temperatures whereas the partial carbogenic Cdots were produced when high temperatures were used. They concluded that the fluorescence of the carbogenic Cdots was due to both the surface/molecule state and the synergistic effect of the carbogenic core whereas that of the polymer-like Cdots was due to the surface/molecule

state only, which might have been due to the fluorophore from the nitrogen-containing groups[13]. In **Chapter 4**, two different types of Cdots were studied (Cdots from citric acid plus ethylenediamine and fumaronitrile). In this section, Cdots from CA together with EDA were selected to be studied further in order to investigate the effect of reaction conditions due to the higher product yield and smaller sizes as compared to Cdots made from fumaronitrile (FN). Therefore, this section is a compilation of NCdots results obtained from CA and EDA (NCdots-CAEDA) at different reaction conditions in order to have a better insight on the fluorescence properties of Cdots.

In addition, other researchers found out that the functional groups on the surface of Cdots have a strong impact on their fluorescence properties[14-16]. Wang *et al*. investigated the effect of carboxyl groups on the fluorescence of Cdots by utilizing three different carbon sources that contained different contents of carboxyl groups[16]. The carbon sources used in their work included: glycolic acid, malic acid and citric acid, and urea was used as both nitrogen precursor and surface passivation agent. Their results demonstrated that the Cdots prepared from a carbon source with a higher content of carboxyl group (CA), exhibited the best fluorescence properties[16]. In this section, we will investigate the fluorescence properties of NCdots-CAEDA by removal of the functional groups on the surface of Cdots using annealing methods.

6.2 Synthesis procedures

6.2.1 Materials

Citric acid (CA, ACS reagent, ≥ 99.5%), 1,2-ethylenediamine (EDA, absolute, ≥ 99.5%), acetone (ACS reagent, ≥ 99.5%), ethylene glycol (EG, anhydrous, 99.8%) and dimethyl sulfoxide (DMSO, ≥ 99.5%), were obtained from Sigma-Aldrich. All these materials were used as received without further purification. Distilled water was obtained from the laboratory.

6.2.2 Synthesis of NCdots using different reaction conditions via microwave-irradiation method

Different conditions were used for the preparation of NCdots to investigate the effect of reaction conditions on these materials. In a standard experimental procedure, CA (1.0 g) and different amount of EDA (0, 0.5, 1.0, 1.5 and 2.0 ml EDA) were dissolved in 10 ml of different solvents (water, ethylene glycol (EG), dimethyl sulfoxide (DMSO) and acetone). The mixture was then transferred into a microwave tube and heated for various times (3, 5, 10, and 15 min) at different microwave power levels (500, 600, 700 and 800 W). The obtained yellow/brown

solutions were then centrifuged at a speed of 15000 rmp for 15 min to remove large particles. Lastly, the final product was filtered with a 0.2 microfilter for further purification. The rotary evaporator was then used to evaporate off the water from the Cdots solution. The resultant product was allowed to dry in a vacuum oven at 70 ºC. Several characterisation techniques such as transmission electron microscopy (TEM) and photoluminescence spectroscopy (PL) were then used to characterise the final product.

6.2.3 Annealing method.

In order to investigate the effect of annealing, NCdots-CAEDA obtained from Chapter 4 were annealed using a horizontal chemical vapor deposition (CVD) setup as shown in **Figure 6.1**. The functional groups were removed in order to investigate the fluorescence properties of NCdots-CAEDA. In a standard procedure, 1.0 g NCdots-CAEDA was added into a quartz boat and placed in a quartz tube. The quartz tube was then placed in the horizontal temperature-controlled furnace. The sample was heated at 500 ℃ for 2 h at a heating rate of 10 ℃/min in the presence of argon as a carrier gas. The flow rate of argon was 100 ml/min. Upon completion of the reaction, the resultant product was allowed to cool to room temperature under a continuous flow of argon gas. The product was then collected and characterized by several techniques including: thermogravimetric analysis (TGA), Fourier transform infrared spectroscopy (FTIR), PL, Raman spectroscopy and powder X-ray diffraction (PXRD).

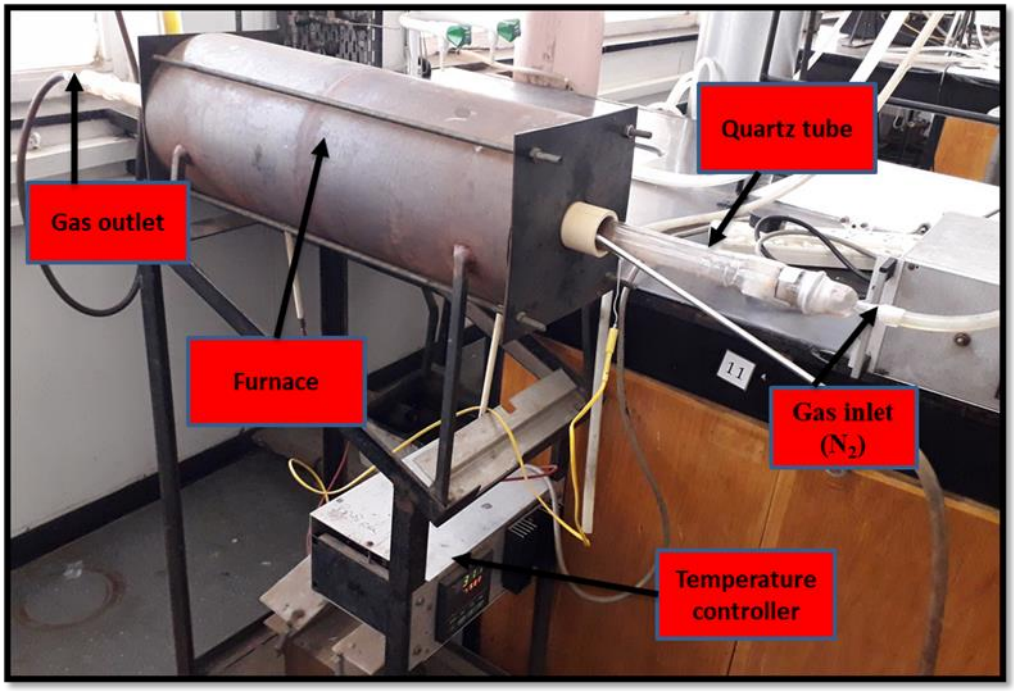

Figure 6.1: Horizontal CVD reactor used for annealing NCdots-CAEDA.

6.3. Results and discussion

6.3.1. Effects of EDA amount on the fluorescence properties of carbon dots

In this section the amount of EDA added to CA was varied from 0 to 2.0 ml (precursor ratio), while the solvent, reaction time and microwave power were kept constant as shown in **Table 6.1**. The morphology and particle sizes of the as-synthesized Cdots prepared from different amount of EDA were determined by TEM and the images are shown in **Figure 6.2**. When Cdots were prepared with just CA (without passivation agent or nitrogen precursor), no Cdots were observed from TEM studies. From this result, we speculated that 10 min was not long enough for Cdots to be formed, meaning that no carbonization took place. This was also indicated by the lack of color change after the completion of the reaction.

TEM images of the as-synthesized Cdots prepared using 0.5, 1.0, 1.5 and 2.0 ml EDA showed that Cdots were quasi-spherical and less than 10 nm in diameter. **Figure 6.2.a** shows TEM image of Cdots prepared from 0.5 ml EDA. Only a few Cdots were observed. This could be due to the small amount of EDA added. The Cdots prepared with 1.0 ml **(Figure 6.2.b**) were well-dispersed as compared to other Cdots prepared from other amounts of EDA used. For Cdots prepared with 1.5 and 2.0 ml EDA (**Figure 6.2.c and d**), TEM revealed that the nanoparticles were aggregated, forming larger materials. TEM image of Cdots prepared with 2.0 ml EDA (**Figure 6.2.d)** demonstrated a clearer agglomeration of nanoparticles.

The results showed that the average sizes of Cdots increased with an increasing amount of EDA as indicated in **Table 6.1** and **Figure 6.3**. The average sizes of Cdots prepared using 0.5, 1.0, 1.5 and 2.0 ml EDA were found to be 1.4, 3.5, 5.1 and 5.6 nm, respectively. These results were similar to the results reported by Gong *et al*. where it was concluded that adding more nitrogen precursor and/or surface passivation agent tended to facilitate the growth of the carbon core, thus leading to the formation of large Cdots[17]. The TEM image of the Cdots prepared with 2.0 ml EDA were found to be the largest as compared to other samples.

Table 6.1: Effect of EDA amount on the preparation of Cdots.

EDA amount (ml)	Precursor ratio (CA:EDA)	Solvent (10 ml)	Time (min)	Power (W)	Cdots size (nm)
0	1:0	Water	10	700	-
0.5	1:1	Water	10	700	1.4
1.0	1:3	Water	10	700	3.5
1.5	1:4	Water	10	700	5.1
2.0	1:6	Water	10	700	5.6

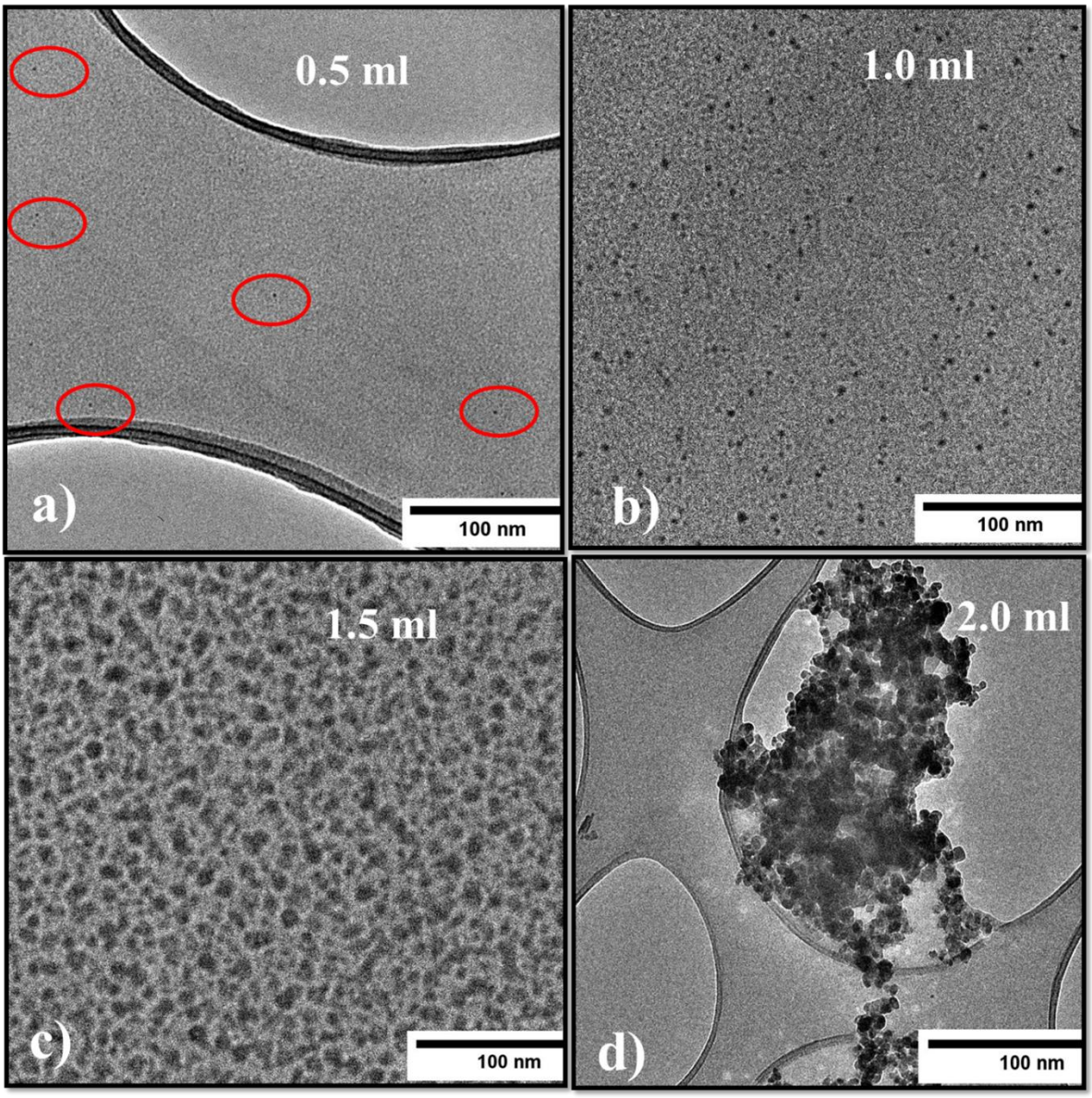

Figure 6.2: TEM images of Cdots prepared from CA with different amount of EDA: a) 0.5 ml b) 1.0 ml c) 1.5 ml and d) 2.0 ml.

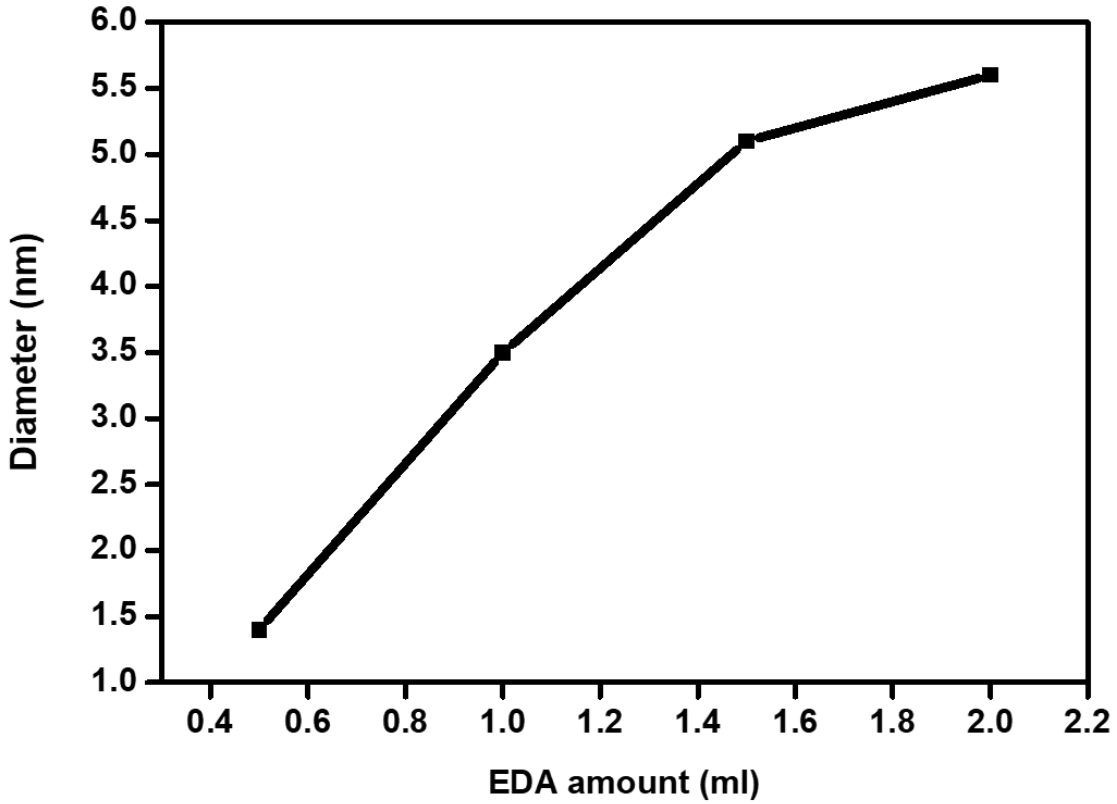

Figure 6.3: A plot of the Cdots diameters versus EDA amounts.

The PL spectra of the aqueous solution of the as-synthesized Cdots prepared from different amount of EDA, together with the corresponding plot of EDA amount against emission wavelength is shown in **Figure 6.4**. The samples showed a broad PL emission peak which was symmetrical on the scale of the wavelength, and this is a characteristic for highly fluorescent Cdots[11,18]. The PL emission peak positions are always associated with the excitation wavelength. All samples were excited at a 365 nm excitation wavelength. There was no PL emission peak observed from Cdots prepared with no EDA (0 ml EDA) and these results are in agreement with TEM results as no Cdots were observed.

The amount of EDA added during the preparation of Cdots plays an important role in the formation of highly fluorescent Cdots. The PL emission peak positions of Cdots prepared from 0.5, 1.0, 1.5 and 2.0 ml were located at 460, 457, 452 and 446 nm, respectively (**Figure 6.4.a**). The PL results showed that there was an obvious trend between the PL emission peaks and the amount of EDA added as shown in **Figure 6.4.b**. As the amount of EDA increased, the PL emission wavelength decreased. Therefore, Cdots prepared with different amount of EDA exhibited a blue-shift with an increasing amount of EDA. Devi *et al*. produced similar results

when they used soot powder and EDA as the carbon and nitrogen precursor, respectivly[19]. As they increased the amount of EDA, the PL emission peaks shifted to shorter wavelengths at a 370 nm excitation wavelength.

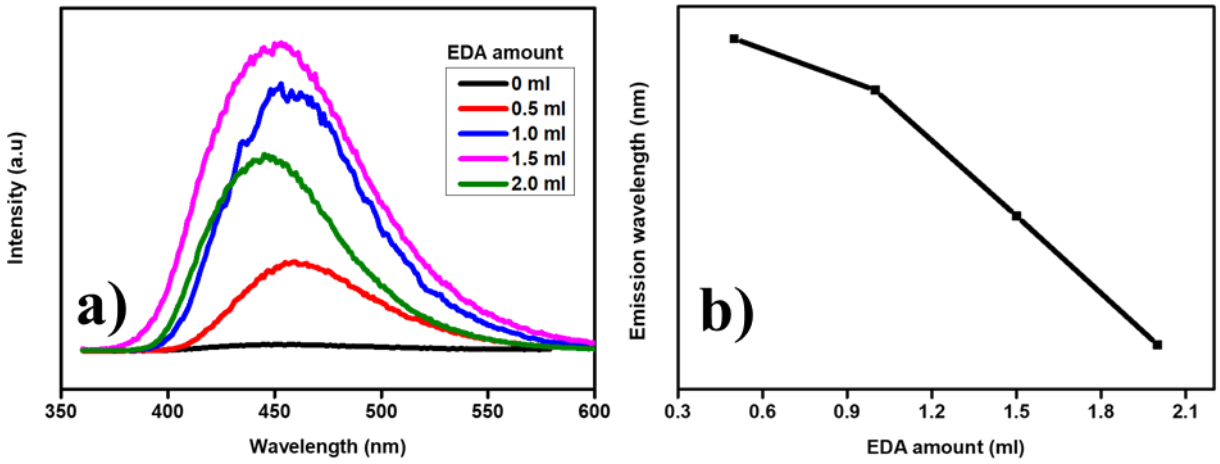

Figure 6.4: a) PL spectra of the aqueous solution of the Cdots prepared with various amount of EDA b) with their corresponding plot of EDA amount against emission wavelength.

6.3.2 Effect of solvent on the fluorescence properties of carbon dots.

In this section, Cdots were prepared using various solvents, viz; water, DMSO, EG and acetone. Their structures are shown in **Figure 6.5**. Other reaction conditions such as the amount of EDA, microwave power and reaction time were kept constant as shown in **Table 6.2**. Cdots prepared with 1.0 ml of EDA (1:3 (CA:EDA)) was chosen as the optimal amount of EDA in preparing Cdots from different solvents as TEM results showed well-dispersed image and PL revealed reasonable PL emissions in water.

TEM images of Cdots prepared from different solvents are depicted in **Figure 6.6**. The results showed that the resultant Cdots prepared with different types of solvents were quasi-spherical with diameters less than 10 nm. In addition, Cdots prepared from different solvents showed no sign of agglomeration. The average sizes of Cdots prepared from water, DMSO and EG were determined to be 3.5, 2.7 and 3.4 nm, respectively. The Cdots prepared from water as a solvent were the largest (3.5 nm) (**Figure 6.6.a**). The Cdots prepared from acetone (**Figure 6.6.b**) were very small and few, hence it was difficult to determine their average size. TEM image of Cdots prepared with DMSO and EG demonstrated a mixture of small and large particles (**Figure 6.6.c and d**). According to the results obtained, it was observed that different solvents produced Cdots with different sizes. Tian *et al*. used different types of solvents such as: water, glycerol

and dimethylformamide (DMF) to prepare Cdots from CA and urea as the carbon and nitrogen precursor, respectively[20]. Their results demonstrated that indeed different solvents produce Cdots with different sizes (Cdots-water = 1.70 nm, Cdots-glycerol = 2.80 nm, Cdots-DMF = 4.50 nm)[20].

Table 6.2: Effect of solvent on the preparation of Cdots.

EDA amount (ml)	Precursor ratio (CA:EDA)	Solvent (10 ml)	Power (W)	Time (min)	Cdots size (nm)
1.0	1:3	Water	700	10	3.5
1.0	1:3	Acetone	700	10	-
1.0	1:3	EG	700	10	3.4
1.0	1:3	DMSO	700	10	2.7

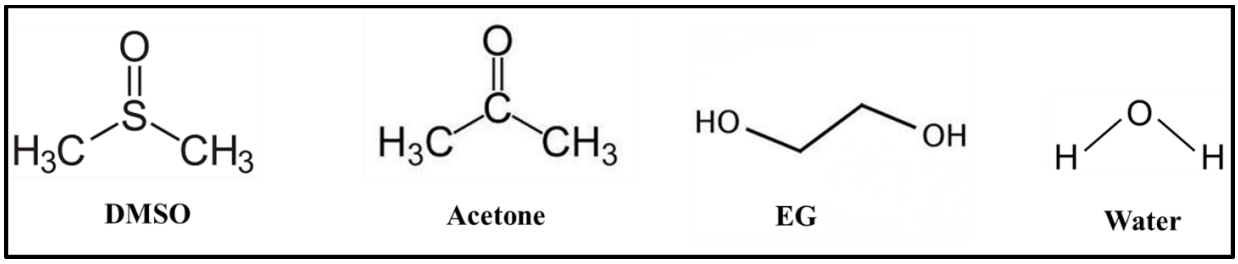

Figure 6.5: The structures of different solvents used to prepare the Cdots to investigate the solvent effect on the fluorescence of the Cdots.

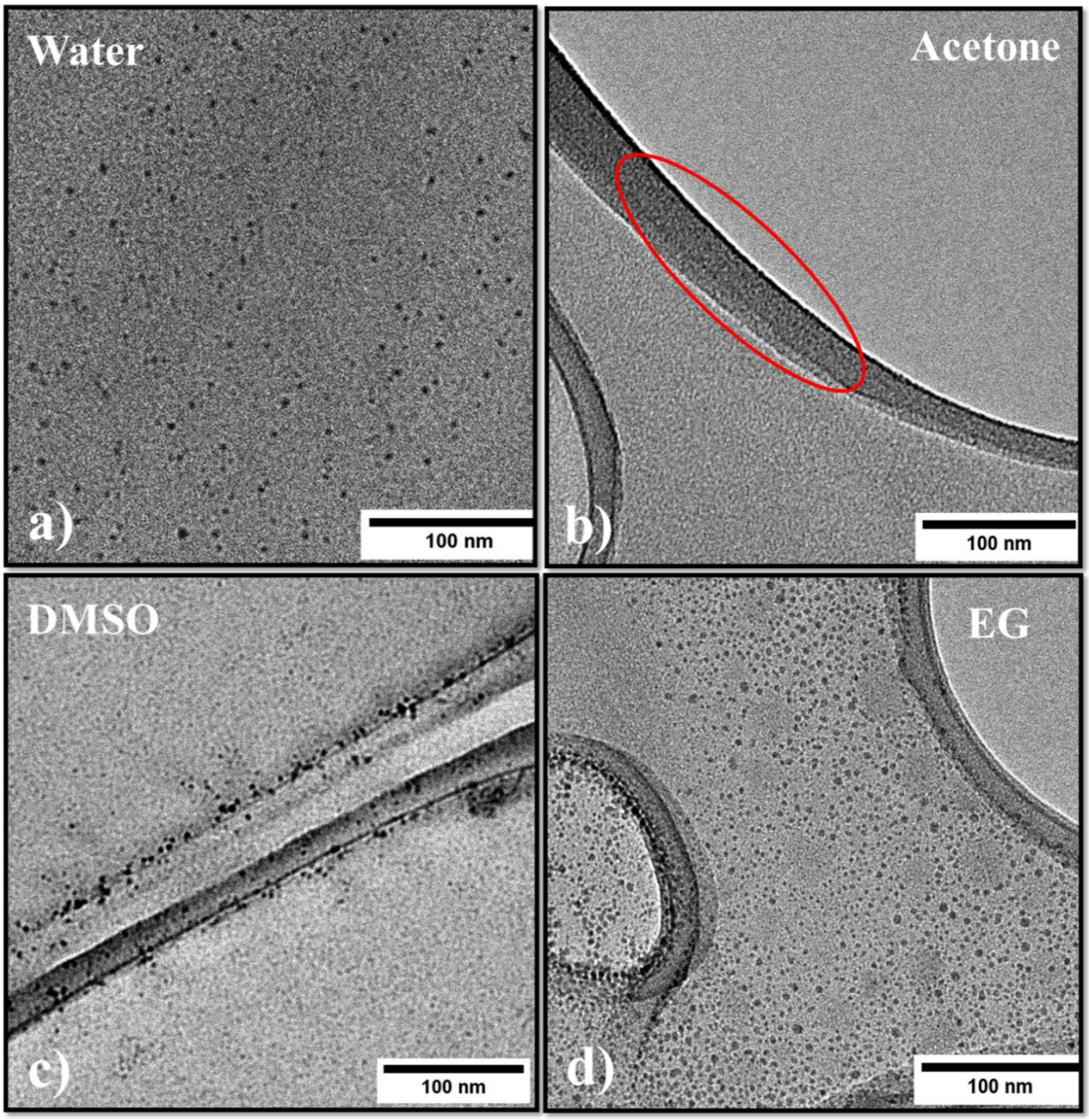

Figure 6.6: TEM images of the Cdots prepared from CA and EDA using different solvents: a) water b) acetone c) DMSO and d) EG.

The fluorescence properties of the Cdots prepared from different solvents were studied and investigated using PL spectroscopy and their spectra are shown in **Figure 6.7.a**. The PL measurements of the Cdots prepared from different solvents were performed at 365 nm excitation wavelength. The PL emission of the Cdots prepared from water, DMSO and EG were not the same and were centered at 455, 431 and 466 nm, respectively. The plot of solvents as a function of their PL emission wavelength is shown in **Figure 6.7.b**. The Cdots prepared from water demonstrated the strongest fluorescence emission at 455 nm. The Cdots prepared

from acetone did not show any PL emission peak. We speculated that the difference in PL emissions of these Cdots might be due to the fact that these solvents possess different dielectric constants and polarities. The dielectric constant of acetone, water, DMSO and EG are 21.0, 78.5, 47.0 and 37.7, respectively[21]. Acetone has a lower dielectric constant (21.0) and this might have contributed to the absence of the PL emission peak.

The PL emission peaks of Cdots prepared from water, DMSO and EG were broad but that from DMSO was broader and unsymmetrical. We speculated that the broadness of the PL emission peak of Cdots prepared from DMSO might be due to a range of functional groups/defects on their surface and heterogeneity of the particle sizes[22]. The PL emission peak position of Cdots prepared from water and EG were similar, but the PL emission peak position of those prepared from DMSO was different. This might be due to the polarity of these solvents as DMSO is the least polar solvent. The polarity of these solvents increase as the following trend: acetone < DMSO < EG < water.

From the results obtained in this section, water was chosen as the optimal solvent because it demonstrated the strongest fluorescence emission. In addition, water is a safe and green solvent as compared to other solvents used in this study[23]. In order to investigate the effect of solvents on the fluorescence properties of Cdots, Chao *et al*. dispersed Cdots synthesized from o-phenylenediamine as both carbon and nitrogen precursor, in various solvents such as water, EG, methanol, DMF, acetone and tetrahydrofuran (THF)[24]. Their results showed that there was a red-shift in the PL emissions with an increasing polarity of the solvent except for water[24]. Their results are similar to our results as there is a red shift from the Cdots prepared from DMSO compared to those prepared from EG.

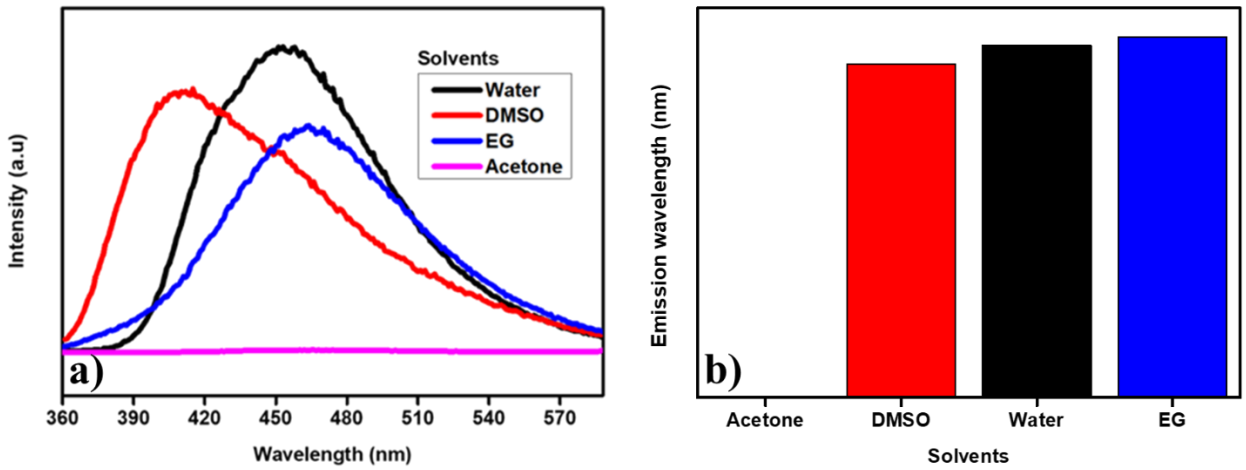

Figure 6.7: a) PL spectra of the Cdots prepared from water, DMSO, EG and acetone, (in water) b) The plot of the types of solvents against emission wavelength.

6.3.3 Effect of reaction time on the fluorescence properties of carbon dots.

In this section, we present the synthesis of the Cdots samples prepared at different reaction times. The amount of EDA, reaction power and reaction solvent were kept constant as shown in **Table 6.3**. The reaction time utilized in this section were 3, 5, 10 and 15 minutes (min). When the reaction was run for 3 min, the obtained solution was pale yellow in colour. As the reaction time was increased from 3 min to 5 min, the colour of the solution changed from pale yellow to light brown and then dark brown when the reaction was prolonged to 10 and 15 min. The colour change indicated the formation of Cdots. The microwave reaction time had a significant impact on the formation of the Cdots as TEM images of the Cdots prepared at different reaction times demonstrated different sizes of the resultant products (**Figure 6.8**). The average sizes of the Cdots prepared at 3, 5, 10 and 15 min were determined to be 1.5, 1.7, 3.5 and 20.2 nm, respectively. The Cdots prepared at 3 and 5 min **(Figure 6.8.a and b)** were similar in size but the once prepared at 5 min were better dispersed than the 3 min ones.

The Cdots prepared at 10 min **(Figure 6.8.c)** were also well-dispersed but bigger than the ones prepared at 3 and 5 min. At 15 min, the starting materials reacted and carbonized completely and grew into bigger structures and there were no smaller particles observed in the TEM image **(Figure 6.8.d).** The product obtained after 15 min are not Cdots. It is worth noting that the Cdots particle sizes increases with an increasing reaction time[25] as shown in **(Figure 6.9)**.

Table 6.3: Effect of reaction time on the preparation of the Cdots.

EDA amount (ml)	Precursor ratio (CA:EDA)	Solvent (10 ml)	Time (min)	Power (W)	Cdots size (nm)
1.0	1:3	Water	3	700	1.5
1.0	1:3	Water	5	700	1.7
1.0	1:3	Water	10	700	3.5
1.0	1:3	Water	15	700	20.2

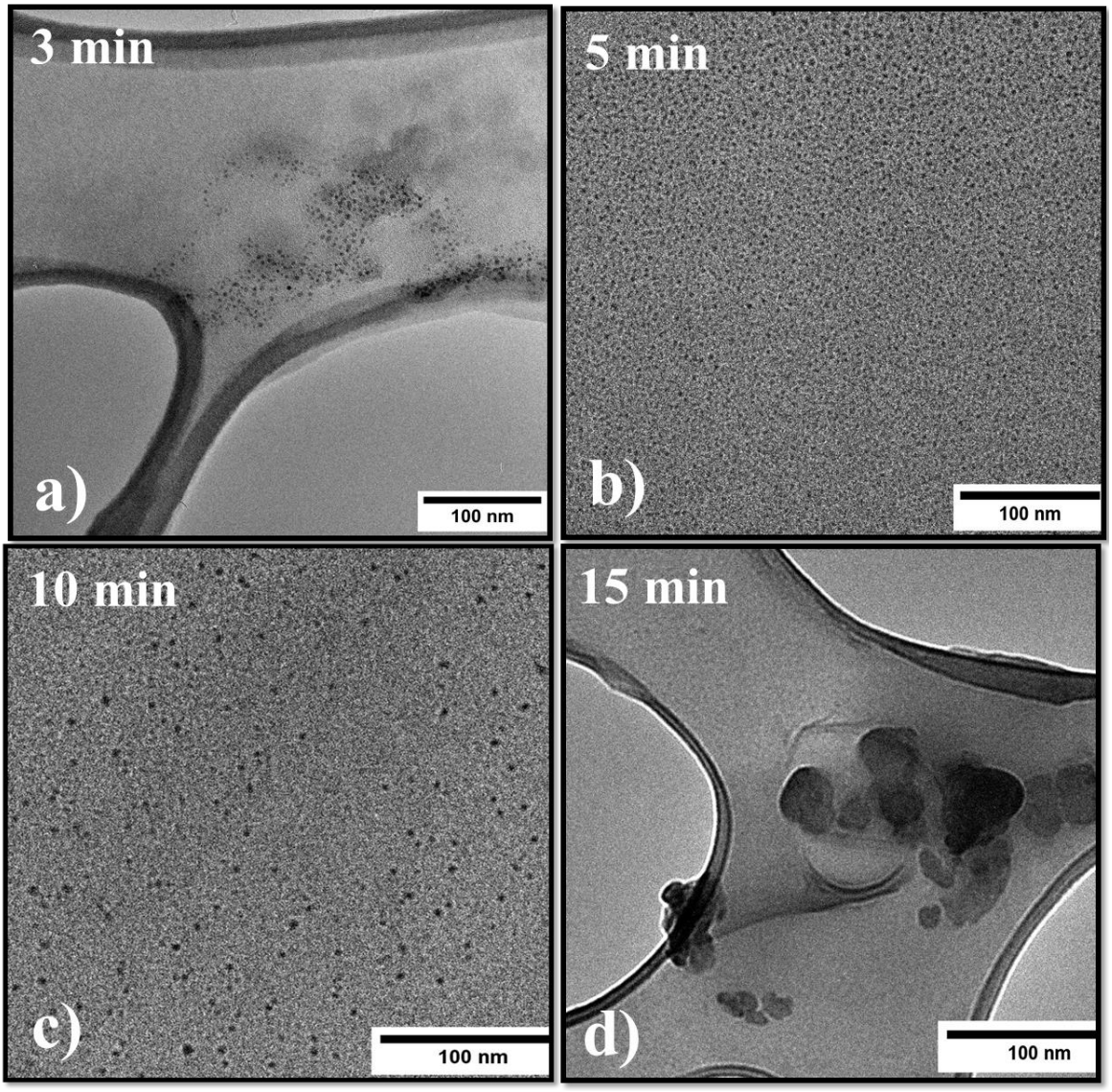

Figure 6.8: TEM images of Cdots prepared from CA and EDA at different reaction times: a) 3 min b) 5 min c) 10 min and d) 15 min.

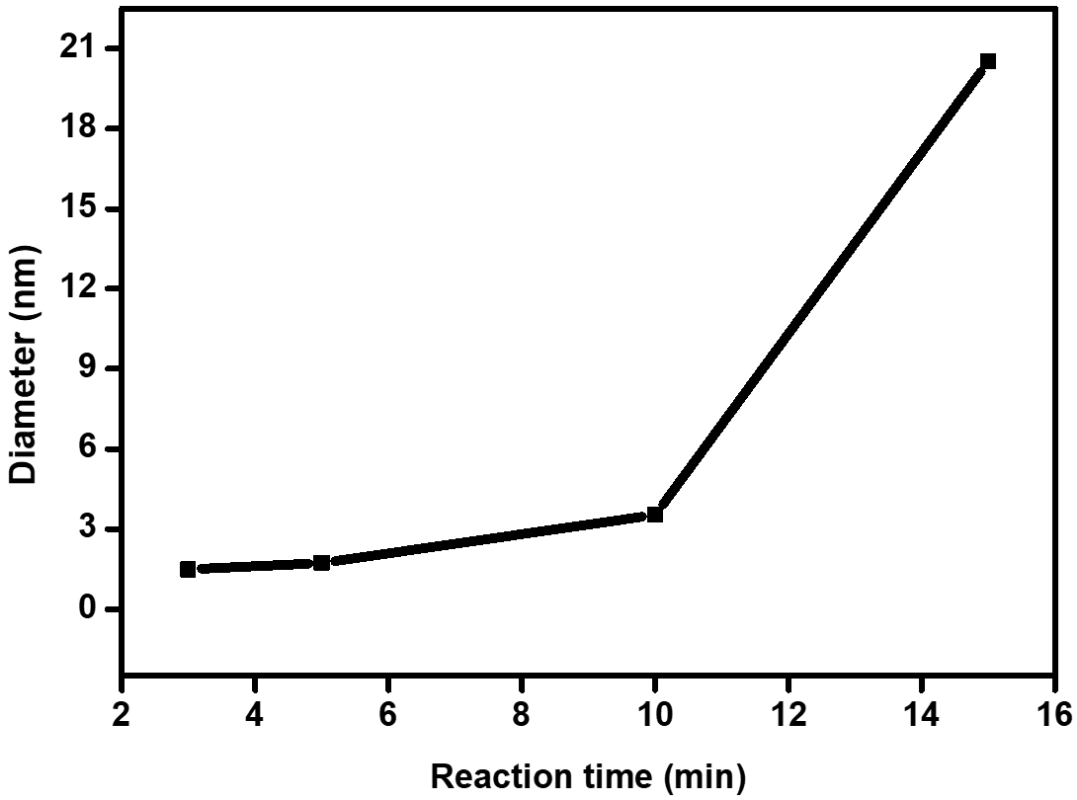

Figure 6.9: A plot of the Cdots diameters versus reaction time.

PL spectroscopy was used to investigate the fluorescence properties of Cdots prepared at different reaction times and their spectra are shown in **Figure 6.10.a**. The PL emission was affected by the reaction time. The PL emission peaks of Cdots prepared at 3, 5, 10 and 15 min were centered at 461, 457, 465 and 450 nm, respectively. A blue-shift was observed as we increased the reaction time (except the 10 min reaction) **(Figure 6.10.b)**. The fluorescence emission of the Cdots prepared at 15 min was very weak. This is because they have grown to bigger structures as shown by TEM images.

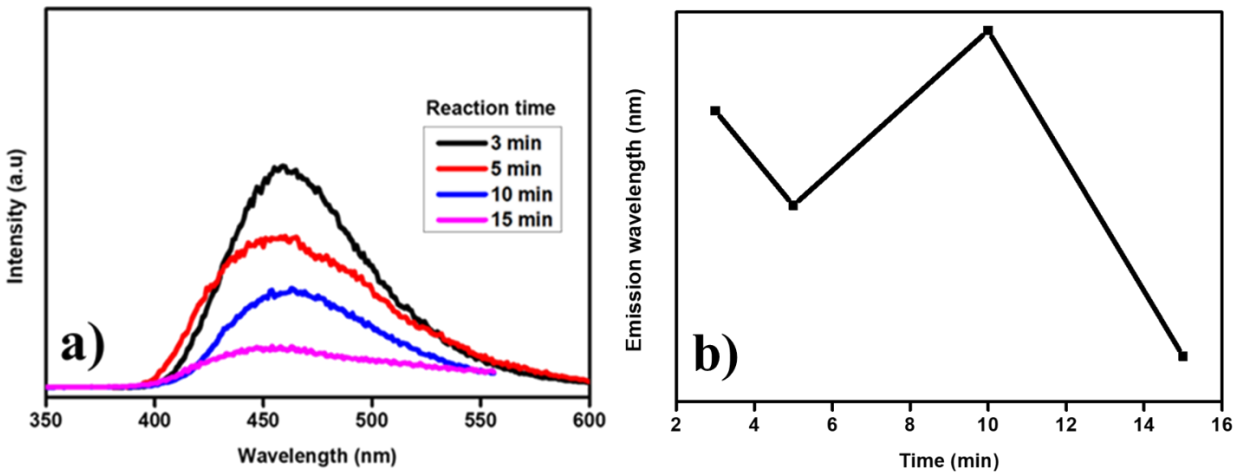

Figure 6.10: a) PL spectra of the aqueous solution Cdots prepared at various reaction times b) The plot of reaction time against emission wavelength.

6.3.4 Effect of microwave power

In this section, four different microwave powers were chosen for the preparation of Cdots while the amount of EDA, solvent and reaction time were kept constant **(Table 6.4)**. The microwave power utilized were 500, 600, 700 and 800 W. The morphology and the particle size were determined by TEM and the images are shown in **Figure 6.11**. The average sizes of the Cdots prepared at 500, 600, 700 and 800 W were measured to be 2.3, 2.4, 3.5 and 7.7 nm, respectively. There was no a significant different between the Cdots prepared at 500 and 600 W **(Figure 6.11.a and b)**. When the microwave power was increased to 700 W, the size of the particles increased slightly **(Figure 6.11.c)**. The particle size increased significantly when the microwave power was further increased to 800 W **(Figure 6.11.d).** The plot of particle size versus microwave power is shown in **(Figure 6.12)**.

Table 6.4: Effect of microwave power on the preparation of the Cdots.

EDA amount (ml)	Precursor ratio (CA:EDA)	Solvent (10 ml)	Time (min)	Power (W)	Cdots size (nm)
1.0	1:3	Water	10	500	2.3
1.0	1:3	Water	10	600	2.4
1.0	1:3	Water	10	700	3.5
1.0	1:3	Water	10	800	7.7

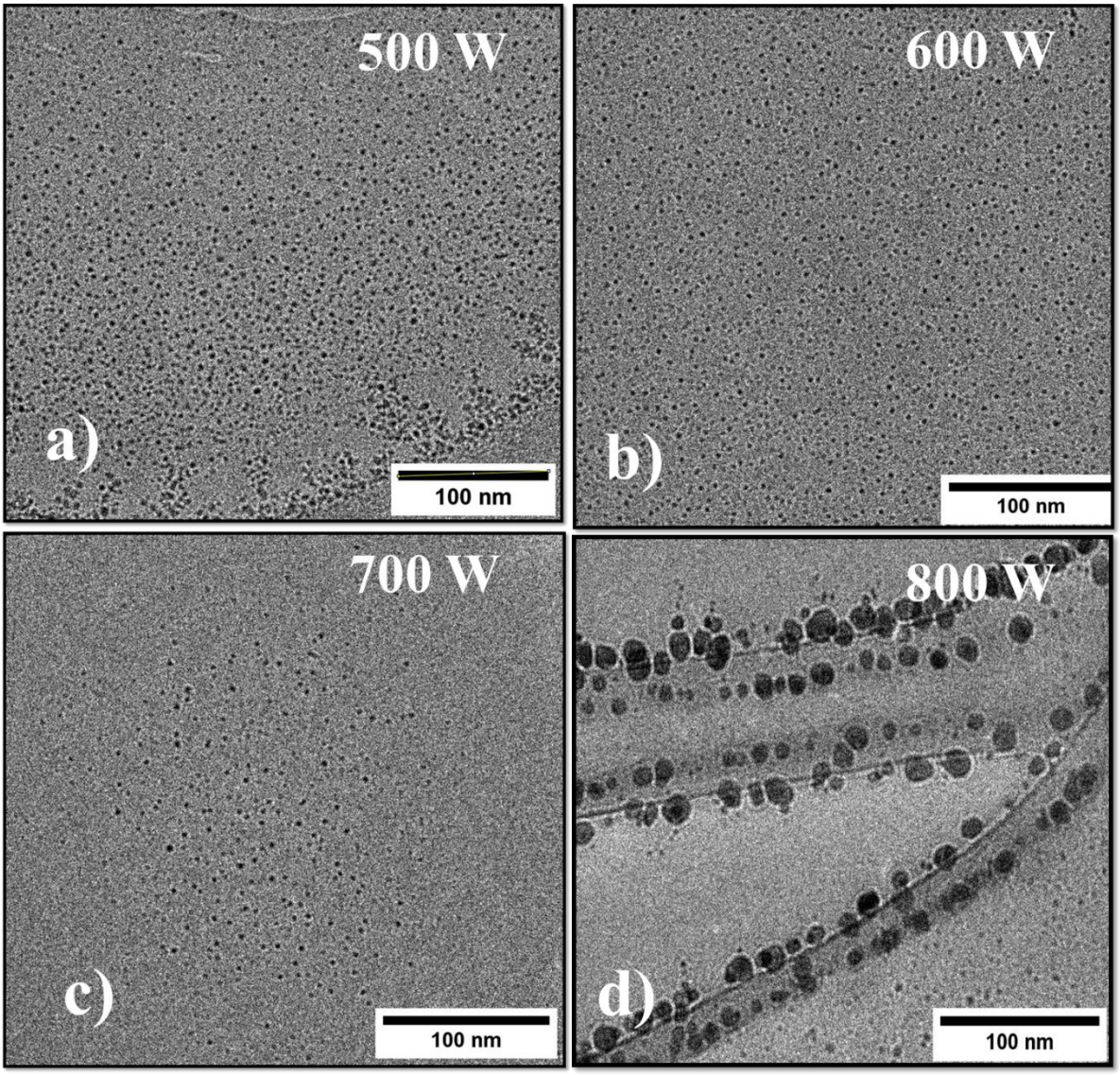

Figure 6.11: TEM images of NCdots prepared from CA and EDA at different microwave powers: a) 500 W b) 600 W c) 700 W and d) 800 W.

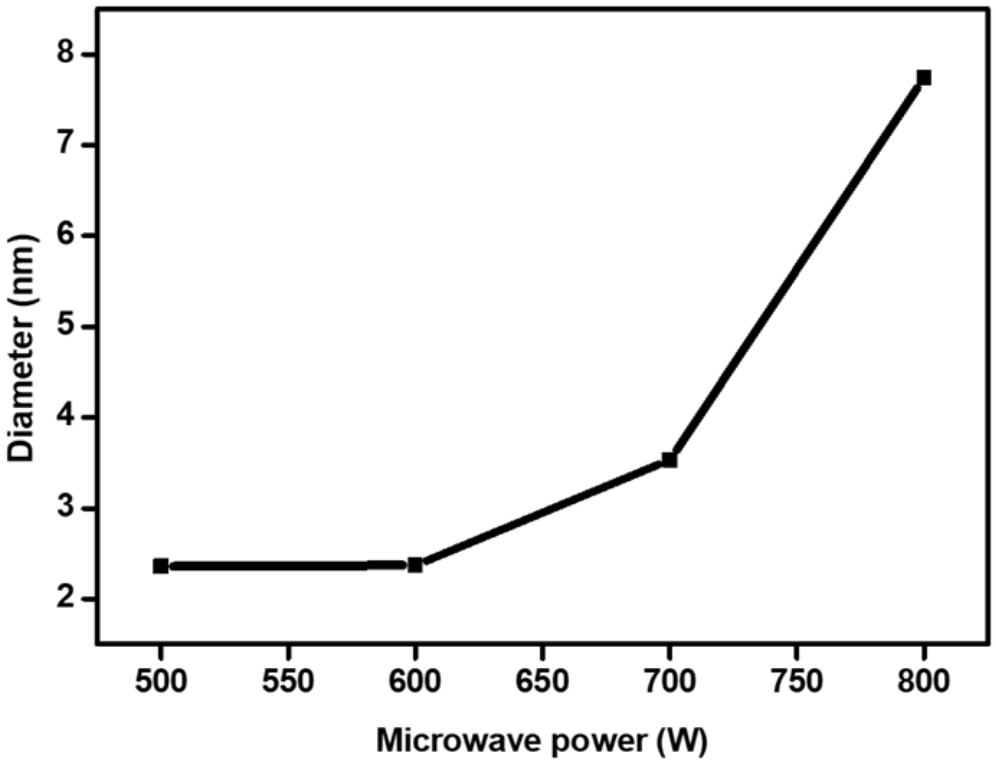

Figure 6.12: A plot of Cdots diameters versus microwave power.

The PL spectra of the Cdots prepared at various microwave powers are shown in **Figure 6.13.a**. The PL emission peaks of the Cdots prepared at 500, 600, 700 and 800 W were located at 506, 497, 466 and 446 nm, respectively. The PL emissions shifted from red to blue with increasing microwave power **(Figure 6.13.b)**. According to the results obtained from TEM, the Cdots prepared at 500 and 600 W had similar particle diameters but their PL emissions differ remarkably. From this, we can therefore assume that the particle sizes or quantum confinement effect, is not the only factor that contributes to the fluorescence of the Cdots as there was a significant impact on the fluorescence properties of the Cdots prepared at 500 and 600 W even though their particle sizes were similar.

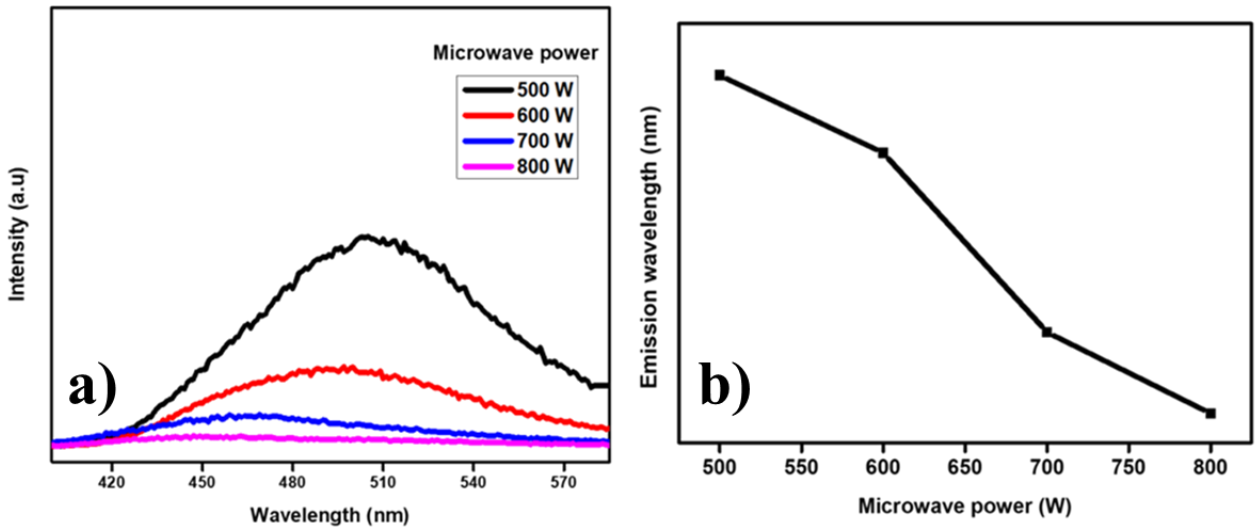

Figure 6.13: a) PL spectra of the aqueous solution Cdots prepared at various microwave power b) The plot of microwave power against emission wavelength.

6.3.5 Effect of annealing NCdots-CAEDA on their fluorescence properties

As mentioned before, the Cdots have different functional groups on their surface and this gives them the opportunity to be modified with different materials such as polymers, inorganic and organic molecules. In this section we have investigated the fluorescence of Cdots based on their functional groups. This was done by removing the functional groups on the surface of the NCdots-CAEDA using annealing methods and the procedure was explained in detail in **section 6.2.3**. TGA, FTIR, PL, Raman and PXRD were used in order to analyze the NCdots-CAEDA after annealed at 500 ℃ for 2 h. **Figure 6.14.a and b** depict the TGA-DTGA profiles of NCdots-CAEDA before and after annealing, respectively. Before annealing **(Figure 6.14.a)**, the TGA profile demonstrated about 30 % weight loss of functional groups at temperatures between 200 and 500 ℃[11]. After annealing **(Figure 6.14.b)**, there were no decomposition peaks observed in the TGA profiles.

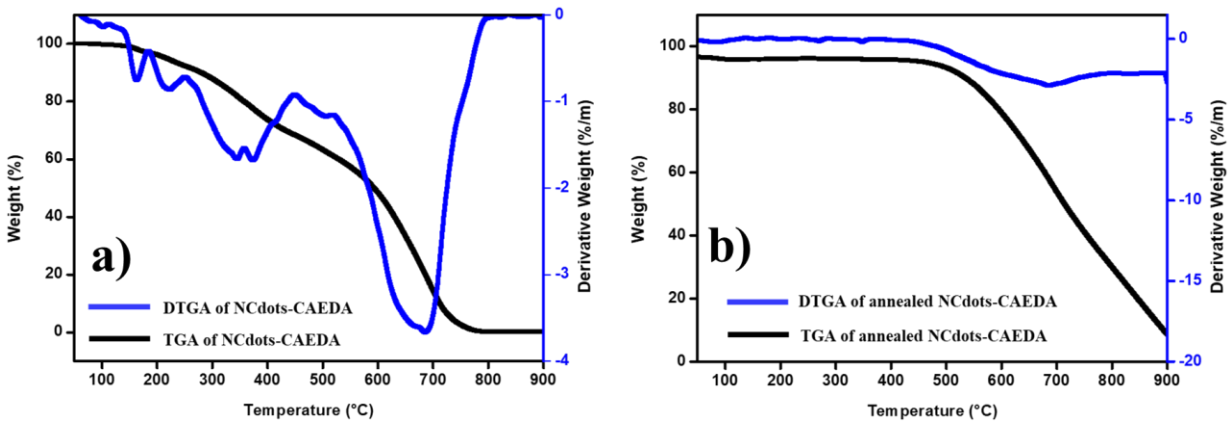

Figure 6.14: TGA-DTGA profiles of NCdots-CAEDA a) before and b) after annealing.

FTIR spectroscopy was used in order to confirm a complete removal of the functional groups on the surface of the NCdots-CAEDA. The FTIR spectra of the NCdots-CAEDA before and after annealing are shown in **Figure 6.15.a**. Before annealing, the FTIR spectrum demonstrated various functional groups on the surface of the NCdots-CAEDA and after annealing, the functional groups were removed completely and these results are in agreement with TGA data. We also used PL spectroscopy to investigate the fluorescence properties of the NCdots-CAEDA. The PL spectra of the NCdots-CAEDA before and after annealing are shown in **Figure 6.15.b**. Before annealing, there was a broad PL emission peak centered at 470 nm upon 365 nm excitation wavelength. After annealing, no PL emission peak was observed from the PL spectrum. This can be an indication that the fluorescence properties of Cdots depend on their surface functional groups.

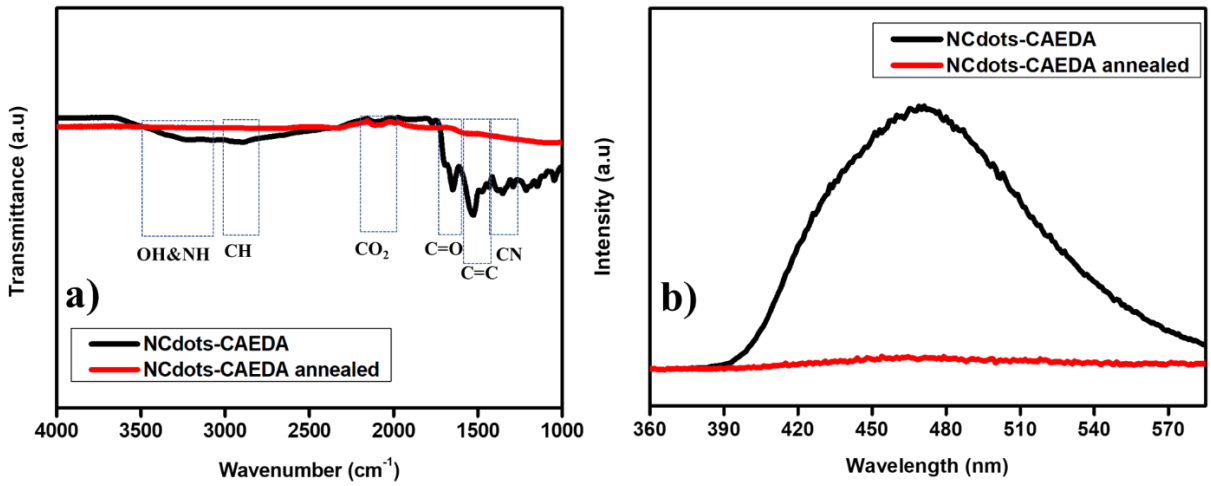

Figure 6.15: a) The FTIR and b) the PL spectra of the NCdots-CAEDA before and after annealing.

We also used laser Raman spectroscopy to determine the degree of graphitization of the sample. It was found out that before annealing the NCdots-CAEDA, no peaks were observed in the Raman data. This is because of the high fluorescence of the NCdots-CAEDA that interferes with the Raman characterization. After annealing **(Figure 6.16.a)**, two prominent peaks were observed at 1351 and 1572 cm^{-1}, which were attributed to the D and G bands, respectively. The D band refers to the structural disorder/defects and sp^3 hybridization whereas the G band is associated with the graphitic order and sp^2 bonding[4,26,27]. The ratios between the D and G intensities (integrated areas) were used to measure the degree of disorder/defects in the resultant product[28]. The I_D/I_G ratio was determined to be 0.62 which indicated that the annealed sample was graphitic in nature.

PXRD data was used for the phase identification and determination of the crystallinity of the resultant product. The PXRD patterns of the NCdots-CAEDA before and after annealing are demonstrated in **Figure 6.16.b**. Before annealing, there was a broad peak centered at 2Theta = 23.1° and a small peak at 2Theta = 40.0 °. After annealing, the broad peak became narrow and sharp, and shifted to 2Theta = 25.2 °. The small peak after annealing was more pronounced than before annealing and shifted to 2Theta = 44 °. The sharpness of the peak and the more pronounced small peak indicate that the annealed NCdots-CAEDA have a higher degree of graphitization than the un-annealed NCdots-CAEDA and these results are in agreement with the Raman data.

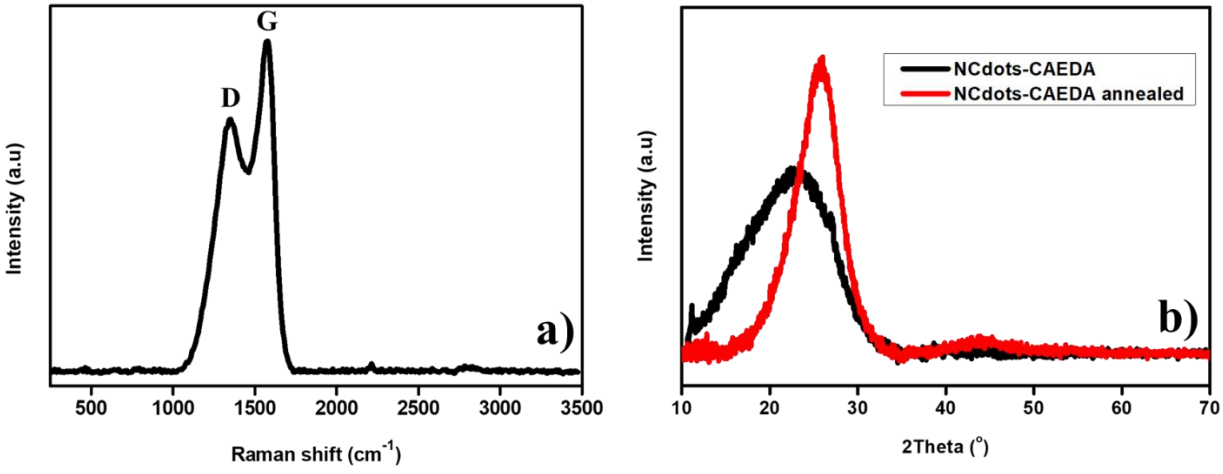

Figure 6.16: a) Raman spectrum of the annealed NCdots-CAEDA b) PXRD patterns of NCdots-CAEDA before and after annealing.

6.4 Conclusions

In conclusion, the fluorescence properties of Cdots prepared from CA and EDA as carbon and nitrogen precursors, respectively, were investigated. Different reaction conditions such as the reaction time, microwave power, solvent and the amount of EDA were used in order to investigate the fluorescence properties of NCdots-CAEDA. According to the results obtained, 1.0 ml EDA, water, 10 min and 500 W were found to be the optimal synthesis conditions for the preparation of the NCdots-CAEDA with good fluorescence properties. The fluorescence properties of NCdots-CAEDA were found to be highly dependent on the reaction conditions. Using different reaction conditions resulted in Cdots with different PL emissions and particle sizes. The NCdots-CAEDA was also annealed in order to remove the surface functional groups and to investigate the fluorescence properties of NCdots-CAEDA. It was found that after annealing, the fluorescence of NCdots-CAEDA were destroyed. We can therefore conclude that the fluorescence properties of NCdots-CAEDA strongly depend on the quantum confinement effect as well as the functional groups on their surface.

References

1) Gu, J.; Li, X.; Hu, D.; Liu, Y.; Zhang, G.; Jia, X.; Huang, W.; Xi, K. Green Synthesis of Amphiphilic Carbon Dots from Organic Solvents : Application in Fluorescent Polymer Composites and Bio-Imaging. *RSC Adv.* **2018**, *8*, 12556–12561.
2) Ortega-liebana, M. C.; Chung, N. X.; Limpens, R.; Gomez, L.; Hueso, J. L.; Santamaria, J.; Gregorkiewicz, T. Uniform Luminescent Carbon Nanodots Prepared by Rapid Pyrolysis of Organic Precursors Con Fi Ned within Nanoporous Templating Structures. *Carbon N. Y.* **2017**, *117*, 437–446.
3) Milosavljevic, V.; Moulick, A.; Kopel, P.; Adam, V.; Kizek, R. Microwave Preparation of Carbon Quantum Dots with Different Surface Modification. *J. Met. Nanotechnologies* **2014**, *3*, 16–22.
4) Vasimalai, N.; Vilas-boas, V.; Gallo, J.; Cerqueira, M. D. F.; Menéndez-miranda, M.; Costa-fernández, J. M.; Diéguez, L.; Espiña, B.; Fernández-argüelles, M. T. Green Synthesis of Fluorescent Carbon Dots from Spices for in Vitro Imaging and Tumour Cell Growth Inhibition. *Beilstein J. Nanotechnol.* **2018**, *9*, 530–544.
5) Hill, S.; Galan, M. C. Fluorescent Carbon Dots from Mono- and Polysaccharides : Synthesis , Properties and Applications. *Beilstein J. Org. Chem.* **2017**, *13*, 675–693.
6) Rao, L.; Tang, Y.; Lu, H.; Yu, S.; Ding, X.; Xu, K.; Li, Z.; Zhang, J. Z. Highly Photoluminescent and Stable N-Doped Carbon Dots as Nanoprobes for Hg^{2+} Detection. *Nanomaterials* **2018**, *8*, 1–18.
7) Miao, X.; Qu, D.; Yang, D.; Nie, B.; Zhao, Y.; Fan, H. Synthesis of Carbon Dots with Multiple Color Emission by Controlled Graphitization and Surface Functionalization. *Adv. Mater.* **2018**, *30*, 1–8.
8) Shamsipur, M.; Barati, A.; Taherpour, A. A.; Jamshidi, M. Resolving the Multiple Emission Centers in Carbon Dots: From Fluorophore Molecular States to Aromatic Domain States and Carbon-Core States. *J. Phys. Chem. Lett.* **2018**, *9*, 4189–4198.
9) Sarkar, S.; Banerjee, D.; Ghorai, U. K.; Das, N. S.; Chattopadhyay, K. K. Size Dependent Photoluminescence Property of Hydrothermally Synthesized Crystalline Carbon Quantum Dots. *J. Lumin.* **2016**, *178*, 314–323.
10) Zhai, X.; Zhang, P.; Liu, C.; Bai, T.; Li, W.; Dai, L.; Liu, W. Highly Luminescent Carbon Nanodots by Microwave-Assisted Pyrolysis. *Chem. Commun.* **2012**, *48*, 7955–7957.

11) Wang, D.; Wang, Z.; Zhan, Q.; Pu, Y.; Wang, J.; Foster, N. R.; Dai, L. Facile and Scalable Preparation of Fluorescent Carbon Dots for Multifunctional Applications. *Engineering* **2017**, *3*, 402–408.
12) Wu, Z. L.; Liu, Z. X.; Yuan, Y. H. Carbon Dots: Materials, Synthesis, Properties and Approaches to Long-Wavelength and Multicolor Emission. *J. Mater. Chem. B* **2017**, *5*, 3794–3809.
13) Zhu, S.; Meng, Q.; Wang, L.; Zhang, J.; Song, Y.; Jin, H.; Zhang, K.; Sun, H.; Wang, H.; Yang, B. Highly Photoluminescent Carbon Dots for Multicolor Patterning , Sensors , and Bioimaging. Angewandte. *Angew. Chemie* **2013**, *125*, 4045–4049.
14) Li, X.; Wang, H.; Shimizu, Y.; Pyatenko, A.; Kawaguchi, K.; Koshizaki, N. Preparation of Carbon Quantum Dots with Tunable Photoluminescence by Rapid Laser Passivation in Ordinary Organic Solvents. *Chem. Commun.* **2011**, *47*, 932–934.
15) Hu, S.; Niu, K.; Sun, J.; Yang, J.; Zhao, N.; Du, X. One-Step Synthesis of Fluorescent Carbon Nanoparticles by Laser Irradiation †. *J. Mater. Chem.* **2009**, *19*, 484–488.
16) Wang, H.; Gao, P.; Wang, Y.; Guo, J.; Zhang, K.-Q.; Du, D.; Dai, X.; Zou, G. Fluorescently Tuned Nitrogen-Doped Carbon Dots from Carbon Source with Different Content of Carboxyl Groups. *APL Mater.* **2015**, *3*, 1–8.
17) Gong, X.; Lu, W.; Chin, M.; Hu, Q.; Wu, X.; Shuang, S.; Dong, C.; Choi, M. M. F. Facile Synthesis of Nitrogen-Doped Carbon Dots for Fe^{3+} Sensing and Cellular Imaging. *Anal. Chim. Acta* **2015**, *861*, 74–84.
18) Wang, Z.; Long, P.; Feng, Y.; Qin, C.; Feng, W. Surface Passivation of Carbon Dots with Ethylene Glycon and Their High-Sensitivity to Fe^{3+}. *R. Soc. Chem. Adv.* **2017**, *7*, 2810–2816.
19) Devi, S.; Gupta, R. .; Paul, A. .; Kumar, V.; Sachdev, A.; Gopinath, P.; Tyagi, S. Ethylenediamine Mediated Luminescence Enhancement of Pollutant Derivatized Carbon Quantum Dots for Intracellular Trinitrotoluene Detection : Soot to Shine. *RSC Adv.* **2018**, *8*, 32684–32694.
20) Tian, Z.; Zhang, X.; Li, D.; Zhou, D.; Jing, P.; Shen, D.; Qu, S.; Zboril, R.; Rogach, A. L. Full-Color Inorganic Carbon Dot Phosphors for White-Light-Emitting Diodes. *Adv. Opt. Mater.* **2017**, *5*, 1–9.
21) https://www.organicdivision.org/wp-content/uploads/2016/12/organic solvents.pdf (Accessed on the 6th February 2019)
22) Li, H.; He, X.; Kang, Z.; Huang, H.; Liu, Y.; Liu, J.; Lian, S.; Tsang, C. H. A.; Yang,

X.; Lee, S. Water-Soluble Fluorescent Carbon Quantum Dots and Photocatalyst Design. *Angew. Chemie - Int. Ed.* **2010**, *49*, 4430–4434.

23) Varisco, M.; Zufferey, D.; Ruggi, A.; Zhang, Y.; Erni, R.; Mamula, O. Synthesis of Hydrophilic and Hydrophobic Carbon Quantum Dots from Waste of Wine Fermentation. *R. Soc. Chem.* **2017**, *4*, 1–11.

24) Chao, D.; Lyu, W.; Liu, Y.; Zhou, L.; Zhang, Q.; Deng, R.; Zhang, H. Solvent-Dependent Carbon Dots and Their Applications in the Detection of Water in Organic Solvents. *J. Mater. Chem. C* **2018**, *6*, 7527–7532.

25) Vinci, john C.; Ferrer, I. M.; Guterry, N. W.; Colon, V. M.; Destino, J. F.; Bright, F. V; Colon, L. A. Spectroscopic Characteristics of Carbon Dots (C-Dots) Derived from Carbon Fibers and Conversion to Sulfur- Bridged C-Dots Nanosheets. *Appl. Spectrosc.* **2015**, *69*, 1082–1090.

26) Ortega-liebana, M. C.; Chung, N. X.; Limpens, R.; Gomez, L.; Hueso, J. L.; Santamaria, J.; Gregorkiewicz, T. Uniform Luminescent Carbon Nanodots Prepared by Rapid Pyrolysis of Organic Precursors Con Fi Ned within Nanoporous Templating Structures. *Carbon N. Y.* **2017**, *117*, 437–446.

27) Lee, V.; Whittaker, L.; Jaye, C.; Baroudi, K. M.; Fischer, D. A.; Banerjee, S. Large-Area Chemically Modified Graphene Films : Electrophoretic Deposition and Characterization by Soft X-Ray Absorption Spectroscopy. *Chem. Mater.* **2009**, *21*, 3905–3916.

28) Zafar, Z.; Ni, Z. H.; Wu, X.; Shi, Z. X.; Nan, H. Y.; Bai, J.; Sun, L. T. Evolution of Raman Spectra in Nitrogen Doped Graphene. *Carbon N. Y.* **2013**, *61*, 57–62.

CHAPTER 7: GENERAL CONCLUSIONS AND RECOMMENDATIONS

7.1 Conclusions

The main purpose of this research project was to synthesize nitrogen-doped carbon dots (NCdots) from different precursors using microwave-irradiation method and apply them in organic solar cells in the active layer. The NCdots were synthesized using citric acid (CA) with ethylenediamine (EDA), and fumaronitrile (FN). The product yield of the NCdots derived from CA with EDA (NCdots-CAEDA) was higher than those derived from FN (NCdots-FN). The properties of the two types of NCdots were investigated and evaluated by transmission electron microscopy (TEM), powder X-ray diffraction (PXRD), Ultraviolet-visible spectroscopy (Uv-vis), Photoluminescence spectroscopy (PL), Thermal gravimetric analysis (TGA), Fourier transform infrared spectroscopy (FTIR) and X-ray photoelectron spectroscopy (XPS). TEM analysis revealed the both types of NCdots were quasi-spherical with diameters less than 10 nm. However, the average particle size of NCdots-FN was larger than that of NCdots-CAEDA. PXRD revealed that the NCdots-FN possessed a higher degree of graphitization than NCdots-CAEDA. FTIR spectroscopy demonstrated the presence of different functional groups on the surface of both types of NCdots. XPS confirmed the composition and functional groups of the NCdots. This was further confirmed by TGA as it weight loses of functional groups at temperatures between 200 and 500 °C. Both types of NCdots exhibited excitation-dependent fluorescence behaviour (redshift). The organic solar cells modified with both types of NCdots in the active layers were successfully fabricated. The device modified with NCdots-FN performed better than the device modified with NCdots-CAEDA. Various reaction conditions such as amount of EDA, solvent, reaction time, microwave power and annealing method were used in order to investigate their effect on the fluorescence properties of NCdots-CAEDA. The fluorescence properties were destroyed after annealing the sample. This implies that the functional groups on the surface of NCdots have a great impact on the fluorescence properties of NCdots. The fluorescence properties of NCdots were affected by the reaction conditions.

7.2 Recommendations

Even though the results demonstrated that the fluorescence properties of NCdots were affected by the reaction conditions, the actual PL mechanism of NCdots is still not understood. Therefore, more research will need to be done in this specific area in the future. Further optimization need to be done on the concentration of the NCdots to determine if they contribute to the broadening or redshift of the emission spectra.

The characterization technique like atomic force microscopy need to be used to determine the morphology the films. This will provide information on whether the 3D network of the acceptor and the donor is interconnected. AFM will also be used to determine the surface roughness of the films. According to the results obtained, the efficiencies of the fabricated devices modified with both types of NCdots and our reference cell were lower than the efficiency of the reference cell from literature review. This is because the measurements were carried out in air. A set-up with controlled environment (vacuum chamber) is recommended to avoid rapid degradation of the cells. Further optimization on the fabrication of the cells is also required.

APPENDIX I

Figure S1: Different fabricated organic bulk-heterojunction devices.

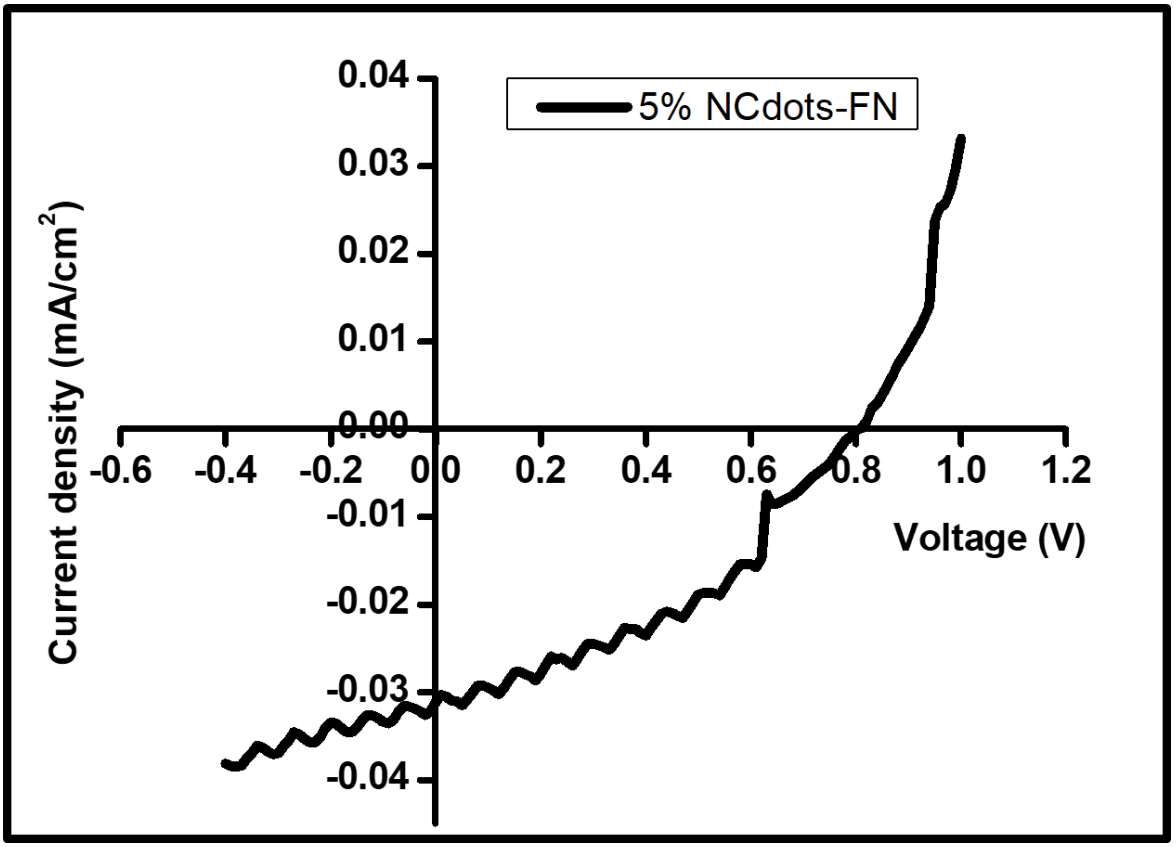

Figure S3: The current density-voltage curve of the organic BHJ device with 5% NCdots-CAEDA in the active layer.